2023

Controls on Thermokarst Lake Water Balances in the Inuvik - Tuktoyaktuk Region

Evan J. Wilcox
Wilfrid Laurier University, wilc0150@mylaurier.ca

Controls on Thermokarst Lake Water Balances in the Inuvik - Tuktoyaktuk Region

by

Evan James Wilcox

B.Sc., Wilfrid Laurier University, 2016

DISSERTATION

Submitted to the Department of Geography and Environmental Studies

in partial fulfilment of the requirements for

Doctor of Philosophy in Geography

Wilfrid Laurier University

Statement of Contributions

This thesis is comprised of multiple co-authored manuscripts. Chapter 2, 3 and 4 are published or under review, while Chapter 5 is to be submitted to a journal. The contribution of co-authors, publication status and citations for each Chapter are outlined below:

Chapter 2: Evan J. Wilcox (EJW), Dawn Keim (DK) and Philip Marsh (PM) conceptualized the study. EJW, DK, Tyler de Jong, Branden Walker (BW) and Philip Mann completed the data collection. EJW performed the statistical analysis with guidance from Anastasia Sniderhan and Oliver Sonnentag (OS). EJW wrote the manuscript with input from all other authors. Status: *Published*. Wilcox et al. (2019): Tundra shrub expansion may amplify permafrost thaw by advancing snowmelt timing, Arctic Science, 5(4), 202–217, 2019.

Chapter 3: EJW developed the study design and sampling plan with input from Brent B. Wolfe (BBW) and PM. EJW completed field sampling and sample preparation for lab analysis. EJW completed the data analysis with input from BBW. EJW lead the writing of the manuscript with input from BBW and PM. Status: *Published*. Wilcox et al. (2022b): Assessing the influence of lake and watershed attributes on snowmelt bypass at thermokarst lakes, Hydrology and Earth System Sciences, 26(23), 6186-6205, 2022.

Chapter 4: The study design and sampling plan was developed by EJW with input from BBW and PM. The field data collection and sample preparation for lab analysis was done by EJW. Analysis of the data was completed by EJW with input from BBW. The manuscript was primarily written by EJW with input from BBW and PM. Status: *Under Review*. Wilcox et al. (under rev.): Hydrological, meteorological and watershed controls on the water balance of thermokarst lakes between Inuvik and Tuktoyaktuk, Northwest Territories, Canada, Hydrology and Earth System Sciences Discussions, 2022.

Chapter 5: The study design and data collection was developed by EJW with input from PM, BW, OS, Julia Boike and Gabriel Hould-Gosselin. Data analysis and the primary writing was completed by EJW, with writing input from PM. Status: *To be submitted to a journal.*

This thesis has been generated alongside a number of co-authored works that contribute to the greater objective of this thesis to better understand the arctic environment. These publications include:

1) Anders et al. (2020): Multitemporal terrestrial laser scanning point clouds for thaw subsidence observation at Arctic permafrost monitoring sites, Earth Surface Processes and Landforms, 45(7), 1589–1600, 2020.

2) Bartsch et al. (2020): Feasibility of tundra vegetation height retrieval from Sentinel-1 and Sentinel-2 data, Remote Sensing of Environment, 237, 111515, 2020.

3) Grünberg et al. (2020): Linking tundra vegetation, snow, soil temperature, and permafrost, Biogeosciences, 17(16), 4261–4279, 2020.

4) Pitcher et al. (2020): Advancing Field-Based GNSS Surveying for Validation of Remotely Sensed Water Surface Elevation Products, Frontiers in Earth Science, 8, 1–20, 2020.

5) Walker et al. (2021): Accuracy assessment of late winter snow depth mapping for tundra environments using Structure-from-Motion photogrammetry, Arctic Science, 7(3), 588–604, 2021.

6) Boike et al. (2022): Standardized monitoring of permafrost thaw: a user-friendly, multiparameter protocol, Arctic Science, 8(1), 153–182, 2022.

7) Meloche et al. (2022): Characterizing tundra snow sub-pixel variability to improve brightness temperature estimation in satellite SWE retrievals, The Cryosphere, 16(1), 87–101, 2022.

The main data used in this thesis has been published in open-access repositories. These data include:

1) Wilcox et al. (2020): Frost table depth with associated snow and landscape variables at Trail Valley Creek, NT, 2015. Borealis. https://doi.org/10.5683/SP2/9ZGR5U, 2020.

2) Wilcox et al. (2022a) Isotope data and associated attributes for 25 thermokarst lakes along the Inuvik – Tuktoyaktuk Highway, 2018. Borealis. https://doi.org/10.5683/SP3/AZE4ER, 2022.

Abstract

There are tens of thousands of thermokarst lakes in the Inuvik-Tuktoyaktuk region, located in the northwest corner of the Northwest Territories, Canada. These lakes formed following the last glacial period in areas where ice-rich permafrost thawed and created depressions in the landscape. The Inuvik-Tuktoyaktuk region is one of the fastest warming regions in the world, leading to changing precipitation patterns, permafrost thaw and deciduous shrub expansion, all of which are affecting the water balance of thermokarst lakes. During the past several decades, lake expansion and contraction have been observed in response to fluctuations in precipitation. While these changes in lake surface area and number have been documented, less is known about how varying meteorological conditions, lake and landscape features, and hydrological processes have regulated these changes in thermokarst lake water balances. Many studies documenting fluctuations in lake surface area often observe some lakes expanding in area while others contract during the same period of time, suggesting that lake and watershed properties regulate how lakes react to climate change. Rapid lake drainage, which can be initiated by extremely high lake levels, is occurring at an increasing rate.

The main objective of this thesis is to quantify the drivers of variability in thermokarst lake water balance components (e.g. inflow, evaporation, lake level, lake water source composition), so that we may better understand how lakes will respond to ongoing climate change. Multiple properties of the environment have the potential to influence thermokarst lake water balances: seasonal and inter-annual variation in meteorological conditions (i.e. air temperature and precipitation), watershed properties (e.g. surface area, vegetation, topography, permafrost), and lake properties (e.g. depth, surface area, outlet channel presence). Achieving the objective of this thesis involves measuring lake water balances and quantifying how the environmental properties described above affect lake water balance components. The four main research chapters of this thesis divide this task into smaller parts, with each chapter quantifying a subset of lake water balance components or environmental conditions at different spatial and temporal scales.

The second chapter explores the interaction between snow and shrubs and their ultimate impact on frost table depth, which influences runoff from lake watersheds. Shrubs are expanding across the Arctic and affecting snow depth, snowmelt timing and soil shading, which in turn influences frost table depth. Hummocks, which are mineral-earth domes 0.5 - 1.0 m across formed over hundreds of years via the cyclical freezing and thawing of the uppermost soil layer (active layer), are common features on hillslopes in the Inuvik-Tuktoyaktuk region. Between hummocks lie a mesh-like network of inter-hummock zones that are filled with peat and form a preferential flow network on hillslopes. When hummocks degrade due to permafrost thaw, they collapse and mineral soils invade inter-hummock zones and reduce the hydraulic conductivity. Frost table depth, snow depth and the snow-free date were measured in hummock and inter-hummock zones at the Siksik Creek watershed throughout the summer of 2015 in shrub-covered and shrub-free locations. Areas of birch shrubs had earlier snowmelt dates, and experienced greater hummock frost table depths. In inter-hummock zones, frost table depth was shallower when adjacent hummocks were taller, indicating that inter-hummock frost table depths increase when hummocks collapse. Future birch shrub expansion may accelerate permafrost thaw, leading to hummock collapse and a reduction in the ability of hillslopes to convey runoff.

Chapter three focuses on the degree to which freshet runoff mixes with lake water, as the snowmelt period represents the largest volumetric input of water to lakes. Previous studies have observed a phenomenon called "snowmelt bypass" whereby water flowing into ice-covered lakes flows underneath lake ice and out of the lake without mixing with the entire water column. Snowmelt bypass occurs when the freshet runoff flowing into lakes (approx. 0°C) is less dense than deeper lake waters (<4°C), a condition that is typically present at the start of snowmelt runoff; however, lakes generally become more mixed towards the end of the snowmelt period. Using lake water isotope data from before and after the freshet, the percentage of lake water replaced by freshet runoff and the average lake source water isotope composition (δ_I) was quantified for seventeen lakes and compared to lake and watershed properties. Lake depth significantly influenced the amount of

lake water replaced by freshet runoff, with deeper lakes retaining less freshet runoff because a larger portion of the lake volume was isolated from mixing with freshet runoff. Additionally, isotope data showed that the source of freshet runoff remaining in lakes contained a mixture of snow-sourced and soil-sourced water. The snowmelt bypass effect was likely stronger earlier in the freshet when runoff was more snow-sourced, while later in the freshet when runoff was likely more soil water-sourced, stronger vertical mixing in the lake was likely present and the snowmelt bypass effect would have been weaker. Earlier snowmelt relative to lake-ice melt caused by shrubification could lead to greater snowmelt bypass in the future, with the freshet runoff remaining in lakes becoming even more soil water-sourced. A shift to more soil-sourced freshet may impact lake chemistry, as soil-sourced runoff has lower concentrations of dissolved organic carbon, lower conductivity and higher pH than snow-sourced runoff. These results are relevant for open-drainage lakes, which can experience snowmelt bypass since any excess water is able to flow through the lake outlet.

The fourth chapter investigates how lake and watershed properties mediate the response of lakes to seasonal shifts in meteorological conditions using an isotope hydrology approach. Twenty-five lakes along the Inuvik-Tuktoyaktuk Highway were water sampled five times during 2018 for isotope analysis, with sampling starting before snowmelt and ending in early September. Lake water isotope compositions were used to estimate the ratio of evaporation-to-inflow (E/I) and (δ_I). Four distinct seasonal phases of lake water balance were identified from the isotope data and prevailing meteorological conditions. The initial Freshet Phase occurred during snowmelt, with lakes experiencing a reduction in E/I and shift in δ_I towards the average isotope composition of precipitation. An Evaporation Phase followed, a period of typically warm air temperatures and minimal precipitation, during which E/I increased and δ_I remained stable due to minimal inflow. As air temperatures declined and precipitation increased, the Soil Wetting Phase began, where E/I and δ_I did not respond to initial rainfall as dry soils had not yet reached a moisture level sufficient to generate runoff. As rainfall persisted and soils become wetter, the Recharge Phase initiated, during which E/I declined and δ_I became more rain-like as inflow to lakes increased and evaporation

decreased as solar radiation and air temperature declined. Variability in E/I among lakes was strongly correlated with the ratio of watershed area to lake area (WA/LA), where lakes with smaller WA/LA had larger E/I ratios because they received less inflow relative to evaporation. The majority of lakes in the region have a WA/LA <10, with many having a relatively low WA/LA between 2 and 4. Given that lakes with larger WA/LA receive relatively more inflow compared to their size, these lakes may see larger fluctuations in lake level and could be more vulnerable to rapid lake drainage as a result.

Chapter five analyzes year-to-year differences in lake water balance components for a single lake in the region. Three years of lake water balance measurements were made at Big Bear Lake near the Trail Valley Creek research station. The water balance was calculated daily between May 1 and October 30, such that $\Delta LL = P + Q_{in} - Q_{out} - E$, where LL is lake level, P is precipitation, Q_{in} is inflow, Q_{out} is outflow, and E is evaporation. Lake level was measured using a pressure-transducer type water level recorder and outflow was estimated using a stage-discharge relationship derived from manual discharge measurements made at the lake outlet. Evaporation was estimated using the Priestley-Taylor method, while precipitation was measured using a shielded weighing gauge. Inflow was calculated as the unknown variable in the lake water balance equation, but was set to 0 if the estimated inflow was a negative value. During the freshet period, the runoff ratio (i.e. the percentage of snowpack and precipitation converted into inflow) was highest when the snowmelt occurred rapidly or when the previous year experienced higher levels of summertime precipitation. Rapid snowmelt also caused higher maximum lake levels at the time of snow dam failure. Summertime runoff ratios were higher in wetter years, but were also affected by the previous year's summertime precipitation, with higher runoff ratios when the preceding year was wetter. Evaporation losses varied between 226 to 296 mm, with the length of the ice-free period largely controlling the amount of evaporation that occurred. There was a large potential for evaporation (4 to 6 mm day^{-1}) in the days leading up to the lake becoming ice-free, implying that the ice-free date has a strong impact on total evaporative losses from lakes. Predicting whether lake

water balances become wetter or drier in the future requires understanding how increasing active layer depths, degrading hummocks and shrub expansion will affect runoff ratios under predicted wetter summers, while ice-free seasons lengthen and lake evaporative losses increase.

Overall, this thesis improves our understanding of the controls on thermokarst lake water balances in the western Canadian Arctic. Specifically, this thesis outlines the strong predictive power of lake and watershed attributes in describing variability in lake water balances, a concept that could be further developed by integrating more variables from remote sensing data and more advanced statistical methods to quantify the influence of less influential lake and landscape attributes on lake water balance. This thesis also advances our understanding of the freshet period, including the influence of different shrub species on snow depth, snowmelt timing and frost table depth, the drivers of lake level maximums and snow dam failure, and the impact of lake depth on the mixing of snow- and soil-sourced water into ice-covered lakes.

The complexity of interactions between climate change and spatially variable landscape elements make it difficult to foresee whether lakes will experience a wetter or a drier future water balance, as climate-induced changes may increase runoff (e.g. more rainfall, wetter soils and increased runoff ratios), or decrease runoff (e.g. shrub expansion, greater rainfall interception, drier soils and decreased runoff ratios), which will either offset or amplify increases in lake evaporation losses. Given our observations of increasing E/I ratios with decreasing WA/LA in Chapter 4, we may expect under drier future conditions that lakes with smaller WA/LA are the first to decrease in surface area, while under wetter conditions lakes with larger WA/LA may be more vulnerable to rapid drainage as they experience greater increases in lake level. These hypotheses could be tested with multi-decadal remote sensing time series and observing how the lake surface area of lakes with different WA/LA behave during wetter and drier periods. Future scenarios for lake water balances may also be investigated with hydrological models, as the capability of models for representing relevant cold-regions processes such as snow redistribution and ground subsidence after permafrost thaw is improving.

Acknowledgements

It has been an incredible experience to do all the work that went into this thesis. I will cherish the many months I spent in the Arctic and all of the friendships I made. I am grateful to my family who always supported me in my endeavours.

Thank you to my supervisor Philip Marsh who gave me the opportunity to do all this rewarding research, and to spend so much time in the Arctic and at conferences around NA and Europe. Thank you also to my supervisor Brent Wolfe, you really helped me get stuff from my brain onto the page in a coherent way. Thank you also to my two committee members Oliver Sonnentag and Julia Boike for your valuable resources and input, and for hosting me in Potsdam, Julia. I will miss my group members and all of those in the Geography Dept. at Laurier where I have spent the last eleven(!) years.

I appreciate the financial support from Ontario Graduate Scholarships and a W. Garfield Weston Award for Northern Research from the Weston Family Foundation that made my education possible. My research was also supported by ArcticNet, Northern Water Futures, the Northern Scientific Training Program, the Polar Continental Shelf Program, and the Natural Sciences and Engineering Research Council of Canada.

Finally, a huge amount of gratitude goes to Carolina, who always was and is there for me.

Author's Declaration

I declare that the entire contents of this dissertation is generated from my own research. This dissertation, in part or whole, has not been submitted for a degree at any university. Ideas taken from others are cited accordingly.

Table of Contents

List of Figures

List of Tables

Chapter 1

Introduction

1.1 Thermokarst lakes and the changing climate

Thermokarst lakes are common features in ice-rich permafrost regions, forming in areas where permafrost has thawed and caused ground subsidence (Plug and West, 2009; Jones et al., 2011). During the past four decades the Arctic has warmed at four times the rate as the rest of the globe (Rantanen et al., 2022), which has influenced the amount of water entering and leaving thermokarst lakes. There has been a varying response of arctic lake surface area to climate warming, including: lake expansion (Smith et al., 2005; Wen et al., 2016), contraction (Jones et al., 2011; Finger Higgens et al., 2019), rapid drainage causing lakes to partially or completely disappear (Marsh and Neumann, 2001; Yoshikawa and Hinzman, 2003), or no long-term changes (Plug et al., 2008). Often, a combination of these changes to lakes are observed within the same region (Smith et al., 2005; Riordan et al., 2006; Karlsson et al., 2012; Chen et al., 2014; Cooley et al., 2019; Nitze et al., 2020; Lindgren et al., 2021), indicating that lake water balances have not responded uniformly to increasing air temperatures. Climate change has altered thermokarst lake water balances through multiple pathways, including:

(i) Rising air temperatures which increase evaporation losses from lakes by increasing the time

that lakes are ice-free, while simultaneously increasing evaporation rates (Prowse et al., 2011; Macrae et al., 2014; Arp et al., 2015).

(ii) Changes in the amount of snowfall and rainfall (Brown and Mote, 2009; Bintanja and Selten, 2014; Bintanja and Andry, 2017; Lee et al., 2021), which alters the volume of water that enters lakes (Stuefer et al., 2017).

(iii) Permafrost thaw, which influences the volume of runoff flowing into lakes by changing the hydrological behaviour of lake watersheds (Liljedahl et al., 2016; Walvoord and Kurylyk, 2016; Koch et al., 2022). Depending on the local permafrost features present in the landscape, permafrost thaw may increase runoff (e.g. Connon et al., 2014) or decrease runoff (e.g. Wan et al., 2020). For example, thaw of ice-wedge polygons increases the hydrological connectivity of tundra landscapes (Liljedahl et al., 2016), whereas the formation of permafrost thaw slumps on lake shorelines can reduce the ability of soils to convey runoff into lakes (Wan et al., 2020).

(iv) Shrub expansion (Sturm et al., 2001; Myers-Smith et al., 2011) which alters the spatial distribution of snow and the timing of snowmelt (Essery and Pomeroy, 2004; Pomeroy et al., 2006). Shrub-induced changes in snow depth and snowmelt timing can either induce or mitigate permafrost thaw depending on the relationship between snow depth and shrub height (Blok et al., 2010; Loranty and Goetz, 2012; Loranty et al., 2018). Shrubs also decrease soil moisture relative to shrub-free tundra via transpiration and rainfall interception (Swann et al., 2010; Wallace and Baltzer, 2019; Zwieback et al., 2019a; Kemppinen et al., 2021), reducing the soil water available to runoff into lakes.

If we are to predict how climate change will influence thermokarst lakes, it is crucial we understand how lake water balances are affected by varying meteorological conditions (e.g. air temperatures, snowmelt timing, precipitation amount) and by landscape elements (e.g. mineral-earth hummocks,

vegetation cover), which are changing as a result of climate warming. Knowledge of how meteorological conditions and lake and watershed properties regulate lake water balances can then be utilized to predict which lakes may be more likely to expand, contract, remain stable, or drain, as temperatures rise, precipitation patterns shift, permafrost thaws and shrubs expand across the landscape.

Lake water balances impact multiple aspects of the permafrost environment, often by linking the terrestrial and aquatic domains via the movement of water into, within, and out of lakes. The number and connectivity of lakes in a permafrost region affects the magnitude and timing of discharge in rivers: when lake levels are lower, runoff is stored for longer in lakes and released more slowly, reducing peak discharge rates downstream and leading to more evaporative water loss from the region (Arp et al., 2012b, 2020b). Carbon and nutrients are carried by runoff into lakes, where their concentrations in the lake are influenced by evaporation, water residence time and mixing in the water column, ultimately impacting the aquatic ecosystem and greenhouse gas flux from the lake (Anthony et al., 2014; Balasubramaniam et al., 2015). High lake levels or ice-wedge cracks can initiate rapid lake drainage by causing runaway thermo-mechanical erosion of the permafrost impounding the lake (Mackay, 1988; Brewer et al., 1993), causing downstream discharge orders of magnitude greater than annual peak flow (Marsh and Neumann, 2001), threatening riparian habitats and infrastructure downstream, while also leading to permafrost aggradation in the former lakebed (Jones et al., 2022).

1.2 Past research and knowledge gaps

Due to their remote location, previous water balance studies of thermokarst lakes often focused on making direct measurements of lake water balance at a single lake (e.g. Woo et al., 1981; Marsh and Bigras, 1988; Hardy, 1996; Pohl et al., 2009; Lopez Caceres et al., 2015; Pan et al., 2017). Direct measurements, using equipment such as water level recorders, can be used to measure the

contribution of specific lake water balance components (lake level, inflow, outflow, evaporation and precipitation) at daily or hourly timescales, and can also be integrated with hydrological models to explore lake water balances under different scenarios. Measuring water balance components at a high temporal resolution provides insight into the physical processes that control lake water balances, but research undertaken at a single lake gives little information about how lake water balances vary within a region. Studies that have surveyed a variety of lakes over multiple years in a region are often able to identify spatially variable lake and landscape properties that drive variability in lake water balance, helping to explain why some lakes in the same region expand while others contract or remain stable. Such lake and landscape attributes include watershed area (Gibson and Edwards, 2002; Turner et al., 2014), landscape position (Brock et al., 2009; Anderson et al., 2013; Gibson and Reid, 2014), hydrological connectivity (Wolfe et al., 2011), ice-free duration (Arp et al., 2015), and vegetation-snow interactions (Turner et al., 2014). These studies examining regional variability over multiple years have predominantly relied on water isotope sampling, which is an efficient method for surveying many lakes across a large area given that only a handful of small water samples per year are required, versus the installation and maintenance of multiple pieces of equipment required for direct water balance measurements. Water isotope samples can be used to calculate the ratio of evaporation to inflow and the relative mixture of sources of water present in lakes (Gibson et al., 1993; Yi et al., 2008), but the temporal resolution of isotope-derived hydrological data is limited by how frequently lake waters can be sampled and the water residence time of the lake. A combined approach using both direct measurements and water isotope samples from lakes can be used to generate a more comprehensive understanding of lake water balances. Direct measurements provide both detailed information about lake water balance components and the hydrological behaviour of the lake and its watershed, which can then be used to interpret information about temporal and spatial variability in lake water balances and variation in water sources provided by lake water isotope sampling.

An important and lesser studied stage of thermokarst lake water balances is the snowmelt

runoff period (freshet), which constitutes the majority of yearly inflow for thermokarst lakes (Woo et al., 1981; Braun et al., 2000). Focused study of the freshet period is necessary for understanding thermokarst lake water balances because of the unique processes influencing snow and lake ice that cause inflow, in-lake mixing, and outflow to behave differently than during the summertime (Fitzgibbon and Dunne, 1981; Roulet and Woo, 1988; Braun et al., 2000; Burn, 2002; Cortés et al., 2017). For example, spatial variability in shrub height can cause areas of taller vegetation to trap snow and increase snow depth, thereby increasing the volume of freshet runoff into lakes (Pomeroy et al., 1997; Essery and Pomeroy, 2004; Turner et al., 2014). During the freshet, inflow is impounded in the lake by snow dams that form in lake outlet channels, causing lake levels to reach their yearly maximums (Woo, 1980); to my knowledge no published research has investigated annual variability in snow dam height or failure date (Heginbottom, 1984; Xia and Woo, 1992; Arp et al., 2020a). Understanding the dynamics of maximum lake level is important because thermokarst lakes are prone to rapid drainage if the water level overtops the lake bank and causes runaway erosion through a new outlet channel (Mackay, 1988; Brewer et al., 1993; Marsh and Neumann, 2001; Turner et al., 2010). While the volume of freshet inflow and snow dams control lake level, the actual replacement of pre-freshet lake water by freshet runoff is affected by snowmelt bypass, a process whereby freshet runoff is unable to mix with deeper lake waters due to density differences between snowmelt and lake water (Henriksen and Wright, 1977; Bergmann and Welch, 1985; Edwards and McAndrews, 1989; Cortés and MacIntyre, 2020). No studies have examined what causes lake-to-lake variability in snowmelt runoff contribution to lake water balances during the freshet, whether it be differences in the volume of freshet inflow or variability in the strength of the snowmelt bypass effect. Given the expected changes to snowfall (Bintanja and Andry, 2017), shrub expansion and therefore snow distribution (Loranty and Goetz, 2012), snowmelt timing (Foster et al., 2008), and lake mixing regimes (Woolway and Merchant, 2019), it can be expected that climate-induced changes to the freshet will affect thermokarst lake water balances.

1.3 Objectives and approach

The general objective of this thesis is to better understand the controls on thermokarst lake water balances, to improve our understanding of how climate-induced changes will affect lake water balances in the tundra uplands between Inuvik and Tuktoyaktuk. This region is an ice-rich continuous permafrost area where lakes have been observed to fluctuate in surface area in response to changing precipitation patterns (Plug et al., 2008; Cooley et al., 2019), and where lakes are vulnerable to rapid lake drainage (Marsh and Neumann, 2001; Pohl et al., 2009). As outlined above, the predicted impacts of climate change on lake water balances are driven by meteorological changes and subsequent impacts, such as longer ice-free seasons and increased evaporation, increasing shrub cover, changing snow redistribution and snowmelt timing, and increasing active layer thickness. Generating the ability to predict how lakes will respond to all these changes first requires an understanding of lake water balance components and how varying meteorological conditions and watershed properties (topography, vegetation, etc.) influence both each other and lake water balance. Knowledge about inter-annual variability in lake water balances was gathered through multi-year direct water balance measurements at a thermokarst lake. At the same location where direct lake water balance measurements were made, data exploring how snow, vegetation, soil, and frost table depth influence each other are also collected in order to generate associations between the various watershed characteristics and how they many impact runoff to lakes. This knowledge, along with other related studies conducted by collaborators, was then used to explain relationships between lake and watershed properties and lake water balance measurements from a set of lakes calculated using water isotope measurements taken during the freshet period and the summertime. This combination of empirical knowledge from direct measurements and a regional survey of lake water balances and watershed properties allows identification of what types of lakes may be vulnerable to change, why those lakes are vulnerable to change, and extrapolate how future changes will affect lake water balance. The objectives of this thesis are addressed by three focused research questions:

1. What is the typical lake water balance for a lake in the Inuvik – Tuktoyaktuk tundra uplands region? (Chapter 4, 5)

2. How do meteorological conditions, lake and watershed components regulate lake water balances? (Chapter 2, 3, 4, 5)

3. What lake and watershed properties make lakes vulnerable or resilient to climate change? (Chapter 4, 6)

1.4 Thesis outline

There are six chapters in this thesis. The first chapter provides a brief introduction to the topic of thermokarst lake water balances in the context of climate change, providing rationale for the objectives of this thesis. Chapters 2, 3, 4 and 5 are a series of interlinked scientific studies aiming to answer the research questions. The final, sixth, chapter synthesizes the findings of the previous four chapters to provide potential trajectories for thermokarst lakes depending on their properties in response to future climate change. Following this section are synopses of Chapters 2 to 5.

1.4.1 Chapter Two

Published in Arctic Science, Wilcox et al. (2019).

Chapter two explores how different landscape features in lake watersheds, namely shrubs, snow, and microtopography, interact with each other to influence frost table depths. Shrub expansion, which is occurring in the Inuvik-Tuktoyaktuk region (Lantz et al., 2013), has been observed to mitigate permafrost thaw in some regions (Blok et al., 2010) and enhance it in others (Grünberg et al., 2020), depending on the interplay between shrubs, snow, and soil. In the Inuvik-Tuktoyaktuk region, runoff is conveyed through inter-hummock zones of highly porous organic soils which form a mesh-like geometry in between mineral-earth hummocks, microtopographical formations 0.5 to

1.0 metres wide and 20 to 40 centimetres tall (Quinton and Marsh, 1998). When inter-hummock zones experience permafrost thaw, mineral soil from the surrounding earth-hummocks collapses into the inter-hummock zone and greatly reduces the hydraulic conductivity of the inter-hummock zone (Kokelj et al., 2007). Therefore, it is important to understand how shrubs will impact snow and permafrost in this region given that changes in watershed runoff are sensitive to permafrost thaw-driven hummock collapse. This chapter unravels the interaction between shrubs, snow and permafrost in this region by using 3056 frost table depth measurements made in hummock and inter-hummock zones and comparing them to snow, shrub and topographical data using a structural equation modelling approach. Results show that hummock frost table depths were deeper in areas that became snow-free sooner, while birch shrubs advanced snow-free timing an average six days earlier than shrub-free tundra. In inter-hummock zones, frost table depth was most strongly related to hummock height, an indicator of hummock development. Based on these results, one can hypothesize that birch shrub expansion will accelerate hummock permafrost thaw, leading to hummock collapse, reducing the hydraulic conductivity of inter-hummock zones.

1.4.2 Chapter Three

Published in Hydrology and Earth System Sciences, Wilcox et al. (2022b).

Chapter three focuses on drivers of lake water balance variability during the snowmelt period, during which snowmelt drives the majority of yearly runoff into lakes. Specifically, this chapter describes how lake and watershed properties cause variability in snowmelt bypass and also observes how the sources of lake water change in response to freshet inflow. This chapter uses stable water isotope methods, sampling lakes along the Inuvik-Tuktoyaktuk Highway before snowmelt and after lakes became ice-free. From isotope data, the percentage of pre-snowmelt lake water replaced by freshet and the change in lake source water isotope composition are calculated and compared to lake and watershed properties. The percentage of pre-snowmelt lake water replaced in lakes varied widely from 5.2 to 52.8%. Lake depth was negatively correlated with the replacement of

pre-snowmelt lake water, as the mixed freshet layer beneath lake ice was restricted from mixing with deeper water. The source of freshet runoff remaining in lakes was a mixture of snow-sourced and soil-sourced water. It is likely that initial runoff flowing into lakes was primarily snow-sourced, but as the freshet period continued the initial runoff that flowed into lakes was replaced by freshet runoff that was more soil-water dominated, as the active layer thawed and allowed soil water to be mobilized. As shrub expansion causes snowmelt to occur earlier relative to lake ice melt, snowmelt bypass may become more amplified in the future, while the freshet runoff remaining in lakes becomes less snow-sourced.

1.4.3 Chapter Four

Under review for Hydrology and Earth System Sciences, Wilcox et al. (under rev.).

Chapter four evaluates how seasonal shifts in meteorological conditions and lake and watershed properties influence lake water balances. Similar to Chapter three, this Chapter also relies on stable water isotope sampling that was completed five times between May and September of 2018 at lakes along the Inuvik-Tuktoyaktuk Highway. For each lake and sampling date, the ratio of evaporation-to-inflow (E/I) and the average source water isotope composition (δ_I) was calculated. The evolution of E/I and δ_I is described and water balance phases (Freshet, Evaporation, Soil Wetting and Recharge) are designated based on how the seasonal meteorological conditions influence E/I and δ_I. The only watershed property that had a significant influence on E/I was the ratio of watershed area to lake area (WA/LA), as lakes with smaller WA/LA had greater E/I ratios because they received less inflow. Extrapolating the relationship between WA/LA and E/I to 7340 lakes in the Inuvik-Tuktoyaktuk region revealed that no lakes are likely to desiccate under current climate conditions, however under a drier future lakes with smaller WA/LA will be more vulnerable to increasing evaporation influence.

1.4.4 Chapter Five

To be submitted to Water Resources Research.

Chapter five uses direct measurements of lake water balance components over multiple years to evaluate how lake water balances vary in response to different meteorological conditions. Measurements were made at Big Bear Lake near the Trail Valley Creek research station using water level recorders, discharge measurements, and a meteorological station. From these measurements a water balance was generated for the lake, where lake level, evaporation, outflow, and precipitation input were measured, and inflow was calculated as a residual. These water balance metrics were then used to calculate the runoff ratio for the watershed for each year during the freshet and summertime. Water balance data show that 53 - 62% of the inflow lakes receive every year occurs during the first few weeks of the freshet, after which lakes receive bursts of inflow periodically from rainfall events if soils are wet enough. Years with rapid snowmelt lead to rapid inflow and higher lake levels before snow dam failure as a result. Runoff ratios during the freshet and summertime were elevated when previous years had wetter than average summertime precipitation, as soil moisture from the previous year is locked in when soils freeze, before being released the following year as the active layer thaws. Yearly evaporation losses varied from 226 to 296 mm and were largely controlled by the length of the ice-free season. There was a large evaporation potential (4 to 6 mm day^{-1}) before lakes became ice-free, suggesting that advancement in ice-off timing may lead to large increases in evaporative losses, in comparison to later ice-on dates. These results highlight the need to understand future changes in lake inflow, as increasing ice-free periods for lakes combined with warmer air temperatures will certainly increase evaporative losses from lakes.

Chapter 2

Tundra shrub expansion may amplify permafrost thaw by advancing snowmelt timing

2.1 Abstract

The overall spatial and temporal influence of shrub expansion on permafrost is largely unknown due to uncertainty in estimating the magnitude of many counteracting processes. For example, shrubs shade the ground during the snow-free season, which can reduce active layer thickness. At the same time, shrubs advance the timing of snowmelt when they protrude through the snow surface, thereby exposing the active layer to thawing earlier in spring. Here, we compare 3056 in situ frost table depth measurements split between mineral earth hummocks and organic inter-hummock zones across four dominant shrub–tundra vegetation types. Snow-free date, snow depth, hummock development, topography, and vegetation cover were compared to frost table depth measurements using a structural equation modeling approach that quantifies the direct and combined interacting influence of these variables. Areas of birch shrubs became snow free earlier regardless of snow depth

or hillslope aspect because they protruded through the snow surface, leading to deeper hummock frost table depths. Projected increases in shrub height and extent combined with projected decreases in snowfall would lead to increased shrub protrusion across the Arctic, potentially deepening the active layer in areas where shrub protrusion advances the snow-free date.

2.2 Introduction

The progression of the frost table in permafrost areas to its maximum annual depth, the active layer (Harris et al., 1988), is controlled by climate at a broad scale and a multitude of other variables operating at smaller scales. These "micro-scale" variables include (micro)topography, snow depth and density, and vegetation type and density (Mackay, 1980; Sturm et al., 2001; Bonnaventure and Lamoureux, 2013; Fisher et al., 2016). Increasing air temperatures promote deeper thaw (Biskaborn et al., 2019), however, the spatially and temporally varying effects of micro-scale variables on ground heat flux mean permafrost thaw does not occur uniformly across the Arctic landscape (Loranty et al., 2018).

Mineral earth hummocks are common microtopographical features in permafrost regions (Schunke and Zoltai, 1988) that are susceptible to degradation when the active layer deepens (Kokelj et al., 2007). Hummocks consist of mineral soil domes roughly 50 – 200 cm in diameter and 10 – 40 cm in height (Tarnocai and Zoltai, 1978; Mackay, 1980). Hummocks formed over thousands of years through cyclical upward frost heaving in their centres paired with subsidence at their perimeters, resulting in a locally deeper active layer beneath the centre of hummocks (Mackay, 1980). Hummocks are surrounded by well-defined, peat-dominated inter-hummock zones with a shallower active layer, and act as areas of preferential flow (Quinton and Marsh, 1999).When hummocks degrade as a result of active layer deepening they become flat and spread out radially, producing a deeper inter-hummock active layer due to the intruding mineral soils (Kokelj et al., 2007).

Shrubs are another main control on active layer thickness in tundra regions. Shrubs are increasing in height, density, and areal extent across the Arctic (Tape et al., 2006; Bjorkman et al., 2018), consequently altering permafrost conditions through multiple, counteracting mechanisms (Chapin et al., 2005; Myers-Smith et al., 2011). When shrubs typically buried by snow were experimentally removed, frost table depth deepened due to increased thermal load on the ground surface during the snow-free period (Blok et al., 2010; Nauta et al., 2015). In contrast, shrubs that protrude through the snow surface emit longwave radiation and advance the timing of snowmelt, which large-scale modeling predicts will offset the shade provided by shrubs (Pomeroy et al., 2006; Marsh et al., 2010; Lawrence and Swenson, 2011; Bonfils et al., 2012). However, shrubs protruding above the snow surface decrease surface wind speed, thereby decreasing the turbulent fluxes of heat and water (Endrizzi et al., 2011). In addition, patches of tall shrubs can trap blowing snow (Pomeroy et al., 1997), which in turn increases wintertime ground temperatures as deeper snow insulates the ground more effectively (Sturm et al., 2001; Hinkel and Nelson, 2003; Myers-Smith and Hik, 2013). Deeper snow also requires longer to melt, and delays the beginning of active layer thaw (Wang et al., 2019).

Previous field studies that described the influence of shrub expansion on active layer thickness did not consider the combined influence of shrubs on snowmelt timing and snow redistribution. This study seeks to identify the relative influence of these variables on frost table depth while also evaluating how they influence each other, using a structural equation modeling approach. We use 3056 in situ frost table depth measurements taken from early June until late August 2015, split between mineral earth hummocks and organic inter-hummock zones across four dominant vegetation types, and explore the effect of multiple known influences on frost table depth. These include hillslope angle and aspect, snow depth, hummock height, vegetation cover and snow-free date.

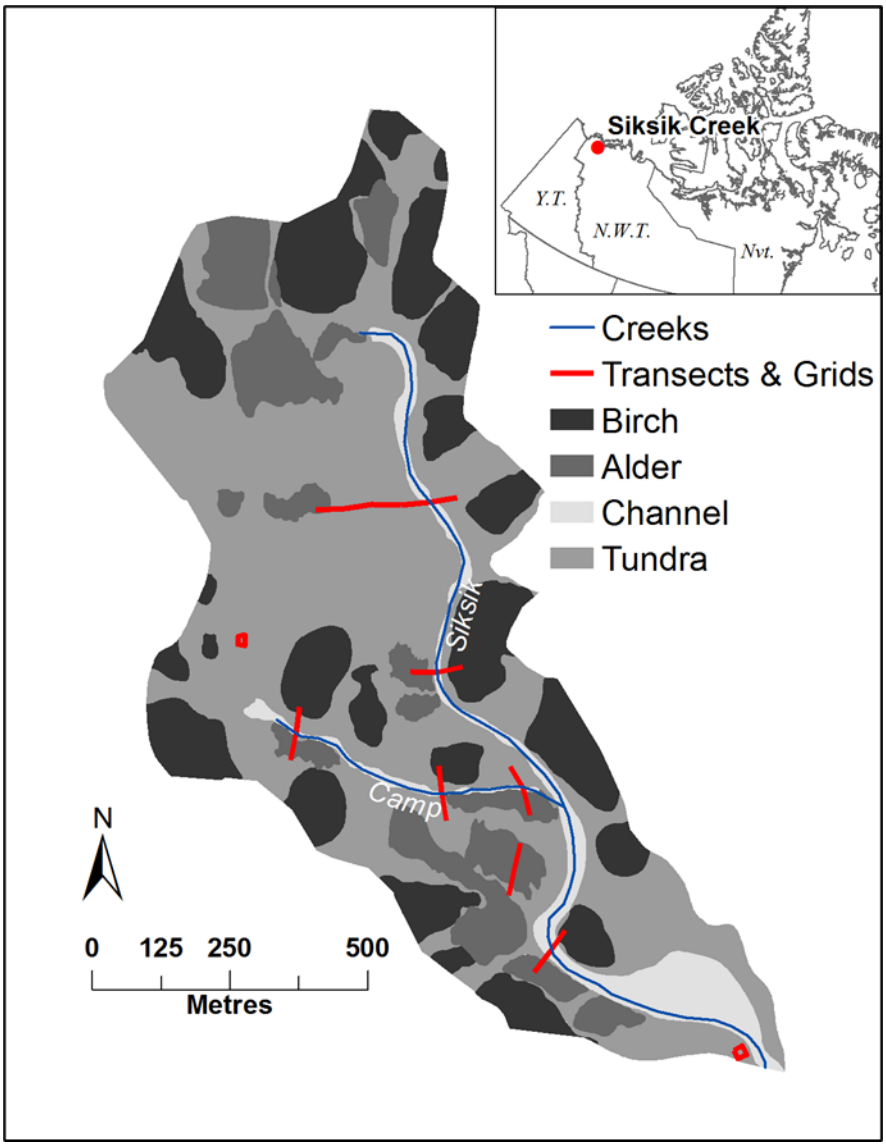

Figure 2.1 The Siksik Creek Basin is located in the continuous permafrost zone in the Northwest Territories, Canada. Frost table depth sampling transects are represented by red lines; red squares represent grids. Hummock and inter-hummock frost table depth was measured at five metre intervals along each grid and transect.

2.3 Study site

All observations were made within the Siksik Creek watershed (68.5° N, 133.75° W) (Figure 2.1), a 1 km^2 catchment that flows into Trail Valley Creek, Northwest Territories (Quinton and Marsh, 1999). The site is located 45 km north of Inuvik and ca. 80 km south of Tuktoyaktuk, at the northern edge of the boreal forest – tundra transition zone. Mean annual total precipitation in Inuvik from 1981 – 2010 was 240 mm of which 66% was snowfall, and mean annual air temperature was -8.2 °C (Environment and Climate Change Canada 2019). Snow cover commonly lasts for 8 months of the year from October to May during which air temperatures remain below 0 °C and south-westerly winds are dominant. The total thickness of the ice-rich permafrost across the region spans from 350 – 500 m and is overlain by an active layer that varies between 0.5 – 0.8 m in thickness (Burn and Kokelj, 2009). The topography of the region between Inuvik and Tuktoyaktuk is characterized by low rolling ice-rich morainal deposits interspersed with thermokarst lakes (Rampton and Wecke, 1987), although no lakes exist within the Siksik Creek watershed. Mineral earth hummocks are present throughout the watershed, surrounded by inter-hummock zones filled with 20 – 50 cm of peat (Figure 2, (Quinton and Marsh, 1998)). The bulk density of hummocks is one order of magnitude greater on average than inter-hummock zones, which are highly porous (Quinton, 1997).

The vegetation cover at the Siksik Creek watershed is broadly characterized as erect low-shrub tundra (S2) (Walker et al., 2005). We identified four unique vegetation cover classes within the Siksik Creek watershed, which occur in patches of tens to hundreds of metres across (Figure 2.1). This type of heterogeneous vegetation cover is common in the treeless region between Inuvik and Tuktoyaktuk (Lantz et al., 2010). Over half of the watershed is covered by a mix of mostly shrub-free "open-tundra", with maximum vegetation heights of 5 – 25 cm, which is predominantly covered by reindeer lichen (*Cladonia rangiferina* L.), Sphagnum moss (*Sphagnum* L.), tussock and non-tussock sedges (*Carex* L.), and Labrador tea (*Rhododendron groenlandicum* (Oeder) Kron & Judd). The second most common vegetation cover type consists of dwarf birch (*Betula glandulosa*

Michx.) patches of 40 – 60 cm in height with open tundra species present beneath, and are generally present on west-facing slopes. Similar, but taller (80 – 150 cm) alder (*Alnus alnobetula* (Ehrh.) K. Koch.) patches exist on east facing slopes and also contain open tundra species beneath. In stream channel areas, 150 – 250 cm alder and willow (*Salix* L.) grow through a Sphagnum moss dominated floor. Open tundra has virtually no canopy cover, while birch and channel areas have dense canopy cover with higher leaf area indexes (Marushchak et al., 2013). Individual alder shrubs have greater leaf area indexes than individual birch shrubs (Zwieback et al., 2019a), however alder shrub patches in Siksik Creek are "open" and less dense than birch shrub patches, resulting in a lower mean leaf area index comparing patch to patch (Marsh et al., 2010; Lantz et al., 2013). Areas of shrub-covered tundra have cooler summer soil temperatures as a result of the shade they provide to the ground (Myers-Smith and Hik, 2013). As a result of their denser canopy, birch shrub patches intercept 15-30% of incoming rainfall, while alder shrub areas have little effective rainfall interception (Zwieback et al., 2019a). Shrub patches are also characterized by larger evapotranspiration rates than tundra areas, and typically have drier soils as a result (Bring et al., 2016). Areas of birch shrubs were observed to protrude through the snow in the Siksik Creek watershed (Figure 2.2), while other areas of vegetation were mostly buried under the snow and were eventually exposed as the snow melted. The greater region between Inuvik and Tuktoyaktuk is experiencing alder and birch shrub expansion (Lantz et al., 2013).

Figure 2.2 Image of birch shrubs protruding through the end of winter snowpack. Their branches lower albedo above the snow pack in spring, enhancing snowmelt.

2.4 Materials and methods

2.4.1 Frost table depth measurements

After snowmelt in early June 2015, frost table depth measurements began at eight transect and two grid locations within the Siksik Creek watershed (Figure 2.1). Transects bisected stream channels in order to capture a wide range of micro-scale variables as efficiently as possible, while grids captured flatter areas. Measurements were made every five metres along 100 m transects and one 150 m long transect, and two 15 m by 20 m grids, resulting in 20 – 30 hummock and 20 – 30 inter-hummock frost table depth measurements at each sampling location. Measurements were taken over the course of a two- to three-day period every one to three weeks. In total eight rounds of sampling were completed between June 11 and August 20 of 2015, resulting in 3056 total frost

table depth measurements.

At sampling points along transects and grids, frost table depth in the nearest hummock and inter-hummock zone was measured by pushing a frost probe into the centre of each feature until submission against the frost table. Measurements were split between hummock and inter-hummock zones to control for the known differences in frost table depth between these two features. While leaving the frost probes in the hummock and inter-hummock zone, a construction level was placed perpendicular to the two probes, resting one end on the hummock. The point where the level intersected the inter-hummock frost probe was recorded (Figure 2.3). Inter-hummock frost table depth was measured perpendicular to the aspect of the hillslope (e.g. if measurements were made on a north-facing hillslope, inter-hummock measurements were made to the east or the west of each hummock measurement) to minimize the influence of the hillslope on the topography of the frost table. Frost table depth measurements were not always performed at the exact same hummock and inter-hummock zone for each sampling location, but still within a one metre radius of each measurement location. This was done to minimize soil disturbance that may affect the thawing beneath the measurement points by creating a preferential pathway for water to reach the frost table. Some sampling points displayed only minimal hummock development, mostly occurring in stream channels which were typically saturated. If no discernible hummocks were present, areas of localized high and low elevation were selected to sample from instead. By sampling regardless of hummock presence or size, the natural variability of hummock development was incorporated into the dataset. If only well-defined hummocks were selected for sampling, then the information gained from the data could only be applied to areas with well-developed hummocks. The spatial distribution of hummocks across the watershed is not known and cannot be estimated using other variables, and defining their state of development relies just on visual inspection. Therefore, the applicability of the knowledge gained from the data would be limited if only well-developed hummocks were measured.

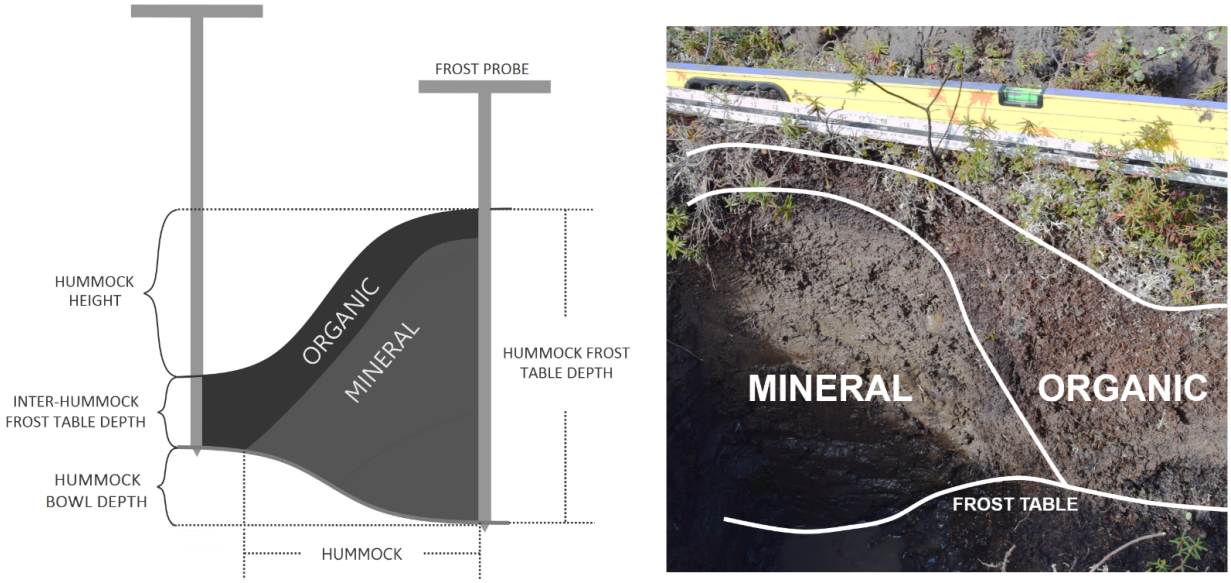

Figure 2.3 Cross-section of the frost table depth measurement protocol. Hummock height was measured using a construction level placed across the two frost probes. The photo on the right shows a cross-section of a typical hummock in mid-July; the hummock and inter-hummock area shown is 65 cm across.

2.4.2 Micro-scale variables

Frost table depth per vegetation cover class was compared to the sample date, hummock height, snow depth, snow-free date, hillslope angle and aspect. Hummock height was considered as an indicator of hummock development (Kokelj et al., 2007). Snow depth was derived by subtracting a bare-ground digital elevation model (DEM) captured by airborne LiDAR (Hopkinson et al., 2008) from a DEM of the snow surface before snowmelt began (De Michele et al., 2016; Mann, 2018). Each DEM contains a grid of one metre by one metre cells which hold an elevation value representing the height of the ground or snow above mean sea level. The snow surface DEM was generated using unmanned aerial system (UAS) imagery obtained by a fixed-wing eBee (SenseFly, 2015) and structure-from-motion photogrammetry analysis in Pix4Dmapper (Pix4D SA, 2019). Raw images taken by the UAS were geotagged and stitched using twelve ground control points placed throughout the Siksik Creek watershed and measured to an accuracy of 2 cm with a real-time kinematic GPS system, to create an orthomosaic using Pix4Dmapper. UAS derived snow depth

from five pre-snowmelt flights were averaged together to create 1 metre raster snow depth product for the entire watershed. As snowmelt had begun before UAS flights took place in 2015, images taken before snowmelt in 2016 were used to create the snow depth product. The spatial pattern of snow remains stable between years in tundra environments due to predominant wind directions and wide-spread snow redistribution, and are therefore comparable between years for this application (Sturm and Wagner, 2010). Measurements of snow depth taken in 2015 using a Magnaprobe (Sturm and Holmgren, 2018), which records GPS positions while measuring snow depth, were compared to the 2016 UAS snow depth product. The mean snow depth of 2459 Magnaprobe measurements made in the Siksik watershed in 2015 was 69.6 ±37.9 cm, while the mean snow depth from the 2016 UAS derived snow depth map at the same points where Magnaprobe measurements were made was 72.5 ±37.1 cm.

Snow-covered area was classified from UAS true colour imagery collected at multiple times over the course of the snowmelt period in 2015. Snowmelt first occurred on April 21, and the UAS was flown on April 28, May 8, May 11, May 12, and May 17, 2015. Approximately 95% of the watershed was snow covered on April 28th, and some areas remained snow-covered until the first week of June. Orthomosaics were then imported into ArcGIS 10.5 (ESRI, 2016), and snow-covered area was delineated using an iso-cluster unsupervised image classification with binary classes. Visual inspection of the classification showed that it was able to classify snow presence vs. snow absence accurately. Each frost table depth measurement location was assigned a snow-free date based on the amount of snow cover within a one metre radius around each frost table depth measurement point. If >90% of the radius around the measurement location was snow-free, it was classified as snow-free.

Vegetation classifications were delineated manually, as different vegetation cover classes were clearly distinguishable, using UAS true colour imagery of the Siksik watershed captured at 5 cm per pixel resolution. Four vegetation classes were delineated: alder shrub-dominated, birch shrub-dominated, open tundra, and channel shrub, as based on the classes outlined in the study site

section. We chose these vegetation cover classes because each cover class encapsulates a variety of biotic and abiotic variables and offers a more simplified assessment of different vegetation covers, compared to measurements of numerous biotic variables in each vegetation cover.

2.4.3 Analysis of frost table depth and micro-scale variables

A piecewise structural equation model (SEM) using the R (R Core Team, 2021) package piecewiseSEM (Lefcheck, 2016) was used to quantify the effect of micro-scale variables on hummock and inter-hummock frost table depth. The SEM incorporates user-defined mixed effects models generated using the package nlme (Pinheiro et al., 2018). Structural equation models determine the effect of explanatory variables on both the dependent variable and other explanatory variables by calculating unstandardized and standardized path coefficients for each causal path of influence defined by the user. Unstandardized path coefficients represent the linear effect of one variable on another, in terms of the explanatory variable's units, and were used to compare how the magnitude of influence of each variable differed between hummock and inter-hummock frost table depths. Standardized path coefficients correct for natural differences in the range of measured variables and allow for the influence of different variables within each SEM to be compared, however they are unitless and do not represent the direct effect of one variable on another. Path coefficients cannot be calculated for categorical variables (vegetation cover class); instead the mean of each category is presented and tested for significant difference from all other categories.

The hummock and inter-hummock SEMs share identical paths for variables which do not influence frost table depth directly, as these measurements are identical for each hummock and inter-hummock measurement. Justification for the SEM paths specified in this analysis are provided in the appendix (Section 2.8.1). As part of the SEM development, a directed test of separation was performed on all unspecified paths to determine if any significant relationships existed between them. The test found that hummock height significantly correlated with snow depth. Based on our understanding of hummock development (Mackay, 1980), there are no physical mechanisms

which would cause areas of deeper snow to develop shorter earth hummocks. This relationship was identified as a correlated error in the SEM, and the path was removed from the analysis. The piecewise SEM approach was chosen over a variance-based approach because it facilitates the use of mixed-effects models, which integrate information about random variability caused by repeated measures across multiple measurement units, such as transects and grids. Hummock and inter-hummock frost table depth were analyzed separately because we hypothesized that hummock and inter-hummock frost table depth may be influenced by different micro-scale variables, due to their different soil and hydrological characteristics. We expected explanatory variables which block incoming solar radiation to the ground to have less of an effect on inter-hummocks due to the insulative properties of peat, and that inter-hummocks would be more affected by variables which control their heat conductivity (e.g. soil moisture). Explanatory variables in each of the mixed effects models included hummock height, sample date, hillslope angle and aspect, snow depth, snow-free date, and vegetation cover class. The transect or grid where measurements were made was used as the random effect in the model. Fitted and residual model values were inspected visually and showed no violations of homoscedasticity or normality, and no transformations were applied to any variables. Significance for all tests was evaluated at alpha = 0.05 in R.

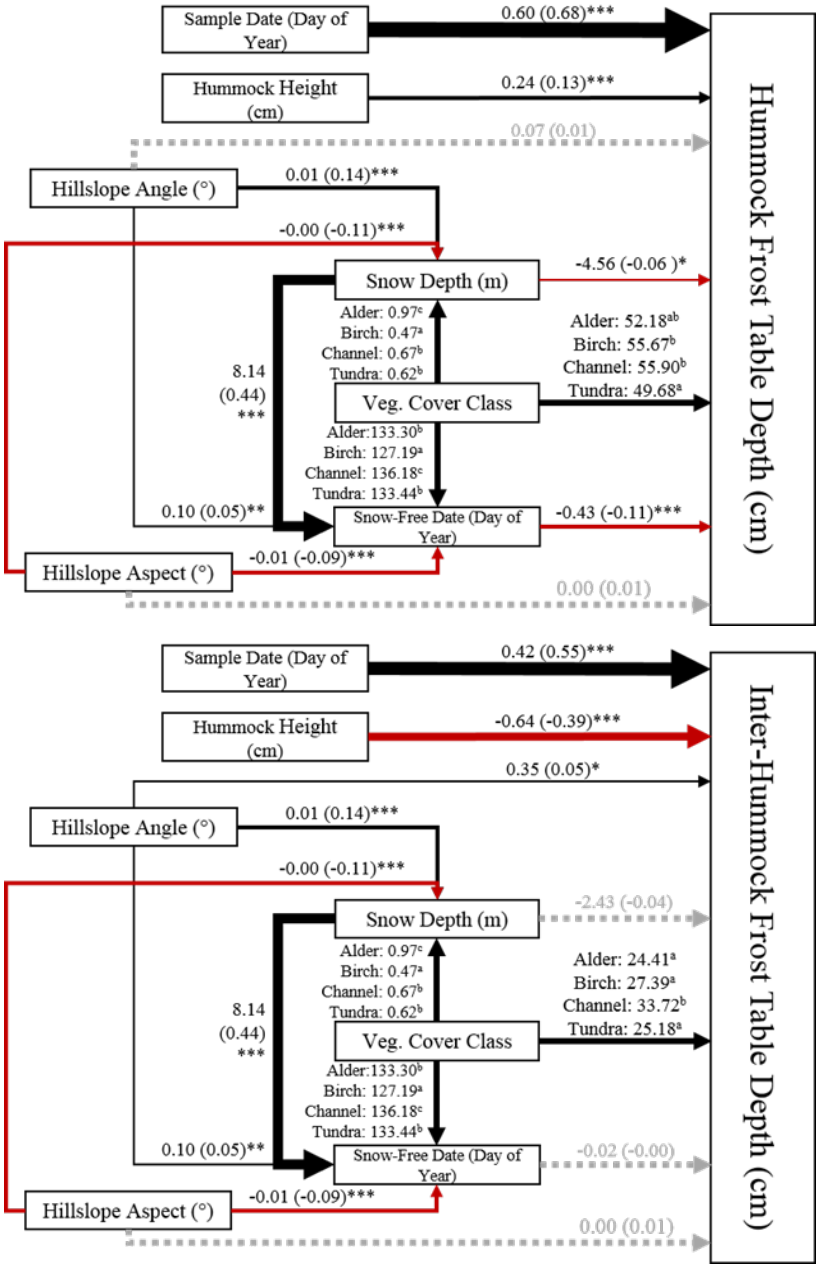

Figure 2.4 Results of the structural equation models for hummock and inter-hummock frost table depth. Paths are labeled with unstandardized path coefficients first, with standardized path coefficients in brackets, and stars which indicate the p-value of the relationship (* <0.05, ** <0.01, *** <0.001). Black arrows indicate positive relationships (i.e. deeper frost table depth), red arrows indicate negative relationships (i.e. shallower frost table depth), and dotted grey lines indicate insignificant relationships (p-value >0.05), with the width of each line corresponding to the size of the standardized path coefficient. Letters beside the means of each category represent significant difference between each category. Both models have a Fisher's C value of 4.944 with a p-value of 0.551 on 6 degrees of freedom.

2.5 Results

Our results show that hummock and inter-hummock zone frost table depths are influenced by different micro-scale variables. Overall, the strongest influence on hummock frost table depth after sampling date was hummock height (Figure 2.4, standardized path coefficient = 0.13), and snow-free date (standardized path coefficient = -0.11). In turn, snow-free date was largely influenced by snow depth (standardized path coefficient = 0.44) and vegetation cover (Figure 2.4). Snow depth had the smallest direct effect of any variable on hummock frost table depth (standardized path coefficient = -0.06), despite its ability to delay the snow-free date by 8.14 days per metre of snow. At points where frost table depth was measured, birch areas became snow-free significantly earlier than other vegetation types (Figure 2.4, $p < 0.001$). On average, birch areas (group "a") became snow-free 6 days earlier than alder or tundra (group "b"), and 9 days earlier than channel shrub areas (group "c"). These earlier snow-free dates in birch areas corresponded with significantly deeper frost table depths compared to tundra areas. Alder areas had average snow depths 56% greater than tundra areas at points where frost table depth was measured, but the average snow-free date in alder was similar to that in tundra (Figure 2.4).

The pattern of snow-free dates across vegetation cover types at points where frost table depth was measured did not match the pattern of snow-free dates observed from watershed-wide measurements of snow depth and snow-free date from UAS-measured values. When controlling for hillslope aspect and snow depth using the UAS data, alder areas became snow-free latest, followed by channel, then tundra, and birch areas became snow-free earliest (Figure 2.5). Areas of deeper snow became snow-free later, and south-west hillslope aspects became snow-free earlier in each vegetation class. The average snow-free date of birch shrub areas was earlier than non-birch shrub areas regardless of the hillslope aspect or snow depth (Table 2.1).

In inter-hummock zones, only sample date, hummock height, hillslope angle, and channel vegetation had a significant effect on frost table depth. Hummock height had a much stronger,

negative influence (i.e. shallower frost table depth with greater hummock height) on inter-hummock frost table depth than on hummock frost table depth (unstandardized path coefficients = -0.64 and 0.24, respectively), and had an eight times larger effect on frost table depth than hillslope angle (standardized path coefficients = -0.39, $p < 0.001$ and 0.05, $p = 0.02$). The effect of hummock height on inter-hummock frost table depth was 70% as strong as sample date, while frost table depth measurements spanned two and a half months (standardized path coefficients = -0.39 and 0.55, respectively). Areas of channel vegetation had significantly deeper inter-hummock frost table depths, 6 – 9 cm deeper than alder, birch and tundra areas. Alder, birch and tundra areas did not significantly differ in average inter-hummock frost table depth. Plots of frost table depth across each micro-scale variable are shown in the appendix (Section 2.8.2).

2.6 Discussion

2.6.1 Effects of snow-shrub interactions on hummock frost table depth

Here we show that differences in hummock frost table depth across alder, birch and tundra vegetation types are partially explained by shrubs' influence on snow. Hummock height had the largest effect on hummock frost table depth after sample date, but snow-free date has a similarly strong influence on frost table depth based on the standardized path coefficients from the structural equation model (0.13 and -0.11 respectively). Snow-free date has been shown to control active layer thickness in large-scale modeling studies (Lawrence and Swenson, 2011; Bonfils et al., 2012; Wang et al., 2019), however, the direct effect of snow-free date on frost table depth has not been reported at the plot scale previously. Our results indicate that the effect of shrub shading is not a dominant control on frost table depth at the Siksik Creek watershed, as areas of birch and channel shrubs had significantly deeper hummock frost table depths than tundra areas, while alder and tundra frost table depths did not differ significantly.

In birch areas, deeper frost table depths were partially explained by advanced snowmelt

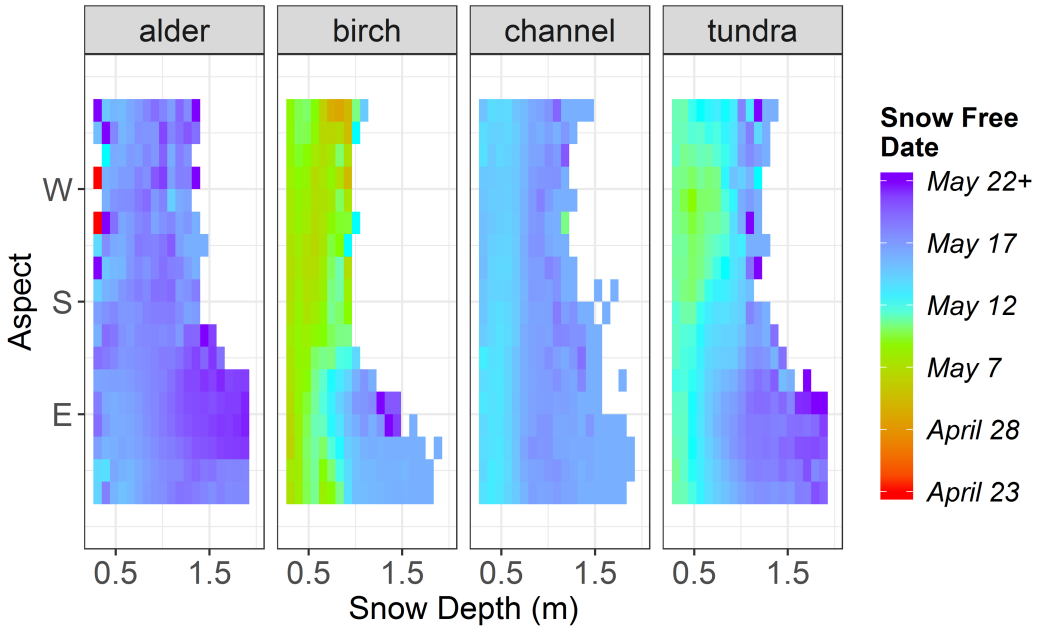

Figure 2.5 Mean snow-free date across snow depth and aspect from all unmanned aerial system measured points in the Siksik Creek watershed (n = 894 523). Each bin has a width of 10 cm snow depth and 18° of aspect, while colour represents the mean snow-free date for each bin.

timing caused by their protrusion through the snowpack (Figure 2.2). While birch shrub areas did have a significantly lower mean snow depth (which contributed to these points becoming snow-free earlier on average (Figure 2.4), birch areas became snow-free significantly earlier than other vegetation cover types regardless of snow depth or hillslope aspect in most cases (Table 2.1). At points where frost table depth was measured alder became snow free at the same time as tundra areas despite having 56% deeper snow. However, the 210 points where frost table depth was measured only represents 0.02% of all UAS snow observations. Utilizing all 894 523 UAS observations shows alder areas became snow free later across the watershed regardless of snow depth or hillslope aspect when compared to other vegetation cover classes (Figure 2.5). Historical snow surveys completed near-yearly in the Siksik Creek watershed from 1991 – 2016 show that tundra and birch shrub areas have similar mean snow densities (0.226 g $cm^{-3}$for birch, 0.222 g cm^{-3} for tundra), while alder areas have a mean snow density of 0.340 g cm^{-3}. Alders tend to grow on steeper slopes within a range of hillslope aspects where snowdrifts would form without alder shrub presence. Wind packed drifts

Table 2.1 The average number of days the snow-free date was advanced in birch shrub areas compared to non-birch shrub areas, as measured by the UAS flights made over the watershed during the snowmelt period (n = 894 523). Positive numbers represent the average number of days birch shrub areas became snow free before non-birch shrub areas. A Welch Two Sample t-test, which is robust against unequal variances and sample sizes, was applied to test for significant differences between alder and birch/tundra areas (italics = p <0.05, bold = p <0.001). The median number of observations in each bin was 9932.

Hillslope Aspect (°)								
315 - 360	6.1	**1.9**	**5**	*10.1*	*3*	1.2	0	—
270 - 315	**5.2**	**2.4**	**4.3**	**5.9**	—	—	—	—
225 - 270	**6**	**2.6**	**4.4**	**4**	—	—	—	—
180 - 225	7.9	**3.6**	**4.4**	**3.2**	—	—	—	—
135 - 180	**6.6**	**3.7**	**4.4**	**4.5**	—	—	—	—
90 - 135	8.4	**3.3**	**3.3**	**3**	**1.5**	-0.7	—	—
45 - 90	**9**	3.1	**3.4**	**3.8**	**2.8**	3.1	*4.4*	4.8
0 - 45	*6.7*	2.6	**4.1**	*4.8*	2.4	**2.4**	**1.8**	**1.8**
Snow Depth (cm)	<25	25-50	50-75	75-100	100-125	125-150	150-175	175-200

have denser snow than other areas and require more energy to melt. Therefore, while alder shrubs still increase energy input into the snow the same way birch shrubs do, denser snow in alder areas likely offset this effect and lead to later snow-free dates when compared to birch areas.

Despite growing in snow-drifting areas, snow depth in alder areas was greater than in birch and tundra areas at almost every given hillslope angle and aspect (Table 2.2). Snow depth was amplified the greatest in areas where alder tend to appear the most in the basin, at hillslope angles greater than 10° and aspects from 0 – 135°. Even though snow drifts would form naturally in these areas without the presence of alder shrubs, snow depth in alder areas was greater in these ranges by 0.26 – 1.35 m on average (Table 2.2).

Previous work which found that removing *Betula nana* shrubs could deepen the active layer (Blok et al., 2010; Nauta et al., 2015) was conducted in areas where shrub heights were shorter than the relatively shallow, homogenous (25 – 35 cm) snow pack. Shrubs likely did not protrude through the snow pack at this site, and may not have been able to initiate earlier snowmelt.

Table 2.2 Mean snow depth (cm) in alder areas minus mean snow depth in birch and tundra areas for given hillslope angles and aspects (n = 894 523). A Welch Two Sample t-test was applied to test for significant differences between alder and birch/tundra areas (italics = p <0.05, bold = p <0.001). Channel shrub areas are excluded as they are also tall and can therefore trap snow, while the purpose of this table is to show that alder shrub areas do increase snow depth. Alder shrubs increase snow depth the most at greater hillslope angles in the range of 0 – 135° hillslope aspect. The median number of observations in each bin was 18 466, and the only bin with a p-value >0.05 had just 28 observations.

Hillslope Aspect (°)					
315 - 360	**0.12**	**-0.28**	**-0.44**	—	—
270 - 315	**0.2**	**0.11**	—	—	—
225 - 270	**0.16**	**0.13**	—	—	—
180 - 225	**0.14**	**0.12**	—	—	—
135 - 180	**0.05**	**-0.12**	*-0.09*	—	—
90 - 135	**0.12**	**0.31**	**0.54**	**0.43**	—
45 - 90	**0.13**	**0.13**	**0.26**	**0.28**	—
0 - 45	**0.08**	**-0.10**	**0.57**	**1.02**	**1.35**
Hillslope Angle (°)	0 - 5	5 - 10	10 - 15	15 - 20	20 - 25

Lafleur and Humphreys (2018) found little difference in snow-free date across three sites of varying shrub height, where mean shrub height and snow depth were closely matched (18.2 – 51.5 cm shrub height, S1, S2, and G4 vegetation types per Walker et al. (2005), 29.4 cm – 57.1 cm snow depth). The similarity in snow-free date across different vegetation heights found by Lafleur and Humphreys (2018) may be caused by a combination of shallower snow depths and minimal shrub protrusion, as mean snow depth was greater than mean shrub height at each site in their study. The different pattern of results found by our study and others (Blok et al., 2010; Nauta et al., 2015) at shrub-tundra sites highlight the need to better understand interactions between shrub height, snow depth, shrub protrusion, and how they influence snow-free date. The opposing physical effects of shrubs on frost table depth can lead to either shallower or deeper frost table depths in different snow and shrub conditions (Figure 2.6). In areas where shrub protrusion does not occur and snow depth is homogenous (Blok et al., 2010), shrubs decreased frost table depth through shrub shading. When shrub protrusion does not occur and snow depth is variable (Nauta et al., 2015), deeper frost table depths occurred in areas of deeper snow. Frost table depth changes in these studies

may also be influenced by changes in transpiration and interception caused by the removal of the shrub canopy, which could alter soil moisture. The larger ranges of snow depth and shrub height in our study found that short protruding shrubs increase frost table depth by advancing snowmelt timing. Therefore, we suggest that with projected increases in shrub height, density, and areal extent (Loranty and Goetz, 2012; Bjorkman et al., 2018) and decreases in snowfall (Bintanja and Andry, 2017), shrub protrusion will increase across the Arctic, leading to earlier snow-free dates that contribute to deeper active layer depths through thawing at the top of the permafrost.

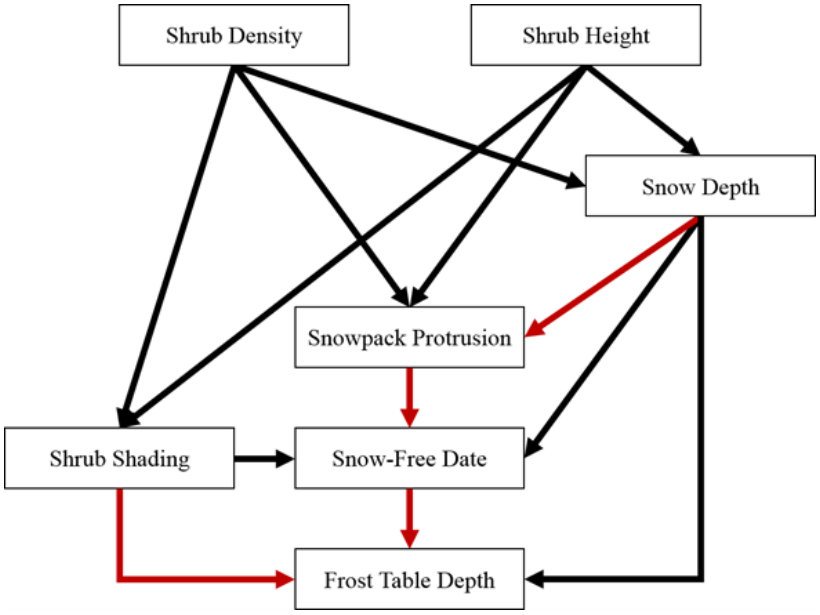

Figure 2.6 Conceptual model of the main short-term physical influences of shrubs on frost table depth. Black arrows represent positive relationships (i.e. larger snow depth → larger frost table depth) and red arrows represent negative relationships (i.e. earlier snow-free date → larger frost table depth).

2.6.2 Influences on inter-hummock frost table depth, and unmeasured micro-scale variables

Inter-hummock frost table depth was dominantly controlled by hummock height, an indicator of overall hummock development. Previous research in this region has also shown inter-hummock frost table depth is closely tied to hummock height, and that hummock height is an overall indication of

Table 2.3 Hummock height differences across different vegetation covers. Difference between classes were tested using the Scheffé multiple comparison test (alpha = 0.05), which is suited for datasets with different numbers of observations (Scheffé, 1953). Only channel vegetation areas had significantly different hummock heights. Superscript indicates classes that were significantly different from one another.

Vegetation Cover Class	Mean Hummock Height (cm)
Alder	24.8[a]
Birch	25.8[a]
Channel	2.0[b]
Tundra	23.6[a]

hummock development (Kokelj et al., 2007). Previous work, however, did not consider the influence of snow or vegetation. Our inclusion of snow and vegetation showed they do not have an impact on inter-hummock frost table depth. Deeper inter-hummock frost table depths in channel shrub areas were likely caused by a lack of hummock development as indicated by significantly lower hummock heights (Table 2.3). Hummock development was likely impeded by the fully saturated soils in channel shrub areas, and not impeded through any mechanism caused by the presence of shrubs themselves. Deeper inter-hummock frost table depths were found in flatter areas (Figure 2.4), which could be due to poorer drainage and more saturated soils that conduct heat more effectively. Future increases in active layer thickness will likely trigger hummock degradation, which would amplify active layer increases in the inter-hummock zone as mineral soils from hummocks invade inter-hummock zones (Kokelj et al., 2007). As inter-hummocks transition to mineral soils, variables which influence hummock frost table depth may become influential on inter-hummock frost-table depth. While hummocks are observed widely across the Arctic (Schunke and Zoltai, 1988), their presence or absence at finer scales is unknown, making it difficult to predict the impact their degradation will have.

In this analysis we did not measure soil properties (e.g. organic layer thickness, soil moisture, moss cover), which can potentially influence frost table depth and correlate with measured variables, namely vegetation cover class. However, at a qualitative level, we expect these unmeasured properties in shrub-covered areas likely decrease overall heat flux into the ground compared to tundra

areas, and would not be confounded with areas which became snow-free earlier. As described in the study site section, birch shrub-covered areas typically experience increased transpiration (Bring et al., 2016), intercept up to 30% of rainfall (Zwieback et al., 2019a), and experience cooler soil temperatures as a result of shading (Myers-Smith and Hik, 2013). This set of properties results in relatively lower soil moisture, which lowers the heat conductivity of the active layer and overall heat flux into the ground, compared to tundra areas. There were also no significant differences in hummock height which may explain differences between alder, tundra, and birch shrub hummock frost table depths (Table 2.3).

2.7 Conclusion

Extensive field measurements of frost table depth were taken over a three-month period across various shrub cover types (alder, birch, channel shrub, and shrub-free tundra dominated areas) in a catchment containing mineral earth hummocks. Unmanned aerial system mapping allowed us to measure snow depth and snow-free date across the 1 km^2 watershed. Our results quantify interactions between snow depth, shrub type, and snow-free date and their influence on frost table depth. Structural equation modeling showed that frost table depth in mineral hummocks and organic inter-hummock zones are controlled by different micro-scale variables. Hummock areas covered by low birch shrub vegetation had deeper frost table depths than tundra areas, likely due to the advancement of snowmelt timing caused by shrubs protruding through the snowpack (Figure 2.5, Table 2.1). However, across the watershed, tall alder shrub areas were able to trap more snow than birch and tundra areas (Table 2.2), creating a deeper snowpack which delayed snow-free timing. This effect is counter-acted by the ability of alder shrubs to amplify snowmelt once the snow has melted enough to where they protrude through the snowpack. As a result, alder hummock areas did not have significantly different frost table depths when compared to tundra areas, despite the two areas experiencing different snow depth conditions. Inter-hummock areas were not affected by

snow or vegetation and are dominantly controlled by hummock height, an indicator of hummock development. Importantly, our results show that low (birch) shrubs increased frost table depth compared to tundra areas at this study site, contradicting previous research which found that shrubs may preserve permafrost by shading the ground. Given projected increases in shrub height, density and areal extent, and decreasing snowfall, shrub protrusion through the snowpack would become more common, and could lead to increases in active layer thickness where shrubs did not protrude before. Further research is required to fully understand how the counteracting forces of shrubs on frost table depth (Figure 2.6) will change and affect permafrost into the future at a circum-Arctic scale.

2.8 Chapter 2 Appendix

2.8.1 Justification of structural equation model

Structural Equation Model paths are specified based on known causal effects between variables included in the model. Here we provide the justification for each of the paths specified in the SEMs used in this article.

Measurement date on frost table depth: Throughout the year, the active layer thaws and increases frost table depth.

Hummock height on frost table depth: Previous work (Kokelj et al., 2007) showed hummock height is a strong indicator of overall hummock development and influences both hummock and inter-hummock frost table depth.

Hillslope angle on frost table depth: We expected flat areas may have deeper frost table depths due to more saturated soils caused by poorer drainage, as saturated soils have greater heat conductivity (Hinzman et al., 1991).

Hillslope angle on snow depth: In shrub tundra environments, snow is redistributed by wind and deposited on steeper slopes where snow drifts form, and eroded from flatter areas.

Hillslope angle on snow-free date: Hillslope angle is a control on incoming solar radiation, which affects the rate of snowmelt.

Hillslope aspect on frost table depth: South-facing hillslopes receive larger amounts of incoming solar radiation, which could increase frost table depth.

Hillslope aspect on snow depth: Predominant winter wind directions in the Arctic mean that larger drifts form on leeward slopes, while windward slopes have snow eroded from them.

Hillslope aspect on snow-free date: South-facing hillslopes receive larger amounts of incoming solar radiation, which could cause earlier snow-free dates by advancing snow melt.

Snow depth on frost table depth: Areas of deeper snow are able to insulate the ground from

cooler winter air temperatures, potentially keeping the ground warmer and leading to deeper frost table depths in summer (Sturm et al., 2001).

Snow depth on snow-free date: Areas of deeper snow require more energy, and take longer to melt entirely.

Vegetation cover class on frost table depth: Vegetation can shade the ground, leading to shallower frost table depths, and also alter soil moisture regimes, changing the thermal conductivity of the soil (Blok et al., 2010; Bonfils et al., 2012).

Vegetation cover class on snow depth: Areas of taller shrub vegetation are able to trap blowing snow, and increase snow depth where their height is taller than the snow would be without their presence (Essery and Pomeroy, 2004; Marsh et al., 2010).

Vegetation cover class on snow free date: Some vegetation is able to protrude through the snow pack, lowering the albedo of the snow and increases the rate of snow melt (Endrizzi and Marsh, 2010).

Snow-free date on frost table depth: Areas which become snow-free earlier are exposed to warmer spring air temperatures and incoming solar radiation, allowing the active layer to begin warming at a greater rate than snow-covered areas.

2.8.2 Frost table depth of each micro-scale variable

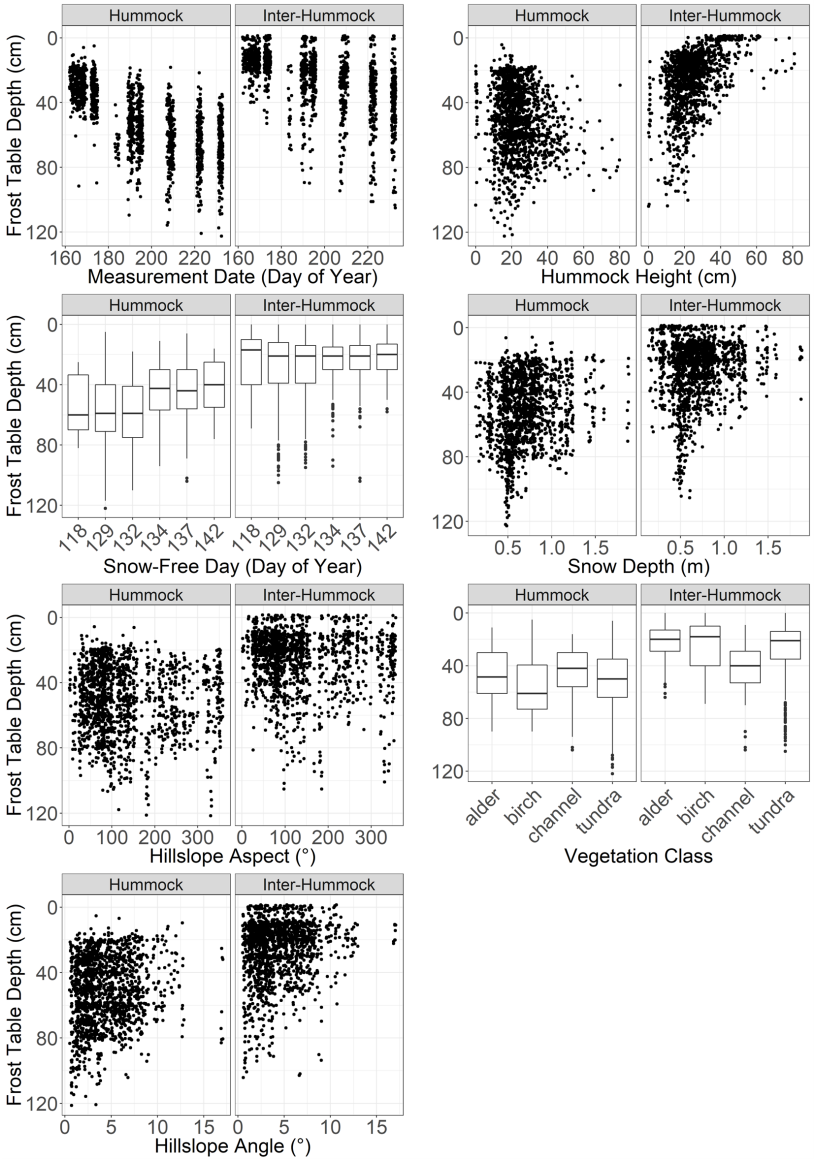

Figure 2.7 All measured frost table depth points for each micro-scale variable are shown. Points are placed randomly within a small range of the measured values so that points do not overlap.

Chapter 3

Assessing the influence of lake and watershed attributes on snowmelt bypass at thermokarst lakes

3.1 Abstract

Snow represents the largest potential source of water for thermokarst lakes, but the runoff generated by snowmelt (freshet) can flow beneath lake ice and via the outlet without mixing with and replacing pre-snowmelt lake water. Although this phenomenon, called "snowmelt bypass", is common in ice-covered lakes, it is unknown which lake and watershed properties cause variation in snowmelt bypass among lakes. Understanding the variability of snowmelt bypass is important because the amount of freshet that is mixed into a lake affects the hydrological and biogeochemical properties of the lake. To explore lake and watershed attributes that influence snowmelt bypass, we sampled 17 open-drainage thermokarst lakes for isotope analysis before and after snowmelt. Isotope data were used to estimate the amount of lake water replaced by freshet and to observe how the water sources of lakes changed in response to the freshet. Among the lakes, a median of 25.2% of lake

water was replaced by freshet, with values ranging widely from 5.2 to 52.8%. For every metre that lake depth increased, the portion of lake water replaced by freshet decreased by an average of 13%, regardless of the size of the lake's watershed. The thickness of the freshet layer was not proportional to maximum lake depth, so that a relatively larger portion of pre-snowmelt lake water remained isolated in deeper lakes. We expect that a similar relationship between increasing lake depth and greater snowmelt bypass could be present at all ice-covered open-drainage lakes that are partially mixed during the freshet. The water source of freshet that was mixed into lakes was not exclusively snowmelt, but a combination of snowmelt mixed with rain-sourced water that was released as the soil thawed after snowmelt. As climate warming increases rainfall and shrubification causes earlier snowmelt timing relative to lake ice melt, snowmelt bypass may become more prevalent with the water remaining in thermokarst lakes post-freshet becoming increasingly rainfall sourced. However, if climate change causes lake levels to fall below the outlet level (i.e., lakes become closed-drainage), more freshet may be retained by thermokarst lakes as snowmelt bypass will not be able to occur until lakes reach their outlet level.

3.2 Introduction

In the continuous permafrost zone of the Arctic, regions with thermokarst lakes have formed where ice-rich permafrost has thawed and the ground surface has subsided. Thermokarst lakes typically range from 1 to 5 m in depth and from 0.01 to 1000 ha in area, can cover over 25% of the land area (Grosse et al., 2008; Burn and Kokelj, 2009; Turner et al., 2014; Farquharson et al., 2016) and mostly formed during a brief warm period following the last deglaciation of the Northern Hemisphere (Brosius et al., 2021). Comparison of aerial photography from the mid-1900s with more recent satellite imagery has revealed both increases and decreases in thermokarst lake area and number (Smith et al., 2005; Plug et al., 2008; Marsh et al., 2009; Jones et al., 2011; Finger Higgens et al., 2019). These changes are partially attributed to shifting thermokarst lake water

balances: increased air temperatures (Woo et al., 2008), longer ice-free seasons (Surdu et al., 2014; Arp et al., 2015), permafrost thaw (Walvoord and Kurylyk, 2016), and shrub expansion leading to increased transpiration (Myers-Smith et al., 2011) and interception (Zwieback et al., 2019a), all causing less inflow and more water to evaporate from thermokarst lakes. In contrast, increasing precipitation can lead to more inflow to lakes, offsetting any rise in evaporation, interception and transpiration (Walsh et al., 2011; Stuefer et al., 2017; Box et al., 2019; MacDonald et al., 2021), while shrub expansion can also increase snow accumulation in lake watersheds resulting in more snowmelt runoff to lakes (Turner et al., 2014; MacDonald et al., 2017). Increased rainfall has also been linked to decreases in lake surface area because lakes are more likely to experience rapid drainage due to permafrost thaw during wet years (Webb et al., 2022).

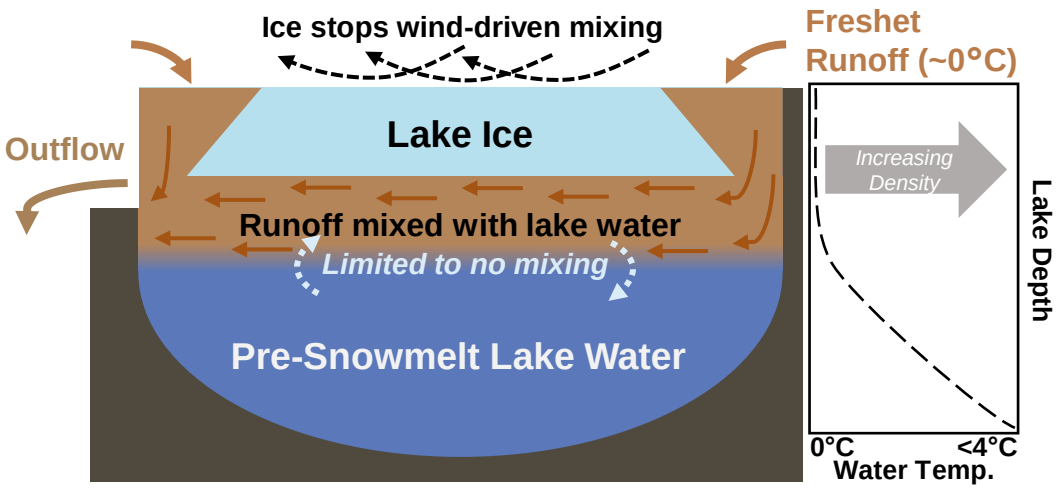

Figure 3.1 A conceptual cross section of a open-drainage lake when freshet has begun. Freshet initially flows into the lake at the edge where lake ice has melted. A layer of snowmelt runoff mixed with lake water then remains buoyant on top of the warmer lake water before flowing through the outlet (i.e., 'snowmelt bypass'). Limited mixing occurs due to density differences between runoff and deeper lake water and the lack of wind-driven mixing due to the presence of lake ice.

Runoff generated by snowmelt in lake watersheds represents a large potential water source for lakes, as snowfall comprises 40 to 80% of total precipitation in the Arctic (Bintanja and Andry, 2017). When snow melts in spring, the volume of snowmelt-driven runoff flowing into lakes (freshet) generally results in the highest lake levels of the year (Woo, 1980; Roulet and Woo, 1988;

Hardy, 1996; Pohl et al., 2009). When freshet is low, thermokarst lakes are prone to desiccation (Marsh and Bigras, 1988; Marsh and Lesack, 1996; Bouchard et al., 2013). It is a reasonable expectation that lakes which receive more freshet will also contain more freshet by the end of the snowmelt if they remain below their outlet level (i.e., closed-drainage lakes). However, for non-bedfast ice-covered lakes at or near their outlet level (i.e., open-drainage lakes), freshet may flow into and out of a lake without mixing with and replacing the pre-freshet lake water, resulting in "snowmelt bypass" (Bergmann and Welch, 1985) (Figure 3.1). While lake ice inhibits wind-driven mixing of lake water, the cooler, less dense freshet (~0 °C) cannot mix with the deeper, warmer and denser lake waters (<4 °C). As a result, freshet water will flow into and out of an open-drainage lake without replacing the deeper, pre-snowmelt lake water until vertical mixing within the lake begins, which is initiated by the warming of lake waters from solar radiation penetrating through snow-free ice and wind-driven mixing after the lake becomes ice-free (Cortés and MacIntyre, 2020). Snowmelt bypass is a common occurrence that has been observed in a wide variety of ice-covered open-drainage lakes around the world (Henriksen and Wright, 1977; Jeffries et al., 1979; Hendrey et al., 1980; Bergmann and Welch, 1985; Schiff and English, 1988; Edwards and McAndrews, 1989; Cortés et al., 2017).

Although previous studies have established the mechanisms and conditions that cause snowmelt bypass, no studies have examined how lake and watershed characteristics affect snowmelt bypass. Given that snowmelt bypass depends on the mixing conditions under lake ice, we hypothesize that lake and watershed characteristics that impact lake mixing may cause variability in snowmelt bypass among lakes in a given region. Understanding the factors that influence the amount of freshet retained by thermokarst lakes is important because of subsequent influence on lake water balance, pH, nutrient composition, and suspended sediment, among other limnological variables (Henriksen and Wright, 1977; Marsh and Pomeroy, 1999; Finlay et al., 2006; Turner et al., 2014; Balasubramaniam et al., 2015).

In this study, we determine factors influencing the magnitude of snowmelt bypass for 17

open-drainage thermokarst lakes in the lake-rich tundra uplands east of the Mackenzie Delta in the Northwest Territories, Canada, during the freshet of 2018. This area contains thousands of thermokarst lakes that constitute up to 25% of the landscape surface area and have changed in area and number during the past several decades in response to changing precipitation and permafrost thaw (Plug et al., 2008; Marsh et al., 2009). We used lake water isotope compositions from before and after snowmelt to estimate the proportion of lake water replaced by freshet during spring 2018 and evaluated relationships with lake and watershed characteristics. We selected lake and watershed characteristics that had the potential to impact under-ice mixing through their influence on the water temperature profile (e.g. lake depth) or by displacing pre-snowmelt lake water (e.g. watershed area). Isotope tracers were also used to assess whether the freshet is sourced solely from snowmelt, or whether other water sources contributed to freshet. Future assessments of hydrological and biogeochemical properties of thermokarst lakes can use the lake and watershed attributes we identify to affect snowmelt bypass and lake water sources to inform their results, given the distinct biogeochemical properties of freshet runoff (Finlay et al., 2006; Balasubramaniam et al., 2015) and the influence of snowmelt bypass on the amount of freshet runoff retained by lakes.

3.3 Study area

The 17 study lakes are situated in the taiga–tundra uplands east of the Mackenzie Delta, in the northwestern region of the Northwest Territories, Canada (Figure 3.2). The landscape is comprised of rolling hills and is strongly influenced by permafrost thaw, as evidenced by the thousands of thermokarst lakes which formed between 13 000 and 8000 years ago (Rampton, 1988; Burn and Kokelj, 2009) that are typically 2 – 4 m in depth with a surface area from 10 to 1000 ha (Pienitz et al., 1997). The study lakes are situated along a ~70 km stretch of the Inuvik-Tuktoyaktuk Highway north of the town of Inuvik (Figure 3.2). The average area of the lakes is 14.2 ha (0.9 – 90.5 ha) and the average maximum depth is 2.2 m (1.0 – 4.1 m) (Table 3.1). All lakes have a defined

outlet channel observed to be active during the spring melt, thus classifying them hydrologically as open-drainage, and many lakes have defined channelized inflows from their watersheds in the form of small streams or ice-wedge polygon troughs.

Soils in the region have evolved from fine-grained morainal tills, ice-contact sediment, and lacustrine deposits (Rampton and Wecke, 1987). Subsurface flow is conveyed efficiently by a network of interconnected peat channels 0.3 – 1.0 m wide that lay between mineral earth hummocks (Quinton and Marsh, 1998). Lake watersheds contain tall–shrub (>1 m), low-shrub (~0.5 m), and shrub-free land cover types comprising lichen, moss, and tussocks (Lantz et al., 2010; Grünberg et al., 2020). Mean annual air temperature in Inuvik is -8.2°C and mean annual precipitation is 241 mm of which 66% is snow, based on 1981-2010 climate normals (Environment and Climate Change Canada, 2019b). Snowmelt usually begins in mid-May, and lakes typically become ice-free in June and freeze up in mid-October (Burn and Kokelj, 2009).

The 2018 snowmelt season was typical in comparison to recent decades. End-of-winter snow surveys conducted in the 58 km^2 watershed of Trail Valley Creek in 2018 (Figure 3.2) recorded an average snow water equivalent (SWE) of 141 mm, close to the average SWE of 147±35 mm based on surveys from 1991 to 2019 (Marsh et al., 2019). At Trail Valley Creek, snowmelt began about May 1, with snow-free areas beginning to appear by May 8, while only the remnants of large snow drifts remained by June 3. Lake ice near Trail Valley Creek became snow-free by May 10, and lakes became completely ice-free on June 14. The mean air temperature at Trail Valley Creek during the sampling period from April 26 to June 15, 2018 was 0.4 °C, which was cooler than the average of 1.7 °C during 1999-2019 (Figure 3.3). Air temperatures roughly followed the average minimum and maximum daily air temperatures, with some temporal variability which can be expected for any given year. Maximum daily air temperatures were mostly above 0 °C after May 8, which was similar to the average timing of the first above-0 °C day during 1999-2019 (Figure 3.3).

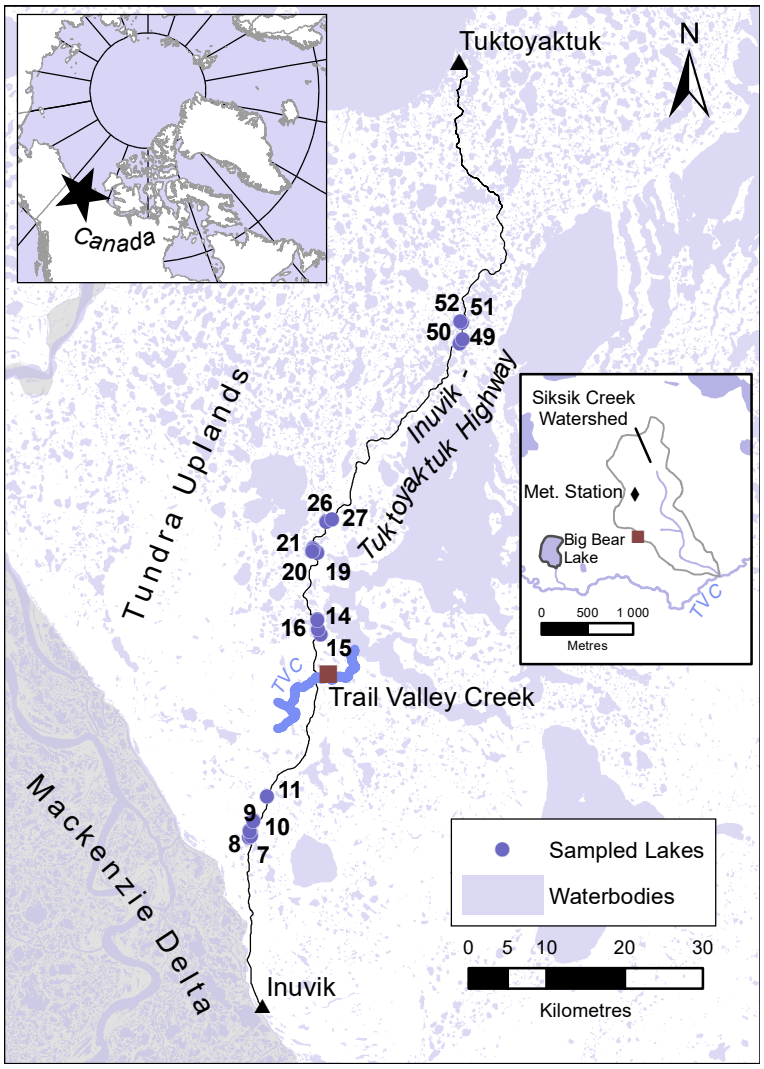

Figure 3.2 Blue circles indicate lakes that were sampled before and after snowmelt in 2018. Tundra uplands are in white while the Mackenzie Delta is in grey. In the inset, key locations near the Trail Valley Creek field station are shown.

Table 3.1 Lake and watershed properties for sampled lakes. Lake locations are shown on Figure 3.2.

Lake	Longitude	Latitude	Lake Elevation (m asl)	Lake Depth (m)	Ice Thickness (m)	Snow Depth (cm)	Lake Area (ha)	Watershed Area (ha)	Watershed Area/Lake Area
7	-133.7614	68.5575	89	2.24	0.81	22	2.81	6.45	2.62
8	-133.7557	68.5588	89	2.30	0.79	15	1.88	15.67	7.55
9	-133.7603	68.5645	86	1.02	0.84	30	59.56	203.56	3.42
10	-133.7465	68.5760	88	1.65	0.85	54	90.48	168.58	1.86
11	-133.7033	68.6039	83	1.91	0.97	11	0.92	21.76	17.32
14	-133.5209	68.7888	52	1.42	0.84	4	10.68	60.64	5.7
15	-133.5289	68.7945	57	1.57	1.14	19	5.66	29.83	4.99
16	-133.5320	68.8055	52	3.18	1.32	7	1.15	19.75	16.02
19	-133.5262	68.8818	39	2.46	1.24	11	5.68	38.98	7.09
20	-133.5430	68.8847	37	2.69	1.27	10	2.30	19.93	9.18
21	-133.5400	68.8872	36	1.78	1.19	11	2.61	10.91	3.96
26	-133.4956	68.9181	38	1.47	1.19	6	4.84	17.89	3.83
27	-133.4771	68.9210	45	3.10	1.22	10	1.13	8.57	6.7
49	-133.0528	69.1188	9	2.18	0.91	23	17.50	46.23	2.54
50	-133.0420	69.1233	8	1.65	0.86	19	8.16	31.92	3.67
51	-133.0414	69.1422	4	2.31	0.84	24	2.24	12.01	5.26
52	-133.0473	69.1439	6	4.14	0.86	18	23.52	49.92	2.05
Min	-133.7615	68.5575	4	1.02	0.79	4	0.92	6.45	1.86
Mean	-133.4748	68.8394	48	2.18	1.01	17	14.18	44.86	6.10
Max	-133.0414	69.1439	89	4.14	1.32	54	90.48	203.56	17.32

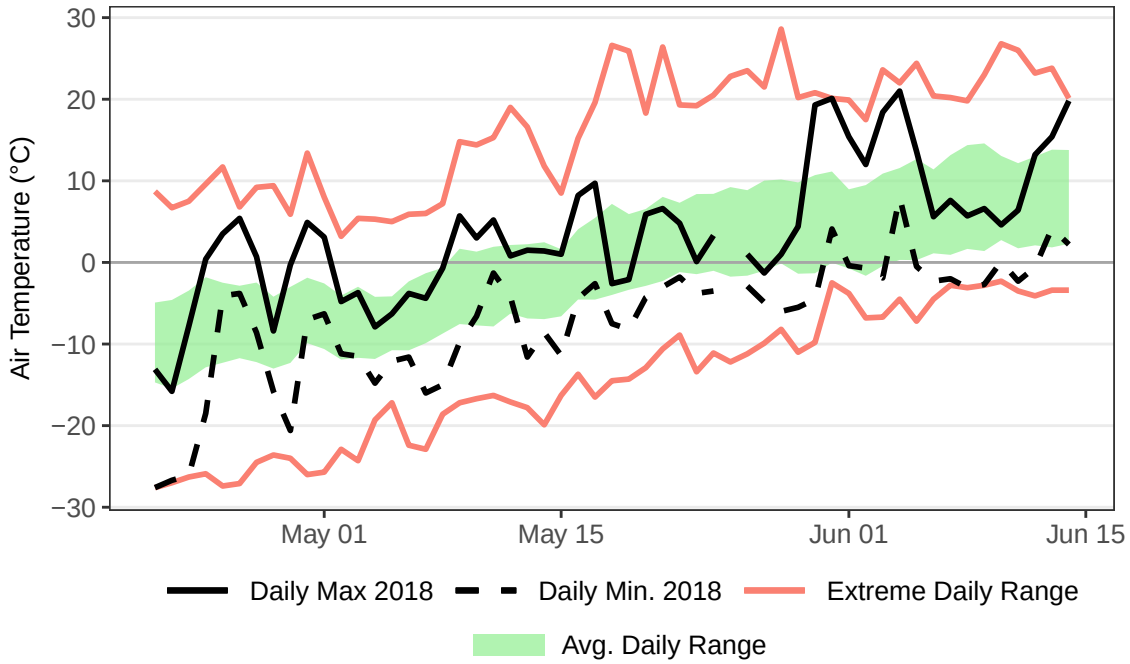

Figure 3.3 Maximum and minimum daily air temperature in comparison to the average and extreme values at the Trail Valley Creek field station for the period of 1999-2019.

3.4 Methods

3.4.1 Lake water and precipitation sampling for isotope analysis

Lake water samples for stable isotope analysis were first collected from the 17 study lakes while they were ice-covered (April 26 – May 1, 2018) and again soon after the lakes became ice-free (June 15, 2018). Pre-snowmelt water samples were obtained from a hole augured through the ice near the centre of each lake. These water samples were taken 10 cm below the water surface in the augured hole. Lake depth, snow depth on the ice, and ice thickness were recorded at the same time water samples were collected. Snow depth was typically very uniform across the lake ice. Water samples were then collected post-snowmelt at the shore of each lake shortly after the lakes became fully ice-free. Isotope data were then used to estimate the portion of lake water that was replaced by freshet between the two sampling dates.

To estimate the local meteoric water line (LMWL) and the average isotope composition of

precipitation (δ_P) in the study region, which are useful references for the interpretation of lake water isotope compositions, samples of end-of-winter snow on the ground in April 2018 and rainfall for the period May to September 2018 were obtained. Snow samples (n = 11) were collected from the study area by taking a vertical core of snow using a tube, completely melting the snow in a sealed plastic bag, and then filling a sample bottle with the meltwater. Rainfall (n = 13) was collected between May and September in Inuvik using a clean high-density polyethylene container, which was then transferred to a sample bottle shortly after the rain had stopped. The midpoint between the average isotope composition of snow samples and rain samples was used to define δ_P. All samples were collected in 30 mL high-density polyethylene bottles and were measured using an isotope analyzer to determine the ratio of $^{18}O/^{16}O$ and $^{2}H/^{1}H$ in each sample. Isotope concentrations were measured using a Los Gatos Research (LGR) Liquid Water Isotope Analyser, model T-LWIA-45-EP at the Environmental Isotope Laboratory at the University of Waterloo. The instrument was calibrated using Vienna Mean Standard Ocean Water (VSMOW) and Vienna Standard Light Antarctic Precipitation (VSLAP) standards provided by LGR. Calibration of the instrument was checked during the analysis using the VSMOW and VSLAP standards. Isotope compositions are expressed in standard δ notation, such that

$$\delta_{sample} = \frac{R_{sample}}{R_{VSMOW}} - 1 \tag{3.1}$$

where R represents the ratio of $^{18}O/^{16}O$ or $^{2}H/^{1}H$. Every fifth sample was analyzed a second time to determine the analytical uncertainties, which were ±0.1‰ for $\delta^{18}O$ and ±0.6‰ for $\delta^{2}H$, calculated as 2 standard deviations away from the difference between the duplicate samples. All isotope data from lakes are presented in Table 3.2.

Table 3.2 Snow and ice thickness, isotope, δ_I, and lake water replacement (%LWR) values for all lakes. Ice-Corrected δ_L values were used to calculate Ice-Corrected δ_I values following Yi et al. (2008).

			Pre-Snowmelt Lake Water (01-05-2018)						Post-Snowmelt Lake Water (15-06-2018)				
Lake	Ice Thickness (m)	Snow Depth (cm)	$\delta^{18}O$	$\delta^{2}H$	$\delta^{18}O$ Ice-Corr.	$\delta^{2}H$ Ice-Corr.	$\delta^{18}O_I$ Ice-Corr.	$\delta^{2}H_I$ Ice-Corr.	$\delta^{18}O$	$\delta^{2}H$	$\delta^{18}O_I$	$\delta^{2}H_I$	%LWR
7	0.81	22	-15.41	-131.05	-14.07	-123.16	-22.84	-171.44	-15.48	-129.67	-21.11	-159.22	19.1
8	0.79	15	-15.94	-134.71	-14.7	-127.42	-24.68	-184.42	-16.71	-137.71	-22.9	-171.81	23.9
9	0.84	30	-17.17	-140.98	-12.02	-110.51	-17.94	-136.81	-15.45	-128.25	-19.78	-149.79	44.7
10	0.85	54	-15.68	-132.02	-13.54	-119.35	-20.84	-157.31	-14.86	-125.77	-20.29	-153.37	19.3
11	0.97	11	-20.56	-156.48	-18.48	-144.48	-20.47	-154.65	-19	-147.33	-20.59	-155.52	25.2
14	0.84	4	-19.85	-154.24	-17.23	-139.05	-21.3	-160.52	-18.66	-146.31	-21.09	-159.04	36.7
15	1.14	19	-18.17	-144.83	-14.35	-122.41	-19.35	-146.76	-16.03	-132.27	-20.82	-157.11	27.2
16	1.32	7	-20.57	-155.32	-18.99	-146.18	-19.96	-151.05	-19.05	-146.66	-20.05	-151.69	7.2
19	1.24	11	-18.92	-149.63	-16.85	-137.58	-21.86	-164.46	-18.26	-144.16	-21.05	-158.75	32.4
20	1.27	10	-19.32	-149.44	-17.44	-138.52	-20.02	-151.49	-17.86	-140.53	-19.96	-151.07	16.3
21	1.19	11	-19.61	-154.6	-16.33	-135.57	-22.83	-171.31	-17.72	-141.63	-21.29	-160.47	26.2
26	1.19	6	-17.5	-141.72	-12.59	-112.7	-17.47	-133.48	-16.15	-131.84	-19.87	-150.41	49.9
27	1.22	10	-17.95	-144.85	-16.48	-136.26	-22.68	-170.25	-17.79	-142.41	-21.65	-162.98	24.2
49	0.91	23	-14.72	-124.46	-13.12	-114.91	-17.44	-133.22	-14.75	-123.4	-18.51	-140.81	31.6
50	0.86	19	-14.99	-127.6	-12.8	-114.59	-18.86	-143.31	-15.43	-125.22	-17.7	-135.07	52.8
51	0.84	24	-16.28	-133.15	-14.95	-125.31	-19.33	-146.63	-15.8	-129.92	-19.72	-149.36	18.5
52	0.86	18	-13.98	-120.75	-13.29	-116.63	-18.51	-140.79	-13.59	-117.58	-18.03	-137.45	5.5
Min	0.79	4	-20.57	-156.48	-18.99	-146.18	-24.68	-184.42	-19.05	-147.33	-22.9	-171.81	5.2
Mean	1.01	17	-17.45	-140.93	-15.13	-127.33	-20.38	-154.00	-16.62	-134.74	-20.26	-153.17	27.1
Max	1.32	54	-13.98	-120.75	-12.02	-110.51	-17.44	-133.22	-13.59	-117.58	-17.7	-135.07	52.8

3.4.2 Estimating the replacement of lake water by freshet and lake source waters

The percentage of a lake's volume that has been replaced by a given water source can be estimated as follows:

$$\%\ lake\ water\ replaced = \frac{\delta_{L-Post} - \delta_{L-Pre}}{\delta_{I-Post} - \delta_{L-Pre}} * 100 \tag{3.2}$$

where $\delta_{\text{L-Pre}}$ is the lake water isotope composition before snowmelt begins, $\delta_{\text{L-Post}}$ is the lake water isotope composition after snowmelt is complete, and $\delta_{\text{I-Post}}$ is the isotope composition of the source water post-snowmelt. Application of this equation assumes minimal to no change in volume, which is reasonable given the lakes we sampled are all open-drainage. We also assume that lakes are well mixed as they become ice-free when $\delta_{\text{L-Post}}$ water samples were collected. Water temperature measurements at Big Bear Lake (Figure 3.2), previous water temperature profiles made at lakes within 10 km of the Inuvik-Tuktoyaktuk Highway, and lake temperature modelling using FLake-online (Kirillin et al., 2011) all suggest that lakes were well mixed at the time of $\delta_{\text{L-Post}}$ sampling on 2018-06-15 (Appendix 3.8.1).

We calculated δ_{I} following the coupled isotope tracer approach outlined by Yi et al. (2008), using an isotope framework based on 2017 air temperature and humidity data for the typical ice-free period (June 15 – October 15) collected at the Trail Valley Creek meteorological station located 45 km NNE of Inuvik (Figure 3.2). Data from 2017 were used because it was the most recent period when lakes were exposed to meteorological conditions for an entire open-water season. The coupled isotope tracer approach assumes all lakes under the same meteorological conditions will evolve towards the same isotope composition (δ^*, the isotope composition of a lake at the moment of desiccation) as lakes evaporate along lake-specific evaporation lines. These lake-specific evaporation lines are defined by extrapolating from δ^* through δ_{L} until intersection with the local meteoric water line, which is used to estimate δ_{I} (Figure 3.4). We calculated δ_{I} for pre-snowmelt and post-snowmelt lake water isotope compositions to identify whether the isotope

composition of the source water changed after freshet. The percentage of lake water replaced was calculated using both $\delta^{18}O$ and $\delta^{2}H$ using Equation 3.2 and average values are reported. The difference obtained using the two isotopes in the estimate of the percentage of lake volume replaced by runoff was minimal, averaging 1.8% and ranging from 0.6 to 3.7%.

A sensitivity analysis was performed to evaluate uncertainty in the δ_I values and subsequent percentage lake water replaced by runoff. Confidence in the interpretation of δ_I values with respect to rainfall- or snowmelt-sourced waters depends on an accurate estimate of δ_P, which was determined using the average δ_{Rain} and δ_{Snow} values. Also, the calculation of percentage lake water replaced by runoff is sensitive to changes in δ_I, which is sensitive to the average δ_{Rain} value because this parameter is used to determine δ_{As} (Equation 3.10), which is subsequently used to determine δ^* (Equation 3.6). Since there was some variability in the δ_{Rain} and δ_{Snow} values from samples we collected, we tested the sensitivity of our estimates of δ_I and the percentage of lake water replaced by runoff to variation in average δ_{Rain} and δ_{Snow} values. We calculated the probable upper-bound and lower-bound limits of δ_{Rain} and δ_{Snow} values by adding and subtracting the standard error from the average of δ_{Rain} and δ_{Snow} values (Appendix 3.8.2). Upper- and lower-bound cases were propagated through the isotope framework to calculate upper- and lower-bound δ_I and percentage lake water replacement values to evaluate whether the standard error caused enough deviation to meaningfully change the results. Overall, differences between upper- and lower-bound δ_I and percentage lake water replacement values were minimal (Table 3.6, Figure 3.9). Details of the equations and variables used in the isotope framework and the sensitivity analysis are given in Appendix 3.8.2.

As ice forms and preferentially incorporates water containing the heavy isotopes ^{18}O or ^{2}H, the lake water beneath the ice becomes increasingly depleted in ^{18}O and ^{2}H. Consequently, the water samples we collected pre-snowmelt were systematically isotopically depleted relative to pre-freeze-up lake water, and the magnitude of depletion depends on the fraction of lake water that had frozen into ice. We corrected $\delta_{L\text{-}Pre}$ for the fractionation of freezing water into ice using

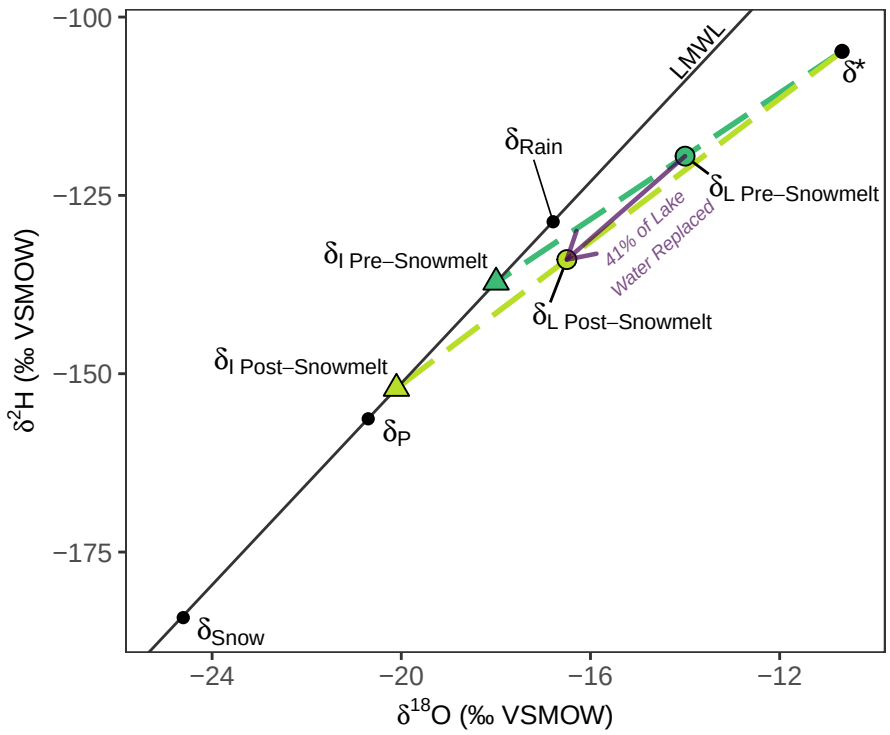

Figure 3.4 A hypothetical change in lake isotope composition from pre-snowmelt to post-snowmelt is shown. A visualization of how δ_{I} is calculated for an individual lake using a lake-specific evaporation line for both pre-snowmelt and post-snowmelt is also shown, where each lake's evaporation line (dashed line) extrapolates from δ^{*} through δ_{Lake} until intersecting the local meteoric water line to give δ_{I}. The local evaporation line (LEL) is defined by the line between δ_{P} and δ^{*} (not shown).

an equation developed by Gibson and Prowse (2002) that describes the fractionation of isotopes between water and freezing ice in a closed system

$$\delta_{L-Pre} = -f^{\alpha_{eff}}(1000 * f^{\alpha_{eff}} - f * \delta_{L-BelowIce} - 1000 * f) \tag{3.3}$$

where $\delta_{\mathrm{L\text{-}BelowIce}}$ is the isotope composition of the water beneath the lake ice, α_{eff} is the effective fractionation factor between ice and water, defined as $\alpha_{\mathrm{eff}} = \mathrm{R_{Ice}}/\mathrm{R_L}$, and f is the fraction of unfrozen water remaining in the lake. α_{eff} is dependent on the thickness of the boundary layer between the forming ice and freezing water and the downwards freezing velocity of the ice. Since we did not have measurements of either of these parameters, we relied on previously estimated values of α_{eff} (Souchez et al., 1987; Bowser and Gat, 1995; Ferrick et al., 2002) and boundary layer thickness

(Ferrick et al., 1998, 2002; Gibson and Prowse, 2002). Using this information, we estimated values of α_{eff} that produced $\delta_{\text{L-Pre}}$ values that closely match lake water isotope compositions measured at the same lakes in August and September of 2018 (Figure 3.10). Additional information about the determination of α_{eff} values is provided in Appendix 3.8.3.

To estimate fraction of unfrozen water remaining in lakes (f, Equation 3.3), bathymetry was collected at Big Bear Lake (Figure 3.2), a typical bowl-shaped thermokarst lake near the Trail Valley Creek meteorological station in June 2017 using a Garmin echoMAP CHIRP 42dv fish finder. Bathymetry data was used to determine a relationship between lake volume and lake depth. We fit a quadratic equation to the bathymetric data to estimate the fraction of lake volume relative to the fraction of lake depth. The best-fit quadratic equation (r^2 = 0.9997) was

$$V_{Lake} = -0.0115 D_{Lake}^2 + 2.1508 D_{Lake} - 0.4857 \tag{3.4}$$

where V_{lake} is the fraction of total lake volume and D_{lake} is the fraction of total lake depth. However, this fitted equation does not reach 100% V_{lake} at 100% D_{lake}, or 0% V_{lake} at 0% D_{lake}, which is required to realistically represent the relationship between lake depth and lake volume. The equation was slightly adjusted to:

$$V_{Lake} = -0.001 D_{Lake}^2 + 2 D_{Lake} \tag{3.5}$$

in order to satisfy these requirements, resulting in a mean offset of 1.7% between the measured bathymetric data and the adjusted equation. Most lakes in this region have a bowl-shaped bathymetry because they were formed through thermokarst processes (Rampton, 1988; Burn and Kokelj, 2009), where subsidence caused by the thaw of ice-rich permafrost results in a water body which then expands outward radially in all directions. Bathymetric data for Big Bear Lake and a comparison of the equation between lake volume and depth are provided in Appendix 3.8.4.

3.4.3 Quantifying lake and watershed properties

We quantified multiple lake and watershed properties to explore relations with the amount of lake water replaced by freshet. These properties included lake depth, lake volume, snow depth on the lake, ice thickness, lake area and watershed area. Lake depth, snow depth on the lake and ice thickness were measured at the same time as pre-snowmelt lake samples were collected. Lake volume was approximated by multiplying the product of lake depth and lake area by 0.7, a relation derived from the measured lake volume of Big Bear Lake. Watershed area was estimated by applying the D8 water routing algorithm (O'Callaghan and Mark, 1984) to the 2 metre resolution ArcticDEM (Porter et al., 2018) using ArcGIS 10.7.1 (ESRI, 2019).

3.5 Results

Correcting for ice fractionation using Equation 3.3 resulted in an increase in estimated $\delta_{\text{Lake-Pre}}$ values as expected, with the median shifting from -17.50‰ (-19.32‰ to -15.68‰ IQR, inter-quartile range) to -14.70‰ (-16.85‰ to -13.29‰ IQR) for δ^{18}O (Figure 3.5a, Table 3.2). The corrected pre-snowmelt lake isotope compositions were distributed across a large range of the predicted local evaporation line (LEL), spanning from near the LMWL to near δ^{*} (Figure 3.5a), reflecting the fact that the lake waters were variably influenced by evaporation. Corrected pre-snowmelt lake isotope compositions also tightly cluster along the LEL, indicating that the predicted LEL is well characterized.

The change in lake isotope composition from pre-snowmelt to post-snowmelt was characterized by a small (~1.5‰ in δ^{18}O) shift towards δ_{P}, with median pre-snowmelt $\delta_{\text{Lake-Pre}}$values of -14.70‰ (-16.85‰ to -13.29‰ IQR) and median $\delta_{\text{Lake-Post}}$ values of -16.15‰ (-17.86‰ to -15.45‰ IQR) for δ^{18}O (Figure 3.5b). The small change in lake isotope composition meant that most lakes retained an evaporated isotope signature post-snowmelt, overlapping with a substantial portion of $\delta_{\text{Lake-Pre}}$ and continuing to plot along the LEL (Figure 3.5b). Post-snowmelt, about

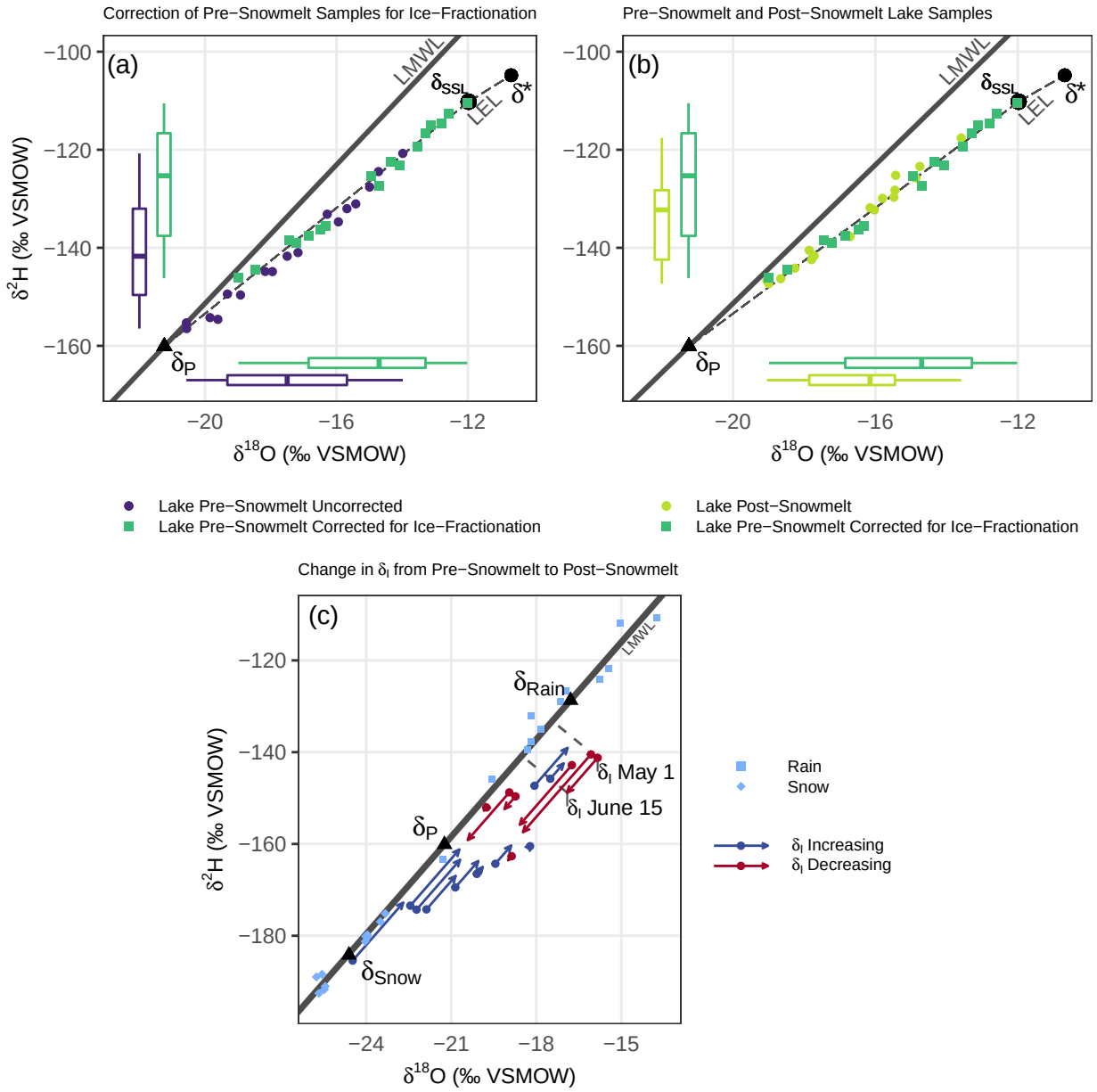

Figure 3.5 Lake water and precipitation isotope data are displayed on $\delta^{18}O$-$\delta^{2}H$ graphs. The local meteoric water line (LMWL: $\delta^{2}H = 7.1*\delta^{18}O - 10.0$) is indicated by the solid line, while the local evaporation line (LEL: $\delta^{2}H = 5.2*\delta^{18}O - 48.9$) is indicated by the dashed line. δ_P represents the average value of precipitation in the region, based on 2018 sampling of end-of-winter snow and rainfall from April to September. (a) Uncorrected and corrected for ice fractionation pre-snowmelt lake isotope data. (b) Corrected pre-snowmelt and post-snowmelt data. (c) The shift in δ_I from pre-snowmelt to post-snowmelt, as indicated by a circle for pre-snowmelt δ_I values and the end of the arrow for post-snowmelt δ_I values. All δ_I values are offset from the LMWL for visibility, as all δ_I values are constrained to the LMWL.

half of the lakes (9 of 17) also plotted above the LEL, indicating that the δ_I of these lakes was more similar to rainfall than snowfall (Figure 3.5b). The shift in δ_I for lakes from pre-snowmelt to post-snowmelt shows a convergence of most δ_I values towards a value near δ_P and away from the isotope composition of the end-of-winter snow (δ_{Snow}) or rainfall (δ_{Rain}) (Figure 3.5c). The convergence of δ_I values towards δ_P and away from end-of-winter snow signifies that a non-snow source of water, with a higher isotope composition than δ_{Snow}, was present in freshet.

Replacement of lake water by freshet ranged widely from 5.2 to 52.8%, with a median of 25.2% (19.1% to 32.4% IQR, Figure 3.6). A substantial proportion of this variation was explained by lake depth: deeper lakes had significantly less of their water replaced by freshet, with a reduction in lake water replacement of 13% for each additional metre of lake depth (R^2 = 0.53, p < 0.001, Figure 3.6, Table 3.3). Lake water replacement was not independently correlated with any other lake or watershed attribute including watershed area, lake volume, snow depth on the lake ice, lake ice thickness, lake area, and the ratio of lake area to watershed area (Table 3.3).

Table 3.3 Results for a linear regression between total lake water replacement with multiple lake and watershed properties. The adjusted R^2 and p-value are shown for each isotope. Linear regressions were performed using the 'lm' function using R 4.0.2 (R Core Team, 2021)

Lake Attribute	% Lake Volume Replaced by Freshet) Adjusted R^2	p-value
Lake depth	0.53	<0.001
Lake area	-0.06	0.849
Lake volume	-0.03	0.486
Snow depth	-0.06	0.771
Ice thickness	-0.05	0.654
Watershed area	0.02	0.274
Watershed area/Lake area	-0.01	0.361

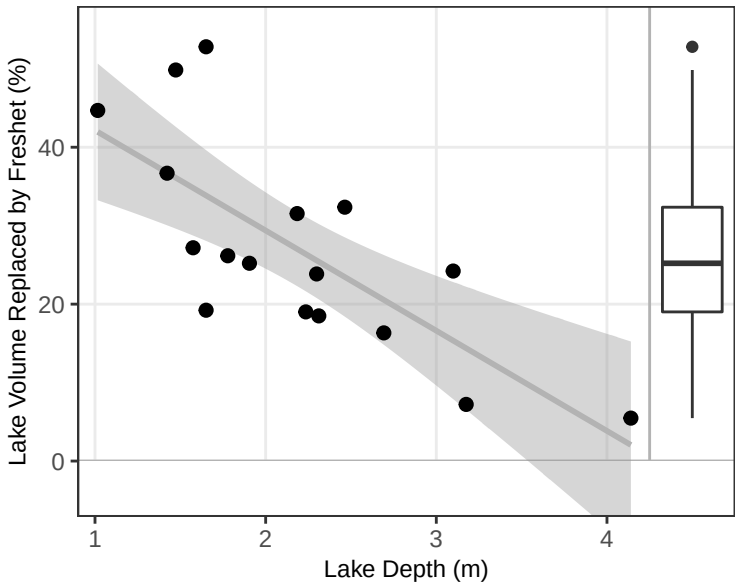

Figure 3.6 The relationship between the amount of lake water replaced by freshet and lake depth. The distribution of lake water replacement by freshet is shown by the boxplot on the right-hand side of the plot. A linear regression is also displayed on the plot ($R^2 = 0.53$, $p < 0.001$). The shaded grey area represents the 95% confidence interval of the linear regression.

3.6 Discussion

3.6.1 Influence of snowmelt bypass on the replacement of lake water by freshet

Characterization of the influence of snowmelt bypass on the replacement of pre-snowmelt lake water required accurate determination of lake water isotope compositions prior to freeze-up. Given that lake water isotope samples are unavailable from autumn 2017, and $\delta_{\text{L-Pre}}$ values were instead obtained from drilling through the lake ice before the lakes became ice-free, their isotope compositions required correction for the isotope fractionation caused by ice formation. Our novel approach to correcting $\delta_{\text{L-Pre}}$ values for the fractionation caused by lake ice formation provides a reasonable estimate of δ_{L} prior to lake ice formation. While our correction of $\delta_{\text{L-Pre}}$ involves some uncertainty, such as having to estimate the relationship between lake depth and lake volume, corrected $\delta_{\text{L-Pre}}$ values closely align with the general distribution of water isotope measurements from August and

September 2018 of the same lakes (Figure 3.10). Corrected $\delta_{\text{L-Pre}}$ values are also situated near or above the LEL, reasonably indicating a more rainfall-sourced δ_{I} that would be present in lakes at the time of freeze-up during the previous autumn. Prior to correction, most $\delta_{\text{L-Pre}}$ values plotted below the LEL (Figure 3.5a), indicating lakes had the majority of their inflow sourced from snow, which would be unlikely at the time when lake ice began forming during the previous autumn. We considered using δ_{L} values from September 2018 instead of correcting for ice fractionation, but 2018 was a cooler and wetter year than 2017, meaning the lake-specific δ_{L} values in September 2018 likely differed somewhat from September 2017.

The presence of a somewhat uniformly thick layer of freshet beneath lake ice (Appendix 3.8.5) likely explains the relationship between lake depth and the amount of lake water replaced by runoff, because the freshet layer represents a relatively smaller portion of lake volume at deeper lakes (Figure 3.6). We calculated the freshet layer thickness to be an average of 0.28 m, ranging from 0.12 to 0.52 m with a standard deviation of 0.11 m (Table 3.8). Previous studies have measured the thickness of the snowmelt bypass layer at the onset of freshet inflow to be ~30 – 200 cm (Henriksen and Wright, 1977; Bergmann and Welch, 1985). Since the mixed layer of pre-snowmelt lake water and freshet comprised a relatively larger volume in shallower lakes compared to deeper lakes (Figure 3.7a), a larger portion of lake water was able to be replaced with freshet in shallower lakes than in deeper lakes. We hypothesized that because shallower lakes likely had colder lake-bed temperatures during freshet (Burn, 2005), more mixing between pre-snowmelt lake water and freshet inflow would occur due to the reduction in the water density gradient between the bottom of the lake and the top of the lake. However, the estimated thickness of the freshet layer was uniform across lakes, indicating that colder lakebed temperatures may not have contributed to greater mixing at shallower lakes. To our knowledge, the relationship between lake depth and freshet retention has not been described in previous literature, although there has been little possibility of observing this relationship because estimates of freshet recharge in more than one lake are scarce (Falcone, 2007; Brock et al., 2008). We expect that a similar relationship between lake

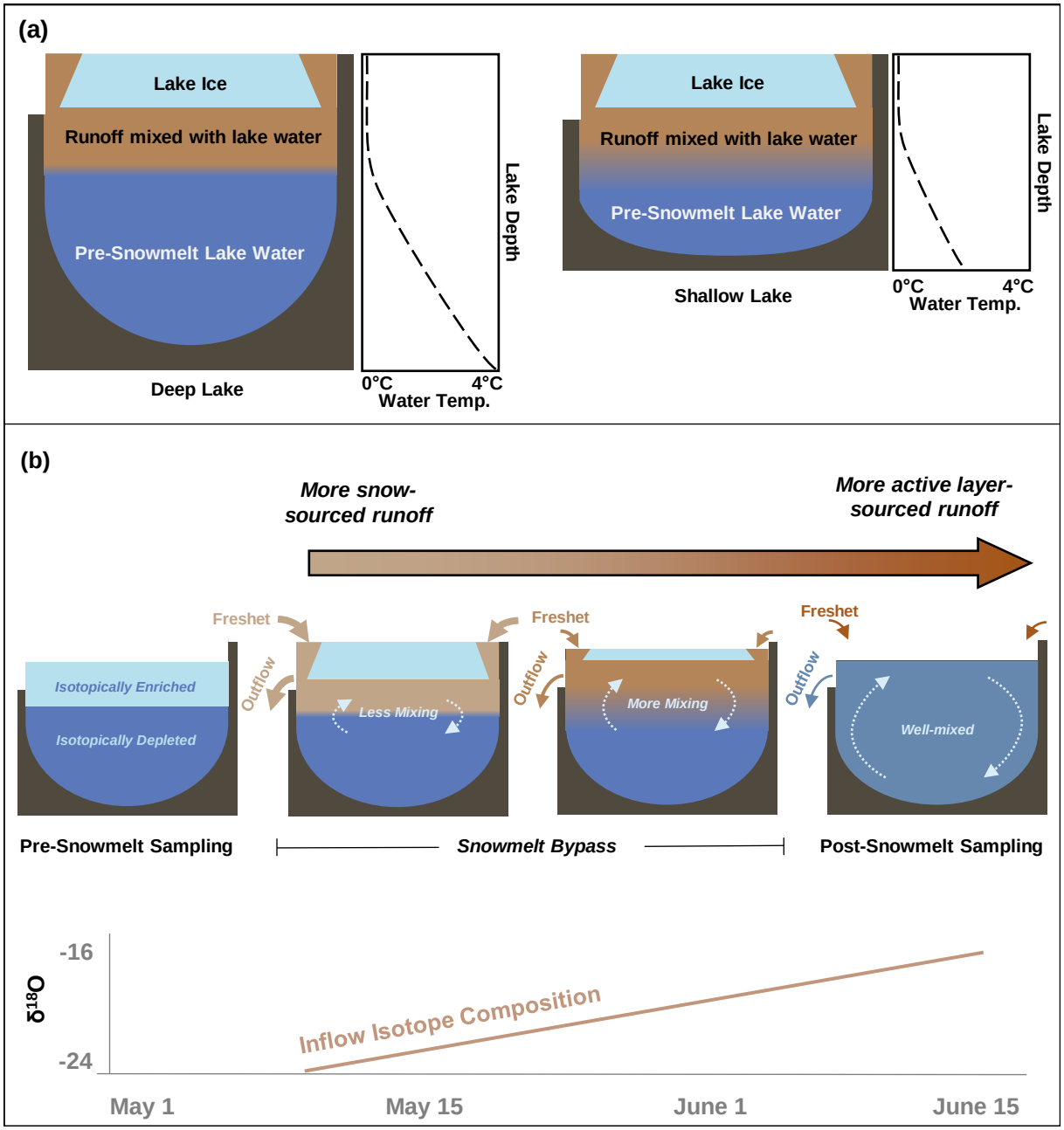

Figure 3.7 (a) A conceptual model showing the relative differences in snowmelt bypass between a shallow lake and a deep lake. Shallower lakes have a larger portion of their volume replaced by the runoff layer that flows beneath the ice, while a larger portion of water is isolated from mixing with runoff in deeper lakes. The estimated freshet layer thickness was somewhat uniform among all the lakes (Appendix 3.8.5). (b) A conceptual model of how snowmelt bypass occurred over the course of the snowmelt period. Pre-snowmelt samples were taken from water beneath lake ice which was isotopically depleted in comparison to the lake ice. As time goes on, the source of freshet shifts from snow-sourced to active layer-sourced, while mixing increases beneath the lake ice simultaneously.

depth and snowmelt bypass could be present in other open-drainage lakes that experience snowmelt bypass, since the relationship between increasing lake depth and greater snowmelt bypass is caused by the typical water temperature gradient which is present in ice-covered lakes at the onset of freshet. However, smaller lakes <1 ha, which are common in the Arctic (Pointner et al., 2019), likely do not experience as strong a snowmelt bypass effect because freshet is able to displace the pre-snowmelt lake water due to the small volume of the lake (Jansen et al., 2019; Cortés and MacIntyre, 2020). However, smaller lakes also typically have smaller under-ice chemical gradients that increase density stratification and limit freshet mixing and retention (Cortés and MacIntyre, 2020). Therefore, a relationship between lake depth and retention of freshet runoff likely does not exist at smaller Arctic lakes.

3.6.2 Sources of freshet

Following the freshet, the δ_I of lakes did not shift towards the isotope composition of snow (δ_{Snow}) as one may expect, but instead shifted towards the average isotope composition of precipitation (δ_P, Figure 3.5c). Other than the 21.3 mm rainfall that fell during the six-week period between the two isotope sampling dates, the only other potential source of water during this time period is water stored in the active layer, which likely mixed with snowmelt runoff as the soil thawed throughout the spring. The high infiltration capacity of the peat channels that convey runoff causes nearly all snowmelt to flow through subsurface routes, as was observed in the field and reported by Quinton and Marsh (1998). As water near the surface of the active layer is most likely to be comprised of rainfall from the previous year, we expect that much of the water stored in the top of the active layer would have been largely sourced from rainfall from the previous summer and autumn. In support of this inference, Tetzlaff et al. (2018) reported δ^2H values between -140‰ and -160‰ from August to September of 2014 in water samples taken at 10 cm soil depth at Siksik Creek, a watershed directly adjacent to the Trail Valley Creek camp (Figure 3.2). This range of soil water δ^2H values is more enriched relative to δ_P (δ^2H = -160.1 ‰, Figure 3.5c), indicating that a mixture

of snowmelt runoff with this active layer water could result in a water source similar in isotope composition to δ_P.

Freshet flowing into lakes later during the snowmelt period likely had a more rainfall-sourced isotope composition, replacing the more snow-sourced runoff that had entered the lake earlier during the freshet (Figure 3.7b). A shift from snow-sourced water towards rainfall-sourced water during the course of the snowmelt period has been observed using water isotope measurements at Siksik Creek by Tetzlaff et al. (2018). Additionally, the mixing of freshet beneath lake ice increases with time as the temperature and density gradient lessens between the top and bottom of the lake water column (Cortés et al., 2017). Based on our results and these previous studies, we conclude that the ability of the active layer to contribute runoff to lakes appears to be maximized at the same time that vertical mixing in the lake is stronger, while snowmelt runoff flows into lakes at a time when little vertical mixing is occurring and is also likely replaced by later runoff (Figure 3.7b). Such interplay between timing of snowmelt runoff, lake ice melt and hydrological behaviour of the active layer explains why the source of water to lakes is not solely snow-sourced, and why incorporation of active layer runoff into lakes is more important than the volume of freshet delivered to lakes for the open-drainage lakes of this study.

3.6.3 Assumptions and improving the utility of water isotope data from ice-covered lakes

In our estimation of lake water replacement by freshet we had to make some assumptions (Appendix 3.8.3) when estimating $\delta_{L\text{-}Pre}$ using Equation 3.3. Future studies could sample lakes in the previous autumn before ice formation begins to avoid these assumptions, as there is minimal water flow in and out of Arctic lakes during the winter months due to frozen soils and ice cover on lakes (Woo, 1980). If lakes cannot be sampled in the previous autumn, another option would be to take a lake ice core and sample the isotope composition at different points along the lake ice core. These isotope

measurements could then be used to estimate the α_{eff} value used in Equation 3.3, as has been done by Souchez et al. (1987) and Bowser and Gat (1995). This approach would avoid the assumptions we made in estimating α_{eff} outlined in Appendix 3.8.3. However with this approach, one still needs to know the volume of the lake ice relative to the volume of the remaining unfrozen water, and must rely on lake bathymetry data or a depth–to–volume relationship, such as the one we derived using bathymetry data from Big Bear Lake (Equation 3.4). Since we only have one survey of lake bathymetry, we do not know how well our depth–to–volume relationship describes other lakes in the region, and it could be that this relationship varies as lakes increase in surface area or in areas of different surficial geology where the intensity of thermokarst processes may have varied during lake formation.

Since we do not have measurements of the lake temperature profile, we also assume that our lakes have the typical thermal structure of cryomictic (Yang et al., 2021) ice-covered lakes that leads to snowmelt bypass. We relied on measurements of water temperature at 1.25 m depth in Big Bear Lake (Figure 3.2) and lake temperature profiles modelled using FLake-online (Appendix 3.8.1) to conclude that our lakes were likely well-mixed at the time lakes were sampled post-freshet. Two scenarios were established in FLake-online, one representing a typical lake from the ones we sampled, and another lake representing a small, deep lake where mixing would be less likely. Even though FLake-online does not simulate under-ice mixing, which typically occurs in Arctic lakes (Hille, 2015; Cortés et al., 2017; Kirillin et al., 2011), the 'typical lake' became fully mixed 1 day after becoming ice-free while the small, deep lake was simulated to become fully mixed 3 days after becoming ice-free. Even though snowmelt bypass is a common phenomenon in many types of ice-covered lakes around the world (Henriksen and Wright, 1977; Jeffries et al., 1979; Hendrey et al., 1980; Bergmann and Welch, 1985; Schiff and English, 1988; Edwards and McAndrews, 1989; Cortés et al., 2017), knowledge about how the thermal structure of our study lakes evolved over time, and varied between lakes of different depth, would have informed interpretation of our results. Such data could have helped better explain why shallow lakes retain more freshet runoff

than deeper lakes, and also could have helped confirm our hypothesis that water flowing into lakes later during the freshet mixes more readily with lake water.

3.6.4 Climate change and snowmelt bypass

Future changes in snowmelt bypass are dependent on whether climate change allows open-drainage lakes to persist, or causes them to become closed-drainage, given that snowmelt bypass can only occur when lakes are at or above their outlet level. There are multiple consequences of Arctic warming that will influence lake water balance: changes in rainfall (Bintanja and Andry, 2017) and snowfall (Brown and Mote, 2009; Ernakovich et al., 2014), increases in active layer thickness (Walvoord and Kurylyk, 2016; Tananaev and Lotsari, 2022; Koch et al., 2022), the proliferation of deciduous shrubs (Loranty et al., 2018), and longer lake ice-free periods (Woolway et al., 2020). Whether the combination of these changes will result in an increase or decrease in runoff to lakes is currently unknown (Blöschl et al., 2019), making it difficult to predict whether open-drainage lakes will persist or if some open-drainage lakes may shift to being closed-drainage under future climate. Due to this uncertainty, we discuss potential future changes in snowmelt bypass under two scenarios: a) where lakes remain open-drainage in the future, and b) where some lakes become closed-drainage in the future.

If open-drainage lakes persist as such in the future, we suspect the freshet that is incorporated into lakes may shift towards being more rainfall-sourced. Projected rainfall increases (Bintanja and Andry, 2017) will likely leave the active layer in a more saturated state when the active layer freezes in autumn, potentially providing more water to lakes during the freshet. Other studies have already established a strong positive relationship between increased rainfall in the previous summer and a more efficient conversion of the snowpack into freshet (Bowling et al., 2003; Stuefer et al., 2017), indicating the presence of a strong connection between snowmelt runoff and water stored in the thawing active layer. Increasing shrub heights will advance snowmelt timing relative to lake ice breakup (Marsh et al., 2010; Grünberg et al., 2020, Chapter 2), causing more snowmelt to flow into

lakes at a time when there is limited below-ice vertical mixing. Combining earlier snowmelt timing with a more rain-saturated active layer could result in more freshet bypassing open-drainage lakes early during the freshet, with the active layer thawing deeper and shifting freshet more towards rainfall-sourced water by the time below-ice mixing begins.

Advancement of snowmelt timing and a shift from snow-sourced to rainfall-sourced freshet may have limnological implications for lakes. Cation and anion concentrations in snowmelt water tend to decrease over the course of the snowmelt period (Marsh and Pomeroy, 1999), while the pH of snowmelt runoff increases with time (Quinton and Pomeroy, 2006). Snowmelt also tends to have higher dissolved organic carbon (DOC) concentrations than summertime runoff (Finlay et al., 2006) and typically contributes the largest input of terrestrial organic matter to lakes in organic-rich landscapes (Townsend-Small et al., 2011; Olefeldt and Roulet, 2012). Balasubramaniam et al. (2015) observed that thermokarst lakes dominated by snow-sourced water tended to have lower pH, higher conductivity and higher DOC concentrations than lakes dominated by rain-sourced water. Based on these observations, as snowmelt occurs earlier in the Arctic, lakes may experience decreases in DOC and conductivity and increases in pH. Such changes to lake biogeochemistry caused by shifts in freshet runoff retention could affect the productivity and ultimately the climate feedbacks of these lakes. Future research could combine estimates of lake water replacement by freshet with water chemistry measurements to further our understanding of the impact of snowmelt bypass on lake chemistry and other limnological properties.

In a future where some open-drainage lakes become closed-drainage due to greater evaporation under a longer ice-free season, for example, we expect that such lakes will retain more freshet runoff than comparable open-drainage lakes, because closed-drainage lakes retain the additional freshet that is required to recharge the lake to its outlet level. Since snowmelt bypass cannot occur until a closed-drainage lake is recharged to its outlet level, we expect that freshet retention by closed-drainage lakes will not be as influenced by lake depth. Lakes with smaller ratios of watershed area to lake area (WA/LA) are more prone to a more negative water balance (Marsh and Pomeroy, 1996;

Gibson and Edwards, 2002; Turner et al., 2014; Arp et al., 2015). Therefore, we expect that lakes with relatively small WA/LA ratios will be more prone to becoming closed-drainage, relying on freshet to recharge them to their outlet level and retain more freshet as a result. A corollary of this prediction is that other ice-covered lakes which currently lie below their outlet level at the onset of the freshet (i.e., closed-drainage lakes) likely retain more freshet than open-drainage lakes of a similar lake depth. A more saturated active layer at the onset of snowmelt, combined with a greater amount of snowfall should increase the ability of freshet to recharge any closed-drainage lake.

An additional complication to predicting the future of snowmelt bypass in response to climate change is caused by the shifting of lake ice regimes from bedfast ice to floating ice. Lakes that freeze completely to the bed in winter (bedfast ice) melt from the surface downwards in spring and likely do not develop the thermal stratification necessary for snowmelt bypass to occur. Remote sensing studies have already observed many bedfast ice lakes shifting to floating ice regimes during the past few decades in response to climate change (Arp et al., 2012a; Surdu et al., 2014; Engram et al., 2018). We are unaware of any lake mixing studies on bedfast ice lakes, making it difficult to hypothesize how shifting from bedfast to floating ice could affect the amount of freshet retained by a lake.

3.7 Conclusions

A portion of the large volume of freshet that flows into lakes every year can bypass ice-covered, open-drainage lakes due to limited mixing between lake water beneath the lake ice and freshet. By estimating the percentage of lake water replaced by freshet at 17 open-drainage lakes, we have been able to explore which lake and watershed attributes affect snowmelt bypass. Our data show that as lake depth increases the amount of lake water replaced by freshet decreases, likely because freshet is unable to mix with deeper lake water when lakes are ice-covered and the water column is stratified; however, we lack data demonstrating the extent of mixing in the lakes we studied. Additionally,

the volume of freshet flowing into the lakes seems to have minimal impact on the amount of lake water replaced by freshet, given that the ratio of watershed area to lake area was not correlated with the percentage of lake water replaced by freshet. Estimation of the isotopic composition of source waters showed that the freshet remaining in lakes was not solely snow-sourced – rainwater left in the active layer from the previous autumn had mixed with snowmelt before entering lakes. Active layer-sourced water likely flows into lakes later in spring and at a time when freshet can more easily mix with pre-snowmelt lake water, replacing the earlier more snow-sourced freshet.

Models specialized for northern environments are rapidly improving their ability to represent the complicated processes present in permafrost regions, such as the effect of shrubs on snow accumulation, snowmelt and active layer thickness (Krogh and Pomeroy, 2019; Bui et al., 2020), lake ice formation and decay (MacKay et al., 2017) and the mixing processes that lead to snowmelt bypass (MacKay et al., 2017). Such models could be used to examine how freshet water sources may change in the future, which could have significant impacts on limnological properties including water chemistry (Finlay et al., 2006; Balasubramaniam et al., 2015). Additionally, current physically based lake models can represent vertical mixing beneath lake ice (MacKay et al., 2017), and could be used to further evaluate the influence of lake depth, lake ice regime, or climate change on snowmelt bypass and resulting impacts on limnology.

3.8 Chapter 3 Appendix

3.8.1 Lake mixing status at ice-off: water temperature data and modelling

The application of Equation 3.2 assumes that lakes are well-mixed at the time that $\delta_{\text{L-Post}}$ water samples were corrected. We investigated if the lakes we sampled were likely to have been well-mixed at ice-off, because some lakes have been observed to be not well-mixed at ice-off (Vachon et al., 2019; Wiltse et al., 2020; Cortés and MacIntyre, 2020). We rely on water temperature data from Big Bear Lake and another lake near the Inuvik-Tuktoyaktuk Highway investigated by Hille (2015), and lake temperature modelling using FLake-online (Kirillin et al., 2011).

Water temperature measurements at Big Bear Lake and a lake nearby the Inuvik-Tuktoyaktuk Highway suggest that lakes in this region become well-mixed during the ice-off period. At Big Bear Lake, water temperature at 1.25 m depth reaches 4°C initially by 05-06-2018, followed by daily fluctuations between 2.3 – 4.1°C, before continuing a warming trend again on 13-06-2018 and reaching 6.8°C on 15-06-2018 (Figure 3.8). Water temperature between 0 and 4 m was measured by Hille (2015) at a 10 m deep lake approximately 10 km from the Inuvik-Tuktoyaktuk highway in 2009. Hille (2015)'s measurements show uniform warming of the water column beneath the ice from 1 to 4 m, with water temperatures reaching ~5°C by the time the lake became ice-free (Hille, 2015, Figure 3.4). Based on these observations, we assume these two lakes were well-mixed at the time they became ice-free.

We also ran two model scenarios using FLake-online (Kirillin et al., 2011, http://flake.igb-berlin.de/model/run) to gather further information about the mixing status of lakes in this region at the time they become ice-free. The first scenario represents a typical lake compared to the lakes we sampled in size and depth (Table 3.4). In the second scenario, lake depth is increased and lake area is decreased to represent the "worst-case scenario" for lake mixing after lakes became ice-free (Table 3.4). Water clarity was set to 2 m, based on an average Secchi depth measurement of 1.88 m based on measurements made by Vucic et al. (2020) at lakes along the Inuvik-Tuktoyaktuk

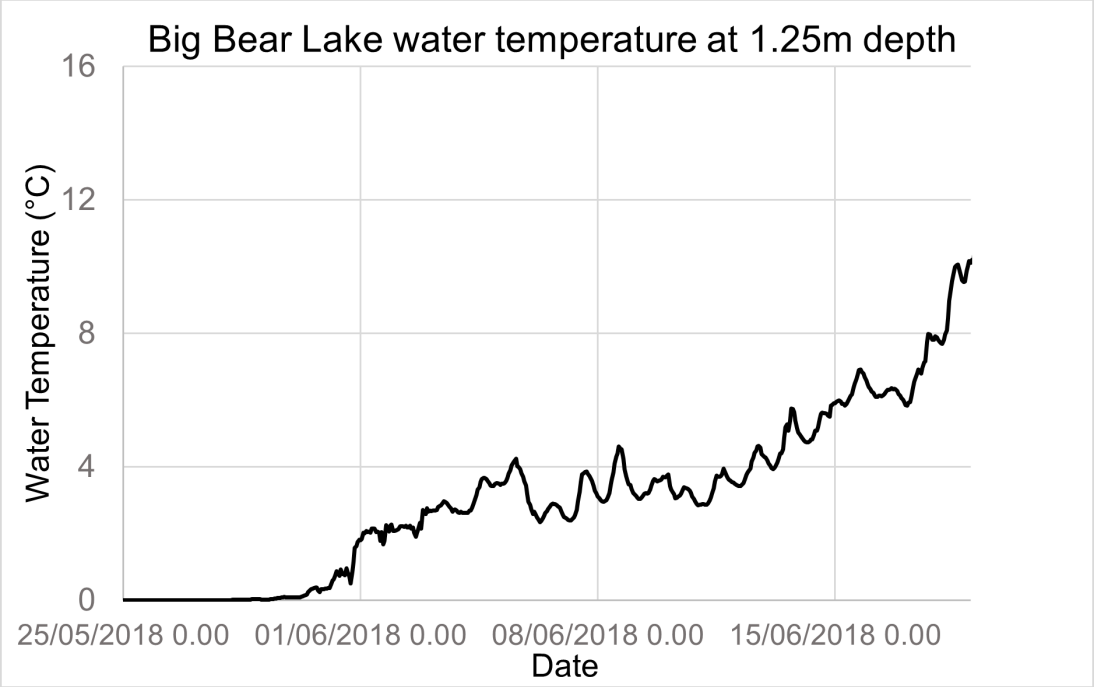

Figure 3.8 Big Bear Lake water temperature at a depth of 1.25 m, between 2018-05-25 and 2018-06-19.

Highway and Dempster Highway south of Inuvik. Both scenarios were run with 'perpetual year' meteorological forcing data, whereby meteorological data from 01-11-2015 to 31-10-2016 forces the model for multiple years until a quasi-steady equilibrium is reached.

In both model scenarios, the mixing depth reached the maximum lake depth rapidly after ice-off, taking one day in the typical lake scenario and three days in the worst chance of mixing scenario. Notably, under-ice warming and mixing does not occur in FLake-online, although under-ice mixing has been observed in other Arctic lakes (Hille, 2015; Cortés et al., 2017; Kirillin et al., 2011). Given that both models indicate full mixing within a few days of lakes becoming ice-free, despite the absence of under-ice warming and mixing that was likely present at our study lakes based on temperature data from Big Bear Lake and Hille (2015), we believe that the lakes we sampled were very likely fully-mixed when we sampled them on 2018-06-15.

Table 3.4 Input parameters and results for the two scenarios used to evaluate the mixing conditions of lakes during the ice-off period.

Parameter/Result	Typical Lake Scenario	Worst Chance of Mixing Scenario
Coordinates	68.74, -133.53	68.74, -133.53
Mean Lake Depth (m)	2	3.5
Water transparency (m)	2	2
Lake Fetch (m)	250	50
Ice-free Date	June 28	June 28
Fully-mixed Date	June 29	July 1
Days from Ice-free to Fully-mixed	1	3

3.8.2 Isotope framework and sensitivity analysis

The isotope framework (i.e., establishment of the predicted local evaporation line (LEL)) used for this study was based on the coupled isotope tracer method developed by Yi et al. (2008), following other studies that have investigated lake water balances using water isotope tracers (Turner et al., 2014; Remmer et al., 2020; MacDonald et al., 2021). Below are the parameters and equations required to calculate δ^*, the terminal point on the LEL. The equation for δ^*, which represents the isotope composition of a lake at the point of desiccation, is as follows (Gonfiantini, 1986)

$$\delta^* = \frac{h * \delta_{As} + \varepsilon_k + (\varepsilon^*/\alpha^*)}{h - \varepsilon_k - (\varepsilon^*/\alpha^*)} \tag{3.6}$$

where α^* is the fractionation factor between the liquid and vapour phase of water (Horita and Wesolowski, 1994), calculated for δ^{18}O as

$$\alpha^*_{L-V} = 2.718^{(-7.685+6.7123*\frac{10^3}{T}-1.6664*\frac{10^6}{T^2}+0.35041*\frac{10^9}{T^3})/1000} \tag{3.7}$$

and calculated for δ^2H as

$$\alpha^*_{L-V} = 2.718^{(1158.8*\frac{T^3}{10^9}-1620.1*\frac{T^2}{10^6}+794.84*\frac{T}{10^3}-161.04+2.9992*\frac{10^9}{T^3})/1000} \tag{3.8}$$

Table 3.5 Variables used in isotope framework and sources of their calculation.

Parameter	Value	Reference
δ^* (‰)	δ^{18}O = -10.77, δ^2H = -104.97	(Gonfiantini, 1986)
h (%)	80.5	(Environment and Climate Change Canada, 2019b)
T (K)	282.32	(Environment and Climate Change Canada, 2019b)
α^*_{L-V}	^{18}O =1.0108, ^{2}H = 1.0981	(Horita and Wesolowski, 1994)
ε^*	^{18}O = 0.0108, ^{2}H = 0.0981	(Horita and Wesolowski, 1994)
ε_k	^{18}O = 0.0028, ^{2}H = 0.0024	(Gonfiantini, 1986)
δ_{Rain} (‰)	δ^{18}O = -16.79, δ^2H = -128.7	This study.
δ_{Snow} (‰)	δ^{18}O = -24.61, δ^2H = -184.2	This study.
LMWL Slope, Intercept (‰)	7.066, δ^2H = -10.0	This study.
LEL Slope , Intercept	5.114, 48.9	This study.

The term ε^* is a separation term where

$$\varepsilon^* = \alpha^* - 1 \tag{3.9}$$

The term h represents the relative humidity of the air above the water and δ_{As} is the isotope composition of atmospheric moisture during the open water season defined as

$$\delta_{As} = \frac{\delta_{Ps} - \varepsilon^*}{\alpha^*} \tag{3.10}$$

where δ_{Ps} is the average isotope composition of precipitation (i.e., rainfall) during the open water season. The term ε_k is the kinetic fractionation separation term, defined as

$$\varepsilon_k = x * (1 - h) \tag{3.11}$$

where x = 0.0142 for δ^{18}O and x = 0.0125 for δ^2H (Gonfiantini, 1986).

Given that there is some variability in δ_{Snow} and δ_{Rain} values from samples collected, we

conducted a sensitivity analysis to evaluate whether uncertainty in these values could affect δ_I and % lake water replacement sufficently to change our interpretation of the results. To conduct the sensitivity analysis, we calculated the standard error of the mean (SEM) for δ_{Snow} and δ_{Rain}

$$SEM = \frac{\sigma}{\sqrt{n}} \tag{3.12}$$

where σ is the standard deviation of δ_{Snow} or δ_{Rain} values and n is the number of δ_{Snow} or δ_{Rain} samples. The SEM was added to δ_{Snow} and δ_{Rain} to calculate an "upper-bound" estimate, and subtracted to calculate a "lower-bound" estimate. These upper- and lower-bound δ_{Snow} and δ_{Rain} values were then used to calculate upper- and lower-bound δ_P, δ_{Ps} and δ^* values (Table 3.6). These upper- and lower-bound values were then used to calculate upper- and lower-bound δ_I (Figure 3.9a) and % lake water replaced values (Figure 3.9b) were calculated. Overall, δ_I and % lake water replaced values change minimally between the upper- and lower-bound cases (Figure 3.9a, 3.9b), and do not alter our interpretation of the results.

Table 3.6 Comparison of isotope framework parameters for upper- and lower-bound cases.

Case	$\delta^{18}O_P$	$\delta^{2}H_P$	$\delta^{18}O_{Ps}$	$\delta^{2}H_{Ps}$	$\delta^{18}O^*$	$\delta^{2}H^*$
Lower-Bound	-24.55	-181.12	-17.40	-133.46	-11.36	-109.40
Base	-24.10	-178.00	-16.79	-129.15	-10.78	-104.97
Upper-Bound	-23.65	-174.88	-16.18	-124.84	-10.16	-100.54
SEM	±0.45	±3.12	±0.61	±4.31	±0.61	±4.43

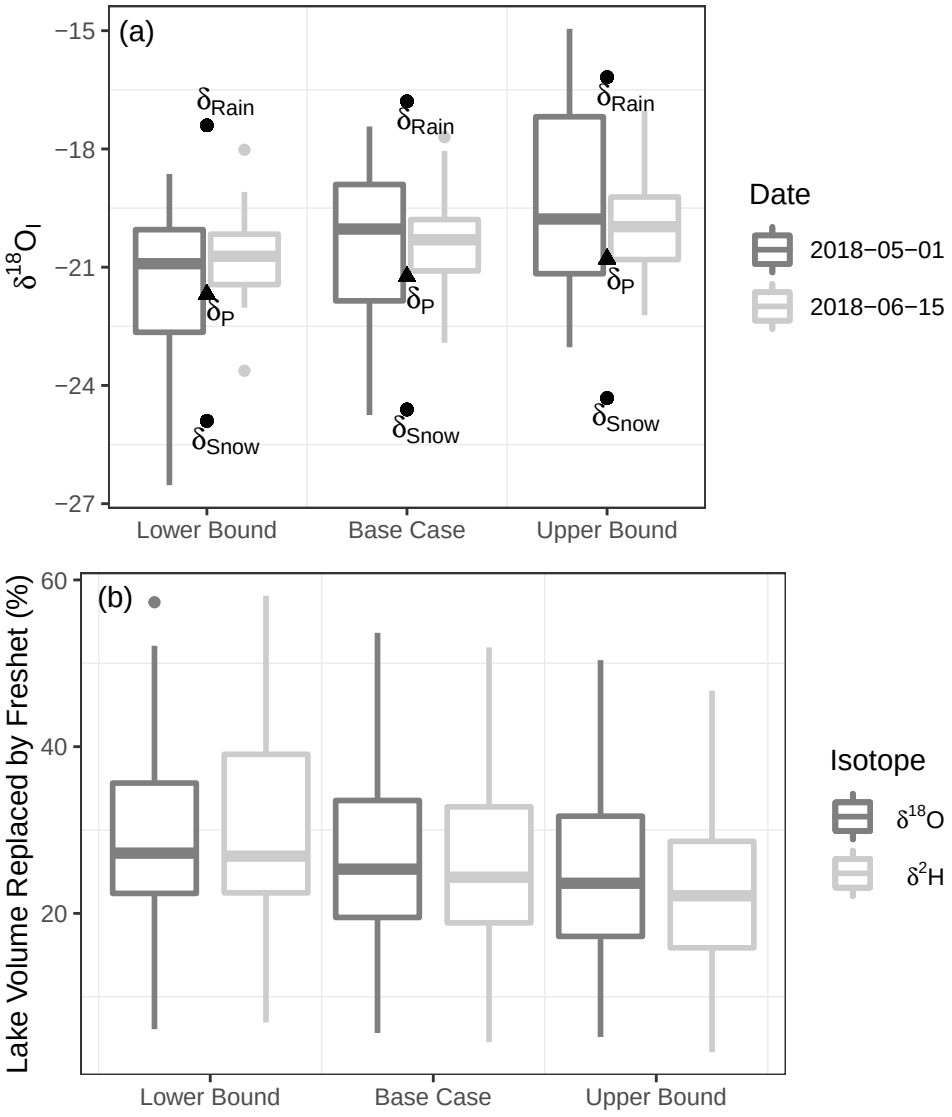

Figure 3.9 Comparison of upper- and lower-bound δ_I and % lake water replacement values against the base case.

3.8.3 Determination of $\alpha_{\mathbf{eff}}$ values

In order to determine α_{eff}, two variables must be taken into account: the thickness of the ^{18}O or ^{2}H boundary layer across which heavy isotopes are diffusing from water into ice, and the downward velocity of the freezing ice (Ferrick et al., 2002). If these two parameters are known, the fractionation factor can be estimated using a linear resistance model developed by Ferrick et al. (1998), which is similar in structure to the Craig and Gordon (1965) linear resistance model for evaporation. Ferrick et al. (1998) define the effective fractionation factor between ice and water as

$$\alpha_{eff} = \frac{\alpha^*_{L-S}}{\alpha^*_{L-S} + (1 - \alpha^*_{L-S}) exp[\frac{-zv}{D_i}]} \tag{3.13}$$

where α^*_{L-S} is the equilibrium fractionation factor between ice and water (1.002909 for $^{18}O/^{16}O$, 1.02093 for $^{2}H/^{1}H$ (Wang and Meijer, 2018)), z is the ^{18}O or ^{2}H boundary layer thickness between the ice and water (mm), v is the velocity of ice growth (cm^2 day^{-1}), and D_i is the self-diffusion coefficient of $^{1}H_2{}^{18}O$ or $^{1}H^{2}H^{16}O$ at 0°C (cm^2 day^{-1}). As the boundary layer and the velocity of ice growth increase, α_{eff} moves from the value of α^*_{L-S} towards a value of 1 (i.e., no fractionation).

As we do not know the boundary layer thickness at the ice-water interface, or the exact ice growth velocity for the lakes studied here, we relied on multiple other sources of information to estimate a probable upper- and lower-bound of α_{eff}. We took into account previous estimates of α_{eff} for ice-water fractionation (Souchez et al., 1987; Bowser and Gat, 1995; Ferrick et al., 2002) and boundary layer thickness from other studies of lakes (Ferrick et al., 1998, 2002; Gibson and Prowse, 2002). The boundary layer thickness between water and freezing ice in a lake was estimated to be between 1 mm and 6 mm by Ferrick et al. (1998), however, they revised this estimate with a more rigorous diffusion model to 1 ±0.3 mm for ^{18}O and 0.4 ± 0.2 mm for ^{2}H (Ferrick et al., 2002). They also found that the boundary layer thickness remained mostly stable across different ice growth velocities, although the lowest ice growth velocity of ~0.9 cm day^{-1} had a boundary layer of ~1.8 mm (Ferrick et al., 2002). The mean ^{18}O α_{eff} values for two ice cores taken from the lake studied

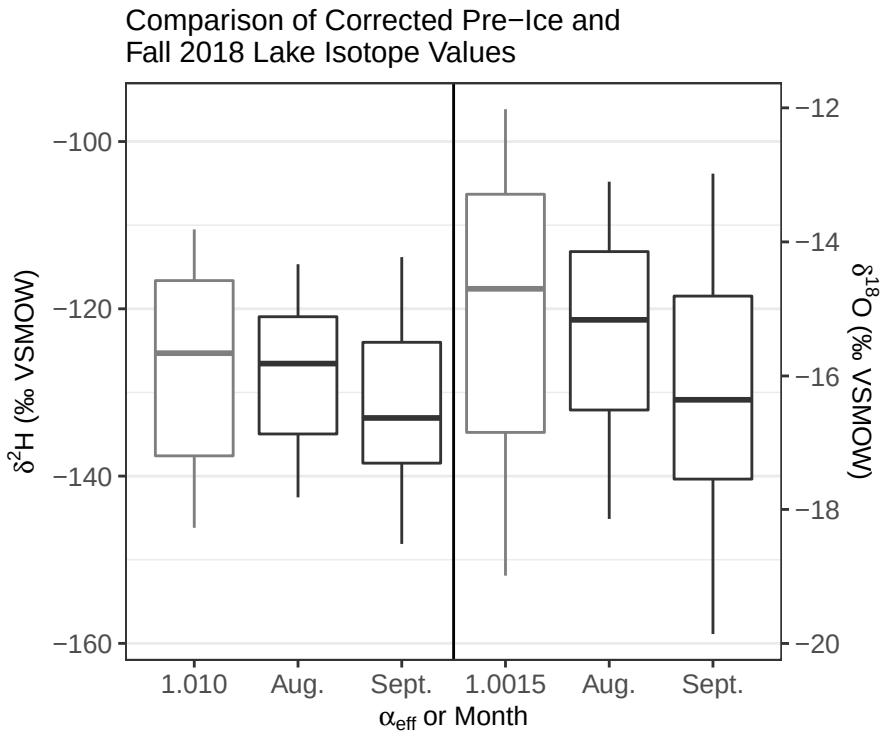

Figure 3.10 Comparison of Pre-Lake Ice Formation and August / September 2018 lake water isotope compositions. The α_{eff} values (δ^2H α_{eff} = 1.010, δ^{18}O α_{eff} = 1.0015) match closely with August and September 2018 lake water isotope compositions. This suggests that these α_{eff} estimates are appropriate to use for estimating the pre-ice formation lake water isotope compositions.

by Ferrick et al. (2002) were 1.0021 and 1.0020, with respective ice growth velocities of 3.7 and 4.1 cm day^{-1}. A 1 mm boundary layer was also estimated by Gibson and Prowse (2002) beneath river ice in northern Canada, however they also suggest that the boundary layer thickness can reach up to 4 mm in quiescent lake water. Therefore, we assume a minimum boundary layer thickness of 1 mm, and a maximum boundary layer thickness of 4 mm.

We estimated the minimum possible freezing velocity of our study lakes using the initial date of ice formation and the ice thickness we measured in spring. Based on Sentinel imagery (Sentinel Playground), all studied lakes became ice-covered by October 16th, 2017. Ice thickness was measured at Big Bear and Little Bear Lake (near Trail Valley Creek camp, Figure 3.1) on March 21st, 2018, and when ice thickness was remeasured again in late April, it had not become any thicker. Therefore, assuming ice growth began on October 16, 2017 and ceased on March 21,

2018, the ice growth velocities for our study lakes range from an average of 0.50 – 0.84 cm day^{-1} (0.78 – 1.32 m ice thickness). This only provides a lower-bound estimate for ice growth velocity, as ice growth likely stopped earlier than March 21, 2018, and was more rapid during initial ice formation.

We further constrained our estimate of α_{eff} by assuming that α_{eff} values that result in lake water replacement estimates of >100% or <0% were not correct. Using all these sources of information, we calculated an upper-bound of α_{eff} values based on the minimum possible ice freezing velocity (^{2}H α_{eff} = 1.0199, ^{18}O α_{eff} = 1.00286) and lower-bound of α_{eff} values which still generate lake water replacement estimates that are >0% and <100% (^{2}H α_{eff} = 1.010, ^{18}O α_{eff} = 1.0015).

Assuming a 2 mm boundary layer, which is within the range of our boundary layer thickness estimates, α_{eff} values of 1.0015 for ^{18}O and 1.010 for ^{2}H correspond to ice growth rates of 3.62 cm day^{-1} for ^{18}O and 3.34 cm day^{-1} for ^{2}H. Similar ice growth rates have been observed in Arctic lakes (Woo, 1980); greater ice growth rates were also estimated for a lake in a warmer climate by Ferrick et al. (2002). These α_{eff} values also compare well with other measured α_{eff} values in lakes: a range of α_{eff} = 1.013 – 1.015 for ^{2}H was found by Souchez et al. (1987) for a 4.4 cm thick lake ice cover; α_{eff} has been found to range from 1.0005 to 1.0027 for ^{18}O in a single 50 cm ice core (Bowser and Gat, 1995). The $\delta_{L\text{-}Pre}$ values calculated using α_{eff} = 1.0015 for ^{18}O and 1.010 for ^{2}H also closely match the distribution of δ_{L} values from August and September of 2018, giving an indication that these α_{eff} values generate realistic lake water isotope compositions (Figure 3.10). Therefore, we chose α_{eff} = 1.0015 for ^{18}O and α_{eff} = 1.010 for ^{2}H as our α_{eff} values, as they correspond well with other estimates α_{eff}, are within a range of probable ice-growth rates and lake water replacement by freshet and generate pre-ice formation isotope compositions that closely match the following summer's lake water isotope compositions.

3.8.4 Bathymetric data and volume – depth relationship

The modelled relationship between lake depth and volume is

$$\%_{LakeVolume} = (-0.01 * \%_{LakeDepth})^2 + 2 * \%_{LakeDepth} \tag{3.14}$$

where $\%_{\text{LakeVolume}}$ is the cumulative lake volume as a percent of total and $\%_{\text{LakeDepth}}$ is the cumulative lake depth as a percent of total (Table 3.7).

Table 3.7 Big Bear Lake bathymetric data and fit between modelled relationship between lake volume and lake depth as a percentage of total lake volume and depth.

Depth (m)	Cumulative Depth (% total)	Cumulative Volume (m^3)	Cumulative Volume (% total)	Modelled Cumulative Volume (% total)	Offset between data and modelled cumulative volume (%)
2.5	100	89326.83	100	100	0.00
2.25	90	88327.68	98.88	99	-0.12
2	80	85881.37	96.14	96	0.14
1.75	70	82441.90	92.29	91	1.29
1.5	60	77491.01	86.75	84	2.75
1.25	50	69384.35	77.67	75	2.67
1	40	58991.30	66.04	64	2.04
0.75	30	46548.63	52.11	51	1.11
0.5	20	32463.34	36.34	36	0.34
0.25	10	16944.40	18.97	19	-0.03
0	0	0	0	0	0.00

3.8.5 Freshet layer thickness

We computed the thickness of the freshet layer using the relationship between lake depth and lake volume, the % of lake volume replaced by freshet, and lake depth measurements made at each sample lake. The freshet layer thickness was calculated by rearranging Equation 3.5

$$freshet\ layer\ thickness\ (m) = \frac{lake\ depth}{-10 * \sqrt{100 - \%lake\ water\ replaced} - 10} \tag{3.15}$$

Lake	Freshet Layer Thickness (m)
7	0.23
8	0.29
9	0.26
10	0.17
11	0.26
14	0.29
15	0.23
16	0.12
19	0.44
20	0.23
21	0.25
26	0.43
27	0.40
49	0.38
50	0.52
51	0.22
52	0.12
Min	0.12
Mean	0.28
Max	0.52
St. Dev.	0.11

Table 3.8 Calculated layer thickness for each lake using Equation 3.15

This calculation represents the thickness the freshet layer would be on 2018-06-15 if it had not mixed with pre-snowmelt lake water. In reality, the unmixed freshet layer during the height of freshet would likely be thicker, due to rises in lake level caused by freshet that are not accounted for in this equation. Layer thicknesses averaged 0.28 m, ranging from 0.12 m to 0.52 m with a standard deviation of 0.11 m (Table 3.8).

Chapter 4

Hydrological, meteorological and watershed controls on the water balance of thermokarst lakes between Inuvik and Tuktoyaktuk, Northwest Territories, Canada

4.1 Abstract

Thermokarst lake water balances are becoming increasingly vulnerable to change in the Arctic as air temperature increases and precipitation patterns shift. In the tundra uplands east of the Mackenzie Delta in the Northwest Territories, Canada, previous research has found that lakes responded non-uniformly to year-to-year changes in precipitation, suggesting that lake and watershed properties mediate the response of lakes to climate change. To investigate how lake and watershed properties and meteorological conditions influence the water balance of thermokarst lakes in this region, we

sampled 25 lakes for isotope analysis five times in 2018, beginning before snowmelt on May 1 and sampling throughout the remainder of the ice-free season. Water isotope data were used to calculate the ratio of evaporation-to-inflow (E/I) and the average isotope composition of lake source water (δ_I). We identified four distinct water balance phases as lakes responded to seasonal shifts in meteorological conditions and hydrological processes. During the freshet phase from May 1 to June 15, the median E/I ratio of lakes decreased from 0.20 to 0.13 in response to freshet runoff and limited evaporation due to lake ice presence that persisted for the duration of this phase. During the following warm, dry, and ice-free period from June 15 to July 26, designated the evaporation phase, the median E/I ratio increased to 0.19. During the brief soil wetting phase, E/I ratios did not respond to rainfall between July 26 and August 2, likely because watershed soils absorbed most of the precipitation which resulted in minimal runoff to lakes. The median E/I ratio decreased to 0.11 after a cool and rainy August, identified as the recharge phase. Throughout the sampling period, δ_I remained relatively stable and most lakes contained a greater amount of rainfall-sourced water than snow-sourced water, even after the freshet phase due to snowmelt bypass. The range of average E/I ratios we observed at lakes (0.00 – 0.43) was relatively narrow and low compared to thermokarst lakes in other regions, likely owing to the large watershed area to lake area ratio (WA/LA), efficient preferential flow pathways for runoff, and a shorter ice-free season. Lakes with smaller WA/LA tended to have higher E/I ratios ($R^2 = 0.74$). An empirical relationship between WA/LA and E/I was derived and used to predict the average E/I ratio of 7340 lakes in the region, which identified that these lakes are not vulnerable to desiccation, given that E/I ratios were <0.33. If future permafrost thaw and warming cause less runoff to flow into lakes, we expect that lakes with smaller WA/LA will be more influenced by increasing evaporation, while lakes with larger WA/LA will be more resistant to lake-level drawdown. However under wetter conditions, lakes with larger WA/LA will likely experience greater increases in lake level and could be more susceptible to rapid drainage.

4.2 Introduction

Thermokarst lakes are common features in ice-rich permafrost terrain, occupying up to 25% of the land area (Woo, 2012). The water balance of thermokarst lakes are changing as arctic warming causes precipitation to shift from snowfall to rainfall (Bintanja and Andry, 2017; MacDonald et al., 2021), permafrost thaw alters the hydrological connectivity of lake watersheds (Wolfe et al., 2011; Walvoord and Kurylyk, 2016; Tananaev and Lotsari, 2022; Koch et al., 2022), longer ice-free periods increase evaporation (Prowse et al., 2011; Arp et al., 2015), and increased vegetation growth changes snow redistribution and snowmelt timing (Sturm et al., 2001; Essery and Pomeroy, 2004; Pomeroy et al., 2006). In many regions, expansion and contraction of thermokarst lakes has been observed demonstrating that lake water balances are not responding uniformly to climate change (Smith et al., 2005; Plug et al., 2008; Marsh et al., 2009; Arp et al., 2011; Jones et al., 2011; Andresen and Lougheed, 2015; Travers-Smith et al., 2021).

Previous studies have demonstrated that knowledge of meteorological conditions and lake and watershed attributes, and their influence on lake water balance, can explain why thermokarst lakes react non-uniformly to climate change (Wolfe et al., 2011; Turner et al., 2014; Nitze et al., 2017; Wan et al., 2020). Key drivers of lake water balances include the relative size of a lake within its watershed (Watershed Area/Lake Area, WA/LA), rainfall and snowfall patterns, permafrost dynamics, wildfire, vegetation cover, and ice-free season length (Turner et al., 2014; Arp et al., 2015; MacDonald et al., 2017; Wan et al., 2020). For example, Turner et al. (2014) found that thermokarst lakes in Old Crow Flats, Yukon, with higher evaporation-inflow ratios (E/I) tended to have smaller WA/LA ratios, reflecting the control of watershed area on the amount of inflow a lake receives. Arp et al. (2015) found that lakes in the Alaskan Coastal Plain with bedfast ice became ice-free sooner than lakes with floating ice, causing bedfast lakes to lose more water to evaporation as a result of a longer ice-free season.

In several studies, water isotope (δ^{18}O and δ^{2}H) analysis has been the primary method used

to efficiently characterize the water balance of a large number of thermokarst lakes because the isotope composition provides an integrated measure of influential hydrological processes (Gibson, 2002; Edwards et al., 2004; Turner et al., 2014; Narancic et al., 2017). Two key metrics of lake water balance modelled using water isotope data include the average isotope composition of lake source waters (δ_I), which can then be related to the measured isotope composition of different water sources (Yi et al., 2008) and the ratio of evaporation-to-inflow (E/I) (Gibson et al., 1993). Sampling lake water for isotope analysis multiple times throughout the year provides data to assess the response of lake water balances to different hydrological processes, which can be related to meteorological conditions and compared to lake and watershed attributes. Recently, MacDonald et al. (2017) compared E/I and δ_I of thermokarst lakes from six regions in northern North America and found a wide range of water balances that were influenced by local meteorological conditions, permafrost extent and vegetation characteristics. In some locations, such as the Alaskan Coastal Plain, E/I ratios were mostly below 0.2, whereas lakes in the Hudson Bay Lowlands of northeastern Manitoba typically possessed E/I ratios >0.5, with some lakes trending towards desiccation.

This study aims to evaluate how meteorological conditions, hydrological processes, and lake and watershed attributes influence the δ_I and E/I of lakes located in the tundra uplands east of the Mackenzie Delta in the Northwest Territories, Canada (Figure 4.1). A previous study in this region showed that only 5-53% of pre-snowmelt lake water is replaced by freshet on average, because snowmelt bypass leads to minimal mixing between freshet and pre-snowmelt lake water (Bergmann and Welch, 1985; Wilcox et al., 2022b). Snowmelt bypass occurs when less dense (~0℃) freshet runoff flows underneath lake ice and passes through a lake without mixing with and replacing the deeper and denser (<4℃) lake water. With this study we explore whether snowmelt bypass influences summertime lake water balances, given that in other regions thermokarst lakes are prone to desiccation when they retain little snowmelt (Bouchard et al., 2013). We also investigate how watershed characteristics that have been identified to influence lake water balance in other regions, such as WA/LA, influence lake water balances. We then use the relationship found between average

E/I and watershed characteristics to predict average E/I for lakes in the region and assess their vulnerability to climate change.

4.3 Study area

The thermokarst lakes in this study are located in the tundra uplands east of the Mackenzie Delta in the northwest region of the Northwest Territories, Canada (Figure 4.1). The landscape is comprised of rolling hills and has been shaped by the thaw of ice-rich permafrost, evidenced by the thousands of thermokarst lakes in the region (Rampton, 1988; Burn and Kokelj, 2009). Hillslopes are well-drained by the network of peat channels that facilitate subsurface flow between mineral earth hummocks (Quinton and Marsh, 1998), while flatter areas are typically drained by high-centred ice-wedge polygons (Burn and Kokelj, 2009). Vegetation consists of tall shrub (>1 m), low shrub (~0.5 m), and shrub-free landcover types containing lichen, moss, and tussocks (Lantz et al., 2010; Grünberg et al., 2020).

We selected 25 lakes that span a range of watershed sizes (6.45 to 203.56 ha) and lake surface areas, among other characteristics, along a ~70 km stretch of the Inuvik - Tuktoyaktuk Highway (Figure 4.1, Table 4.1). Nineteen of the lakes are headwater lakes and the other six lakes are downstream of other sampled lakes (Table 4.1). All lakes have a defined outlet channel and many lakes have defined channelized inflows from their watersheds in the form of small ephemeral streams or ice-wedge polygon troughs.

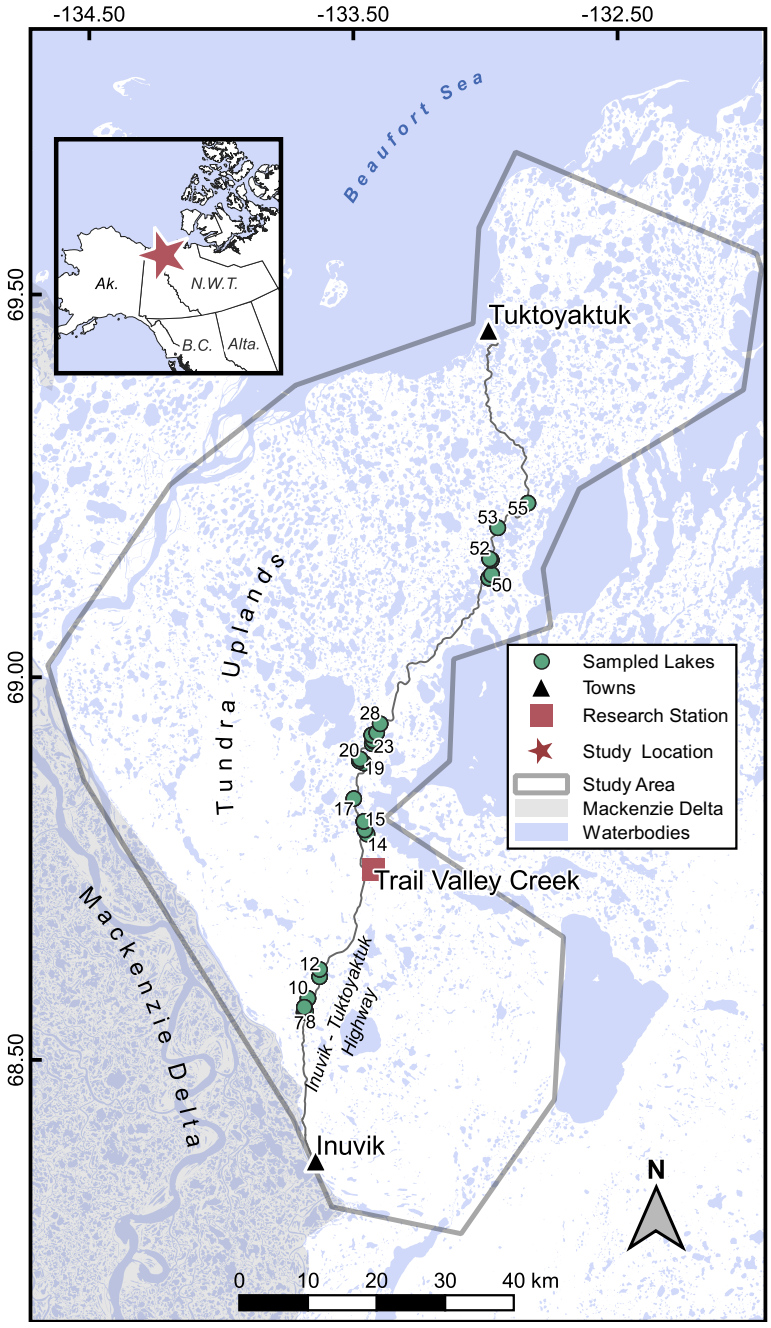

Figure 4.1 Study area showing locations of thermokarst lakes where water samples for isotope analysis were obtained. The study location relative to northwestern North America is shown in the inset map. Not all lakes are labeled on the map, but lakes are numbered sequentially from south to north.

Table 4.1 Lake and watershed attributes and isotope derived hydrological indicators for all lakes.

Lake	Latitude (dec deg.)	Lake Depth (m)	Lake Elevation (m asl)	% Polygon Area	Watershed Slope (°)	Lake Area (ha)	Watershed Area (ha)	WA/LA	Headwater Lake?	Upstream Lake(s)	Drainage Density (m ha^{-1})	E/I Average	δ_I Average (‰ $\delta^{18}O_I$)
7	68.557	2.2	89.0	0.00	1.30	2.94	6.45	2.62	yes	none	0.00	0.278	-19.816
8	68.559	2.3	88.9	0.00	2.63	2.07	15.67	4.41	no	7	0.00	0.205	-20.582
9	68.564	1.0	86.4	29.84	1.20	59.56	203.56	3.77	no	7,8,10	22.28	0.398	-18.193
10	68.576	1.7	87.9	5.17	1.42	90.48	168.58	1.86	yes	none	7.40	0.352	-18.849
11	68.604	1.9	82.7	2.53	2.10	1.26	21.76	17.32	yes	none	12.68	0.039	-19.843
12	68.613	2.6	90.8	0.00	2.45	8.19	23.05	2.81	no	11	0.51	0.429	-21.838
14	68.789	1.4	51.9	8.07	3.01	10.65	60.64	5.70	yes	none	1.24	0.088	-20.348
15	68.795	1.6	57.2	1.62	2.73	5.98	29.83	4.99	yes	none	0.00	0.170	-18.813
16	68.805	3.2	51.5	12.57	4.04	1.23	19.75	16.02	yes	none	4.86	0.043	-19.648
17	68.836	1.1	39.1	8.23	4.38	3.27	39.88	12.20	yes	none	11.53	0.083	-20.214
19	68.882	2.5	39.2	4.91	4.27	5.50	38.98	7.09	yes	none	5.79	0.096	-19.690
20	68.885	2.7	36.7	2.76	4.69	2.17	19.93	9.18	yes	none	3.04	0.095	-19.331
21	68.887	1.8	35.5	1.87	5.33	2.75	10.91	10.31	no	20	6.86	0.155	-20.071
22	68.907	3.7	33.6	4.11	5.33	3.41	23.67	18.25	no	23,24	6.12	0.115	-19.751
23	68.910	3.0	34.9	1.22	5.35	1.83	22.73	20.40	no	24	4.88	0.042	-19.221
24	68.911	3.0	38.3	4.49	4.69	0.37	11.10	30.10	yes	none	9.69	-0.014	-19.152
26	68.918	1.5	38.4	4.71	4.69	4.68	17.89	3.83	yes	none	0.00	0.246	-18.449
27	68.921	3.1	45.4	0.00	6.21	1.28	8.57	6.70	yes	none	0.00	0.166	-20.518
28	68.933	2.2	24.1	9.58	4.66	2.32	92.08	39.69	yes	none	22.73	0.014	-19.278
49	69.119	2.2	8.6	4.06	3.18	18.20	46.23	2.54	yes	none	0.79	0.305	-17.451
50	69.123	1.7	8.3	2.92	3.85	8.70	31.92	3.67	yes	none	0.00	0.230	-17.534
51	69.142	2.3	3.8	0.00	4.90	2.29	12.01	5.26	yes	none	0.00	0.193	-18.455
52	69.144	4.1	6.3	1.26	3.93	24.32	49.92	2.05	yes	none	0.00	0.322	-17.008
53	69.184	2.3	4.8	8.71	6.54	0.46	11.21	24.21	yes	none	10.05	0.131	-19.380
55	69.215	1.8	2.3	0.00	2.12	1.61	8.11	5.03	yes	none	0.00	0.175	-17.706
Min	68.557	1.0	2.3	0.00	1.2	0.37	6.45	1.86	n/a	n/a	0.00	-0.014	-21.838
Avg	68.871	2.3	43.4	4.75	3.8	10.43	39.78	10.40	n/a	n/a	5.218	0.160	-19.246
Max	69.215	4.1	90.8	29.84	6.54	90.48	203.56	39.69	n/a	n/a	22.73	0.429	-17.008

4.4 Methods

4.4.1 Lake water and precipitation sampling and analysis of isotope data

Water samples from the 25 thermokarst lakes were collected on five days (May 1, June 15, July 26, August 2, September 3) during 2018 for water isotope analysis. Samples were collected on May 1 through a hole augured through the ice in the centre of each lake to capture the pre-snowmelt lake water balance conditions. The May 1 samples also represent the hydrological status of lakes during the freeze-up period of 2017, since virtually no hydrological activity occurs during the winter months due to the complete freezing of the soil and lake surface. Because May 1 water samples were influenced by fractionation that occurred during lake ice formation, the isotope compositions were corrected to represent the isotope composition of the lake before lake ice formation took place (Wilcox et al., 2022b). Lake water samples were corrected for ice fractionation by estimating the fraction of lake water that had been frozen and the corresponding amount of isotopic depletion of lake water that would have occurred assuming the lake was a closed system, following Ferrick et al. (2002). June 15 was chosen as it marked the first day of the ice-free season for most lakes and was intended to capture the influence of snowmelt bypass, however the southernmost lakes (Lakes 7-12) became ice-free on June 7, and some of the northernmost lakes (Lakes 49-55) became ice-free on June 17 or June 18. More information about ice-correction and the response of lakes to snowmelt bypass is provided by Wilcox et al. (2022b). Next, samples were obtained on July 26 to capture the effects of evaporation and rainfall in the early open-water season, and before a large, forecasted rainfall event occurred. Samples were then collected on August 2 to capture the influence of a week-long rainy period following the sampling date on July 26. Samples were lastly taken on September 3 to assess lake water balance response to the relatively rainy and cool August weather prior to freeze-up. The four time periods between the five sampling dates are identified as “P1” (May 1 to Jun. 15), “P2” (Jun. 15 to Jul. 26), “P3” (Jul. 26 to Aug. 2), and “P4” (Aug. 2 to Sept. 3).

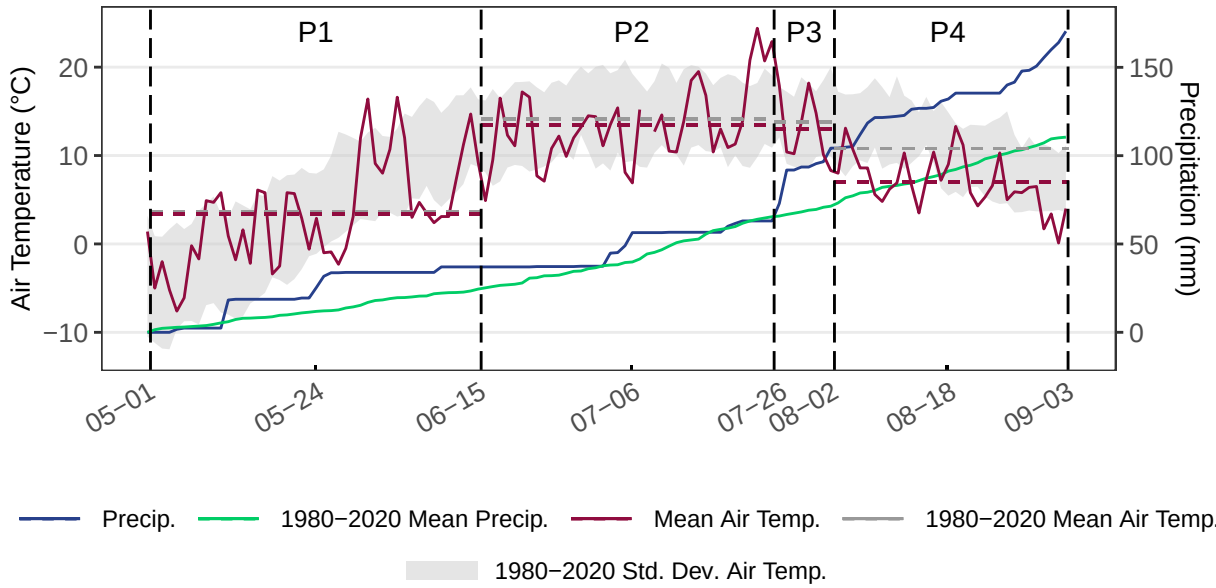

Figure 4.2 Air temperature and precipitation during the sampling period and the 1980-2020 mean, as recorded at Inuvik (WMO ID: 71364) (Figure 4.1). Meteorological data were retrieved from Environment and Climate Change Canada (2019a). The five days when water samples were taken from lakes are shown by the vertical dashed lines. The periods between the sampling dates are labeled P1, P2, P3, and P4. Mean daily air temperature for 2018 and 1980-2020 for each period is indicated by the horizontal dashed lines.

From June 15 onward, water samples were collected at the shoreline of each lake where water was freely circulating. Samples of end-of-winter snow and open-water season rainfall were obtained to determine the average isotope composition of rain (δ_R) and snow (δ_S). Snow samples (n = 11) were collected from the region in late April by taking a vertical core of the end-of-winter snowpack using a tube, completely melting the snow in a sealed plastic bag, and then filling a sampling bottle with the melted snow. Rainfall (n = 13) was collected between May and September in Inuvik using a clean high density polyethylene container, which was then transferred into a sample bottle shortly after precipitation ceased. All samples were stored in 30 mL high-density polyethylene bottles. A Los Gatos Research (LGR) Liquid Water Isotope Analyser, model T-LWIA-45-EP was used to measure the ratio of $^{18}O/^{16}O$ and $^{2}H/^{1}H$ in each sample at the Environmental Isotope Laboratory at the University of Waterloo. Isotope compositions are expressed in standard

δ-notation, such that:

$$\delta_{sample} = \frac{R_{sample}}{R_{VSMOW}} - 1 \tag{4.1}$$

where R represents the ratio of $^{18}O/^{16}O$ or $^{2}H/^{1}H$, and VSMOW represents Vienna Mean Standard Ocean Water. Isotope values are normalized for Standard Light Antarctic Precipitation to $\delta^{18}O$ = -55.5 ‰ and $\delta^{2}H$ = -428 ‰ (Coplen, 1996). Each isotope measurement consisted of 8 injections of roughly 1000nL sample volume, with the first 2 injections being discarded and the remaining 6 injections averaged to produce the measurement value. All samples were pre-filtered to 0.45 micron into 12x32mm septum vials. Every fifth sample was measured a second time to determine the analytical uncertainties, which were ±0.1‰ for $\delta^{18}O$ and ±0.6‰ for $\delta^{2}H$, calculated as two standard deviations from the difference between the duplicate samples. VSMOW and Vienna Standard Light Antarctic Precipitation (VSLAP) standards provided by LGR were used to calibrate the instrument initially, and VSMOW and VSLAP standards were analyzed intermittently throughout the sample run to confirm the accuracy of the instrument.

4.4.2 Isotope framework, δ_I and E/I

The isotope data were initially described and interpreted with respect to an 'isotope framework' that consists of two fundamental linear relationships that form when isotope data is plotted with $\delta^{18}O$ on the x-axis and $\delta^{2}H$ on the y-axis ('$\delta^{18}O$-$\delta^{2}H$ space'). The isotope composition of precipitation from anywhere in the world tends to plot closely to the Global Meteoric Water Line (GMWL), a strong linear correlation in $\delta^{18}O$-$\delta^{2}H$ space which is defined as $\delta^{2}H = 8.0 * \delta^{18}O + 10$ (Craig, 1961). However, the slope and intercept of a Meteoric Water Line can vary for precipitation collected at a single location: the Local Meteoric Water Line (LMWL) represents the expected isotope composition of precipitation in a region. We estimated the LMWL for Inuvik using a linear regression through rainfall and snowfall isotope compositions. The average isotope composition of rainfall (δ_R) and snowfall (δ_S) were calculated by averaging the isotope composition of all the

rainfall and snowfall samples we collected respectively, with δ_P representing the average of δ_S and δ_R. The LMWL equation we derived was $\delta^2H = 7.1 * \delta^{18}O - 10.0$, which compared closely to the LMWL derived by Fritz et al. (2022), who used precipitation samples collected between 2015 and 2018 in Inuvik and estimated the Inuvik LMWL to be $\delta^2H = 7.4 * \delta^{18}O - 6.7$. Both of these LMWLs compare closely with the LMWL derived from the Global Network of Isotopes in Precipitation (GNIP) data set, which is comprised of precipitation samples in Inuvik between 1986 and 1989 and gives an LMWL of $\delta^2H = 7.3 * \delta^{18}O - 3.6$ (IAEA/WMO, 2023). We considered using the LMWL, δ_S, δ_P and δ_R values produced by Fritz et al. (2022), however we decided to use the LMWL we developed since it more closely represented the input waters during the study period, and the δ_S, δ_P and δ_R values derived by Fritz et al. (2022) were within 0.6‰ (δ^{18}O) of the values we obtained.

Evaporated waters tend to plot along a Local Evaporation Line (LEL), which can be defined independent of measured lake water isotope compositions. Using this approach and for the case of a lake fed by waters of mean annual isotope composition of precipitation, the LEL was anchored at δ_P and at the maximum isotopic enrichment that can be achieved for a given set of environmental conditions (δ^*), which is dependent on air temperature, relative humidity and the isotope composition of atmospheric moisture in the region (Gonfiantini, 1986). Along the LEL exists a useful reference point where the amount of evaporation a water body is experiencing is equal to the amount of water input, defined as δ_{SSL} (steady-state lake water isotope composition of a terminal basin). When lake water isotope compositions are plotted in δ^{18}O-δ^2H space, they typically plot near the LEL, with more evaporated lakes plotting closer to δ^* and less evaporated lakes plotting closer to δ_P. Lakes preferentially sourced by rainfall will tend to plot above the LEL, whereas lakes preferentially influenced by snowmelt will tend to plot below the LEL, owing to the normally distinctive isotope composition of rainfall and snowmelt.

Isotope compositions of the lakes were used to estimate the average isotope composition of source water (δ_I, or $\delta^{18}O_I$ when referring to just the oxygen isotope compositions). We followed

the coupled isotope tracer method introduced by Yi et al. (2008) which of has been applied in a variety of northern locations (Turner et al., 2014; MacDonald et al., 2017; Remmer et al., 2020). Calculating δ_I using the approach of Yi et al. (2008) involves generating a lake-specific evaporation line for each lake water isotope composition. This approach assumes that all lakes tend towards δ^* as they evaporate, and the lake-specific evaporation line is defined as the line that intersects the lake water isotope composition and δ^* in δ^{18}O-δ^2H space. δ_I is then calculated as the point of intersection between a lake-specific evaporation line and the LMWL.

We used these δ_I values to calculate the ratio of evaporation-to-inflow (E/I):

$$E/I = \frac{\delta_I - \delta_L}{\delta_E - \delta_L} \tag{4.2}$$

where δ_L is the isotope composition of the lake water and where δ_E is the isotope composition of evaporated vapour from the lake (Gonfiantini, 1986). More detailed information about the calculation of the isotope framework components, δ_I and E/I is provided in Appendix 4.8.1.

4.4.3 Meteorological conditions and lake and watershed attributes

The end of winter snowpack at Trail Valley Creek contained 141 mm of snow water equivalent, similar to the 1991-2019 mean of 147 mm (Marsh et al., 2019). Air temperature at Inuvik was within a degree of the long-term mean during P1, P2 and P3, but P4 was 3.8°C cooler than the long-term mean (Figure 4.2). P1 and P2 experienced a combined 72.9 mm of rainfall, close to the long-term mean of 66.0 mm for this period, while P3 and P4 experienced 107.3 mm of rainfall, more than double the long-term mean of 45.0 mm for this period (Figure 4.2).

Multiple lake and watershed attributes for each lake were quantified for comparison with δ_I and E/I. Lake-specific properties included surface area, depth, latitude, and elevation, while watershed-specific properties included surface area, mean hillslope angle, drainage density, vegetation cover and ice-wedge polygon coverage (Table 4.1). Within each watershed, the areas of

ice-wedge polygons were identified visually from satellite imagery and digitized manually. Drainage density was calculated as the length of all flowpaths with a contributing area greater than 5000 m^2, and then divided by the total area of the watershed. A threshold of 5000 m^2 was chosen as this was roughly the threshold when water tracks became visible in optical satellite images. Vegetation height in each watershed was quantified using the remote sensing vegetation height product produced by Bartsch et al. (2020), which provides vegetation height at 20 metre spatial resolution with a RMSE of 45 cm in vegetation height. All spatial analysis was carried out using ArcMap 10.7.1 (ESRI, 2019).

To evaluate whether lake and watershed properties were correlated with lake water balance metrics derived from water isotope data, linear regressions between lake and watershed properties and E/I and δ_I were tested. Only correlations where $p < 0.01$ were considered significant. The distribution of each variable was plotted on a histogram and data were mathematically transformed if the distribution was non-uniform. Statistical analysis was performed using R 4.1.0 (R Core Team, 2021).

A correlation was identified between WA/LA and average E/I ($R^2 = 0.82$) and we used this relationship to predict average E/I for lakes in the region with areas >0.25 ha (n = 7454, Figure 4.1). Watershed area was estimated, including the 25 lakes sampled for isotope composition, by applying the D8 water routing algorithm (O'Callaghan and Mark, 1984) to the 2 m resolution the digital elevation model ArcticDEM (Porter et al., 2018). The ratio of WA/LA was calculated for each lake by dividing the total watershed area by the total area of the lake(s) in the watershed. In rare cases, watersheds were not delineated accurately and part of the watershed was clipped to the lake boundary due to slight offsets between the lake layer and ArcticDEM. We rejected all watersheds where WA/LA <1.5, as all watersheds we inspected that met this criteria were improperly delineated due to the offset error described. After rejecting all watersheds where WA/LA <1.5, a total of 7340 watersheds remained.

4.5 Results

4.5.1 Seasonal evolution of lake water balances

Lake water isotope compositions span from near the LMWL to exceeding δ_{SSL}, reflecting a range of lake water balance conditions (Figure 4.3). Lake water isotope compositions plot close to the LEL, indicating that the isotope framework has been well estimated using the Trail Valley Creek meteorological data. Only two lakes plot beyond δ_{SSL}, but they lie above the LEL and possess E/I ratios less than 1 (see below) because their δ_I values are higher than δ_P. As expected, rain and snow isotope compositions plot in two distinct clusters along the isotopically-enriched and depleted segments of the LMWL, respectively, permitting rain-influenced and snow-influenced δ_I to be distinguished. Most lakes plot slightly above the LEL, signifying that the δ_I of most lakes is more reflective of rain than snow.

In general, we observed distinct shifts in lake water isotope composition, $\delta^{18}O_I$ and E/I between sampling dates. Shifts in E/I between sampling dates were often more pronounced than shifts in $\delta^{18}O_I$. During P1 (May 1 to June 15), $\delta^{18}O$ decreased from a median of -15.04‰ (-17.53‰ to -13.81‰ inter-quartile range [IQR]) to -16.15‰ (-17.89‰ to -15.43‰ IQR) and $\delta^{2}H$ values decreased from -130.35‰ (-139.08‰ to -120.88‰ IQR) to -132.27‰ (-142.41‰ to -125.77‰ IQR) (Figure 4.3). At the same time, the range of $\delta^{18}O_I$ values decreased and the median decreased slightly from -19.36‰ (-20.33‰ to -18.34‰ IQR) to -19.59‰ (-20.34‰ to -18.81‰ IQR) (Figure 4.4a). The median (and range) of E/I values also decreased during P1 from 0.20 (0.07 to 0.38 IQR) to 0.13 (0.07 to 0.18 IQR) (Figure 4.4b). The median change in E/I was -0.08 (Figure 4.4c). The reduction in E/I values that occurred during P1 was larger than in any other phase (Figure 4.4c).

During P2 (June 15 to July 26), lake water isotope values increased slightly. The median $\delta^{18}O$ increased from -16.15‰ (-17.89‰ to -15.43‰) to -15.63‰ (-17.33‰ to -14.22‰ IQR) and the median $\delta^{2}H$ increased from -132.27‰ (-142.41‰ to -125.77‰ IQR) to -129.50‰ (-137.90‰ to -124.99‰ IQR) (Figure 4.3). During P2, $\delta^{18}O_I$ increased slightly from -19.59‰ (-20.34‰

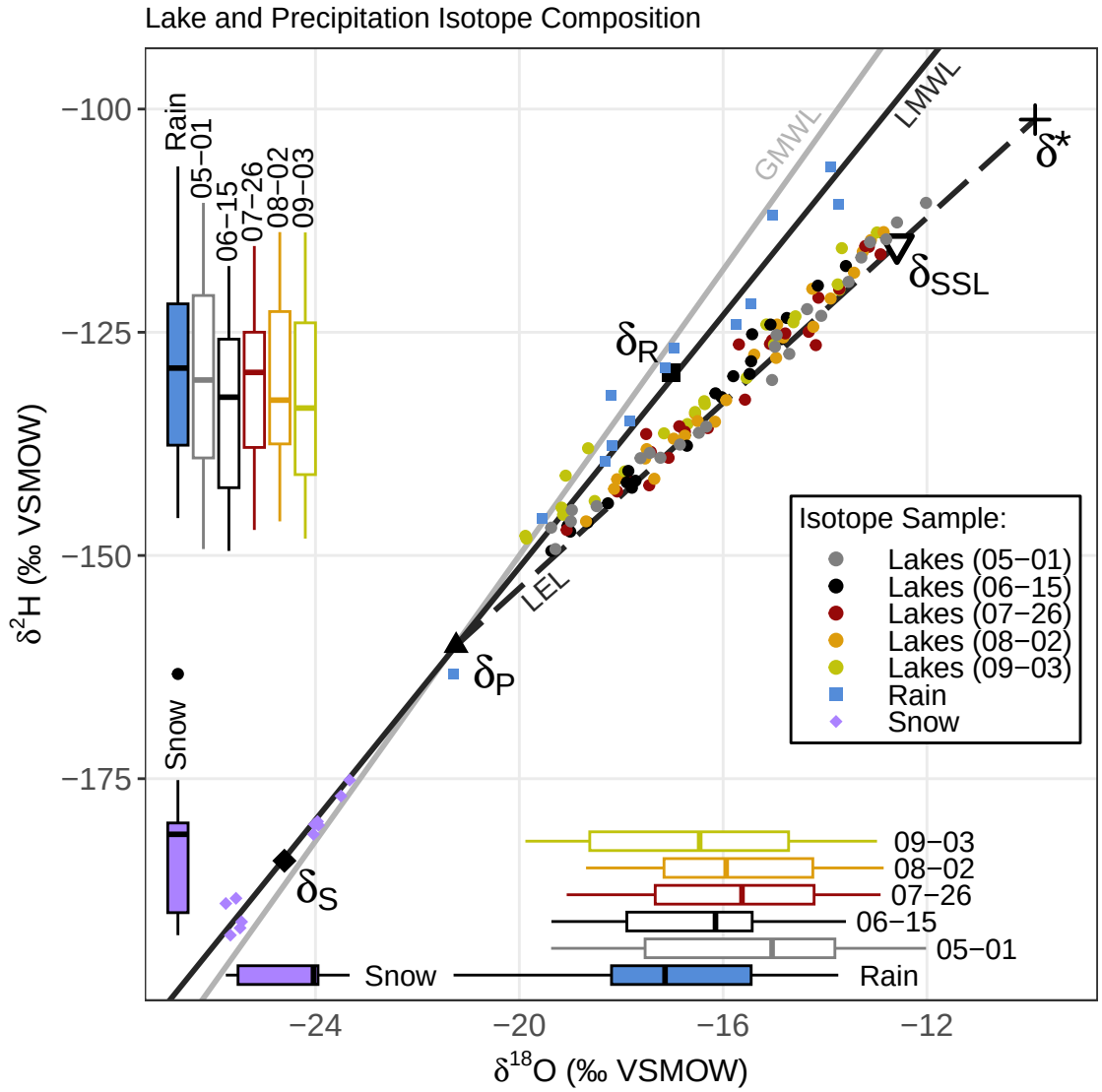

Figure 4.3 Isotope values for all lake and precipitation samples, with their respective ranges along each axis illustrated by boxplots, plotted in δ^{18}O-δ^{2}H space, as deviations per mil from Vienna Standard Mean Ocean Water (VSMOW). Local Meteoric Water Line (LMWL, black solid line, $\delta^2 H = 7.1 * \delta^{18} O - 10.0$) is calculated as a regression through snow samples collected throughout the study region and rain samples collected from Inuvik in 2018 (n = 24). The average isotope composition of end-of-winter snow samples (δ_S), rainfall samples (δ_R), and the average of δ_S and δ_R (δ_P) are labelled along the LMWL. The Local Evaporation Line (LEL, dark grey dashed line), the Global Meteoric Water Line (GMWL, light solid grey line), the maximum isotopic enrichment possible for a waterbody (δ^*), and the point at which evaporation is equal to inflow (E/I = 1, δ_{SSL}) are added for reference.

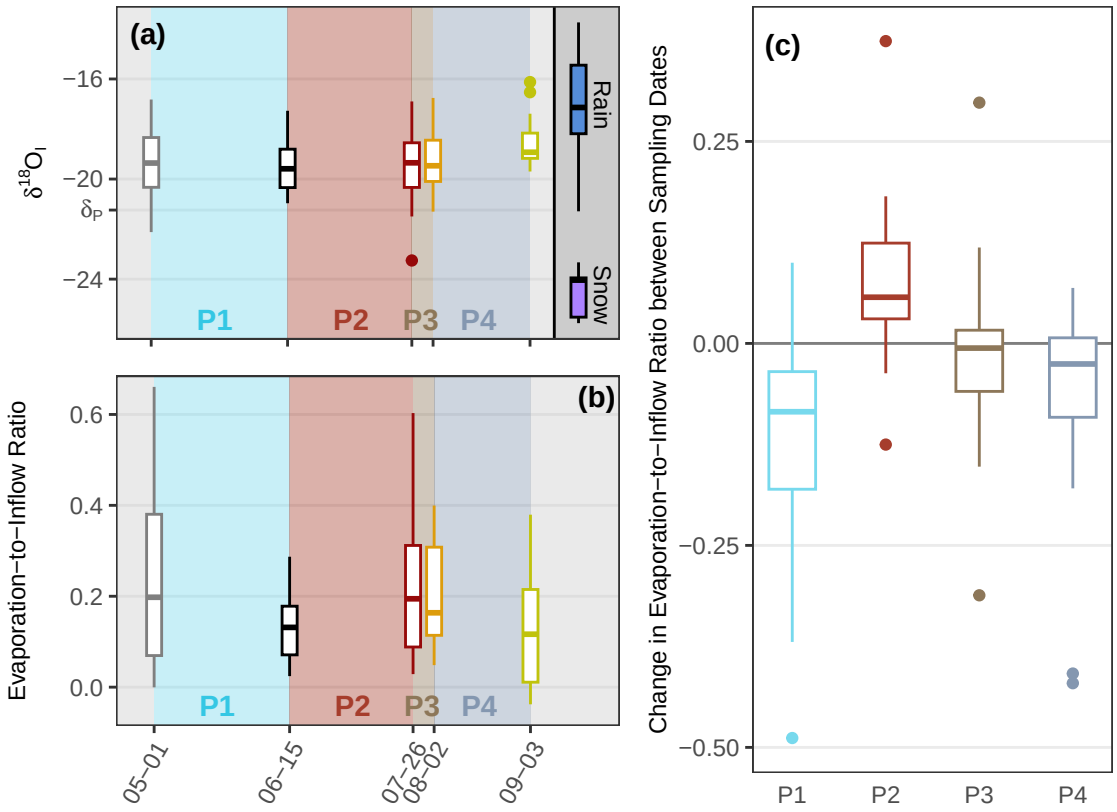

Figure 4.4 (a) The distribution of $\delta^{18}O_I$ for each sampling date with rain and snow isotope compositions for reference. (b) The distribution of E/I values at all lakes across the five sampling dates. (c) The lake-specific change in E/I between the sampling dates was calculated as $\Delta[E/I] = [E/I]^{Ln}_{t_2} - [E/I]^{Ln}_{t_1}$, where Ln represents a specific lake, and t represents a sampling date.

to -18.81‰ IQR) to -19.35‰ (-20.34‰ to -18.55‰ IQR) (Figure 4.4a). The median E/I ratio increased from 0.13 (0.07 to 0.18 IQR) to 0.19 (0.09 to 0.31 IQR) (Figure 4.4b). The median increase in E/I was 0.06 (0.03 to 0.12 IQR) although three lakes experienced a decrease in E/I (Figure 4.4c).

Lake water isotope values decreased marginally during P3 (July 26 to Aug 2). Median $\delta^{18}O$ decreased from -15.63‰ (-17.33‰ to -14.22‰ IQR) to -15.94‰ (-17.16‰ to -14.24‰ IQR) and median $\delta^{2}H$ decreased from -129.50‰ (-137.90‰ to -124.99‰ IQR) to -132.60‰ (-137.51‰ to -122.68‰ IQR) (Figure 4.3). E/I and $\delta^{18}O_I$ values also shifted minimally during P3. Median $\delta^{18}O_I$ decreased from -19.35‰ (-20.33‰ to -18.55‰ IQR) to -19.47‰ (-20.10‰ to -18.45‰ IQR) (Figure 4.4b). The median change in E/I was -0.01 (-0.06 to 0.02 IQR) with a near equal

number of lakes experiencing an increase or decrease in E/I (Figure 4.4c).

During P4 (August 2 to September 3), median $\delta^{18}O$ values decreased from -15.94‰ (-17.16‰ to -14.24‰ IQR) to -16.55‰ (-18.65‰ to -15.00‰ IQR) and $\delta^{2}H$ values decreased from -132.60‰ (-137.51‰ to -122.68‰ IQR) to -133.49‰ (-140.94‰ to -123.94‰ IQR) (Figure 4.3). On September 3, some lakes plotted close to the LMWL, indicating that their waters had experienced negligible amounts of evaporation (Figure 4.3). The median $\delta^{18}O_I$ values increased from -19.47‰ (-20.10‰ to -18.45‰ IQR) to -18.94‰ (-19.18‰ to -18.14‰ IQR) and the range of values narrowed and became more similar to rain (Figure 4.4a). Median E/I values also returned towards June 15 values by the end of P4, decreasing to a median of 0.11 (0.00 to 0.21 IQR) (Figure 4.4b). Two thirds of the lakes experienced a decrease in E/I and the median change in E/I was -0.03 (-0.09 to 0.01 IQR) (Figure 4.4c).

4.5.2 Correlation between lake and watershed attributes and lake water balance metrics

Variability among lakes in average E/I and $\delta^{18}O_I$ was partially explained by statistically significant relationships with lake and watershed properties. Average E/I was negatively correlated with WA/LA ($p < 0.0001$, Table 4.2, Figure 4.5a) and average watershed slope ($p = 0.0085$, Table 2) and was positively correlated with the log of lake surface area ($p < 0.0001$, Table 4.2). Thus, lakes that had higher E/I values tended to have relatively smaller watershed size, have a flatter watershed, and be larger in surface area. When these three variables are combined into a linear model, only WA/LA remained a significant predictor of average E/I ($p = 0.0002$) while lake area ($p = 0.1949$) and average watershed slope ($p = 0.8472$) became insignificant effects (Table 4.2). Both lake surface area and average watershed slope were correlated with WA/LA (Table 4.2). For the relationship between average E/I and WA/LA, the majority of downstream lakes were outliers, having higher than typical E/I ratios for a given WA/LA as they inherited evaporated waters from

Table 4.2 Significant correlations between $\delta^{18}O_I$, E/I, and explanatory variables. In cases where there are multiple explanatory variables, the p-values for each explanatory variable are listed respectively. Adjusted R^2 was used in order to control for the tendency of R^2 to increase as explanatory variables are added to a model (Yin and Fan, 2001). Adjusted R^2 was calculated as $R^2_{adj} = 1 - (1 - R^2) * ((n-1)/(n-m-1))$, where n is the sample size and m is the number of explanatory variables. p-values >0.05 are *italicized*.

Response Variable	Explanatory Variable(s)	p-value(s)	Adjusted R^2
Average E/I	log(WA/LA)	<0.0001	0.7361
Average E/I	log(Lake Area)	<0.0001	0.5092
Average E/I	Average Watershed Slope	0.0085	0.2332
Average E/I	log(WA/LA) + log(Lake Area) + Average Watershed Slope	0.0002, *0.1949*, *0.8472*	0.7339
Average Watershed Slope	log(Lake Area)	0.0040	0.2771
log(WA/LA)	log(Lake Area)	<0.0001	0.5150
log(WA/LA)	Average Watershed Slope	0.0022	0.3128
Average $\delta^{18}O_I$ (‰)	Lake Latitude	0.0027	0.3010
Average $\delta^{18}O_I$ (‰)	Lake Elevation	0.0029	0.2954
Lake Elevation	Lake Latitude	<0.0001	0.9695

upstream waterbodies (Figure 4.5a).

Average $\delta^{18}O_I$ was only correlated with two attributes: lake elevation (p = 0.0029) and latitude (p = 0.0027) (Table 2). Lakes at lower elevations and higher latitudes tended to have higher $\delta^{18}O_I$ values (Figure 4.5b). Lake elevation and latitude are also nearly perfectly correlated (R^2 = 0.97, Table 2), with lake elevation decreasing as latitude increases.

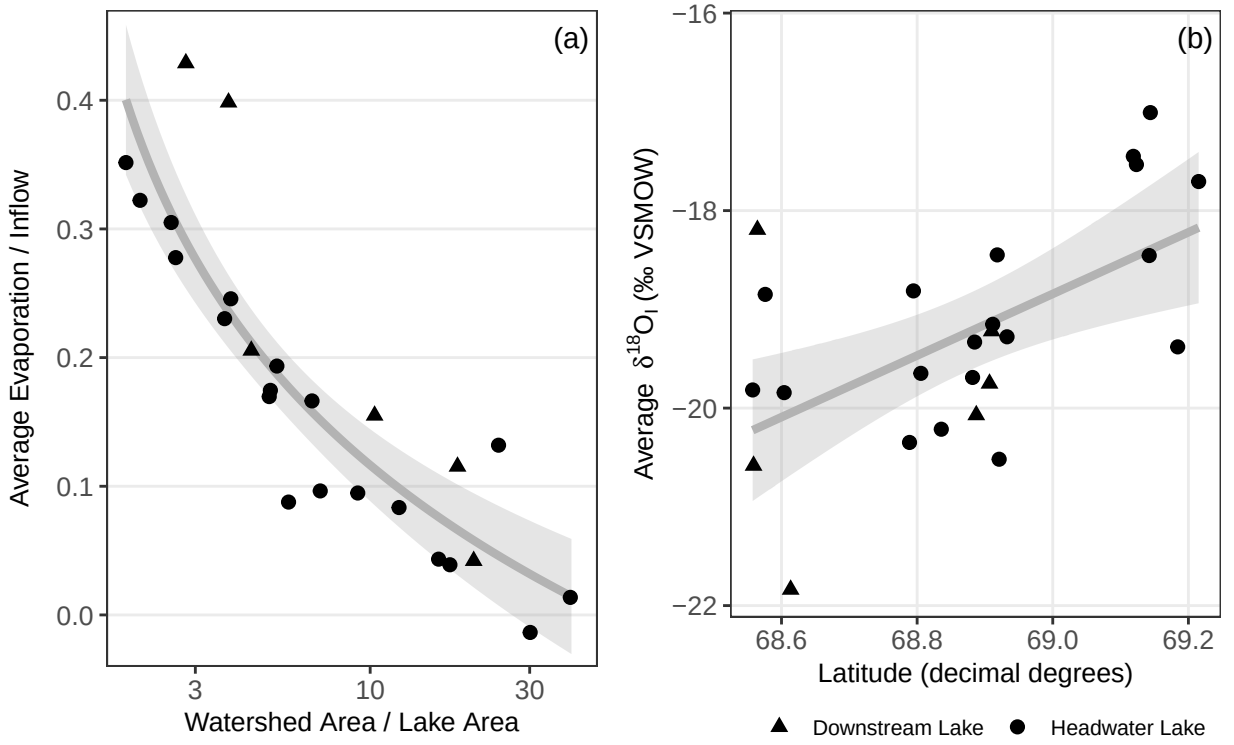

Figure 4.5 (a) Relationship between average evaporation-to-inflow ratio and watershed area/lake area for sampled lakes. The grey line represents a line of best fit between watershed area/lake area and the average evaporation-to-inflow ratio, such that y = log(x), with the 95% confidence interval shown in grey shading (R^2 = 0.74, p <0.0001). Note the logarithmic x-axis. (b) The relationship between latitude and δ_I. The grey line represents a linear line of best fit between δ_I and latitude, with the 95% confidence interval shown in grey shading (R^2 = 0.30, p = 0.0027).

4.6 Discussion

4.6.1 Influence of meteorological conditions on lake water balances

Water isotope measurements from five discrete time points provide context for characterizing the seasonal evolution of thermokarst lake water balances as a series of phases in relation to meteorological conditions and influential hydrological processes (Figure 4.6). A previous study at many of the same lakes by Wilcox et al. (2022b) observed the presence of snowmelt bypass (Henriksen and Wright, 1977; Hendrey et al., 1980; Bergmann and Welch, 1985) during the Freshet Phase (P1; Figure 4.6). Initial snowmelt runoff flowing into lakes did not mix with water

underneath lake ice because the ~0°C snowmelt runoff was less dense than the deeper, warmer waters beneath the lake ice, causing it to flow into and out of lakes without mixing with lake water. This resulted in a much smaller reduction in E/I than would have occurred if freshet runoff was able to mix with the entire lake water column. While snowmelt bypass does limit the recharge of lake waters during the Freshet Phase, the sheer volume of snowmelt runoff and lack of evaporation due to lake ice cover appears to compensate for the impact of snowmelt bypass and results in a greater reduction in E/I than any other period (Figure 4.4c).

During the Freshet Phase, $\delta^{18}O_I$ shifted towards the value of δ_P and not towards δ_S even though minimal rainfall fell during the period (Figure 4.2) and snowmelt runoff was flowing into lakes. Wilcox et al. (2022b) determined that by the time snowmelt runoff could mix with lake waters, the soil had begun to thaw and allowed snowmelt runoff to mix with soil water from the previous year before flowing into lakes. This resulted in a post-snowmelt $\delta^{18}O_I$ that was a mixture of snow-sourced and rain-sourced water (Figure 4.4a). Since only a small amount of snow-sourced water was incorporated into lakes during the Freshet Phase, the $\delta^{18}O_I$ of lakes remained primarily rain-sourced throughout the entire study period (Figure 4.4a).

The Evaporation Phase (P2; Figure 4.6) was characterized by minimal change in $\delta^{18}O_I$ (Figure 4.4a) and rising E/I ratios at nearly all lakes (Figure 4.4c), caused by the relatively dry and warm conditions that are typical for this region. Previous water balance studies conducted in this region also found that lake evaporation rates were higher as a result of substantial incoming solar radiation in June and July compared to August and September, and when inflow is minimal due to low precipitation (Marsh and Bigras, 1988; Pohl et al., 2009).

During the brief Soil Wetting Phase (P3; Figure 4.6), there was minimal change in $\delta^{18}O_I$ (Figure 4.4a) and E/I (Figure 4.4b) despite the 41.2 mm of rainfall, which represented 25% of the rainfall during the study period. This evidence suggests little runoff was generated by this event and that rainfall that fell directly on lakes had only a minor effect on lake water balances. We hypothesize that dry conditions preceding the rainfall event allowed soils to absorb the rainfall

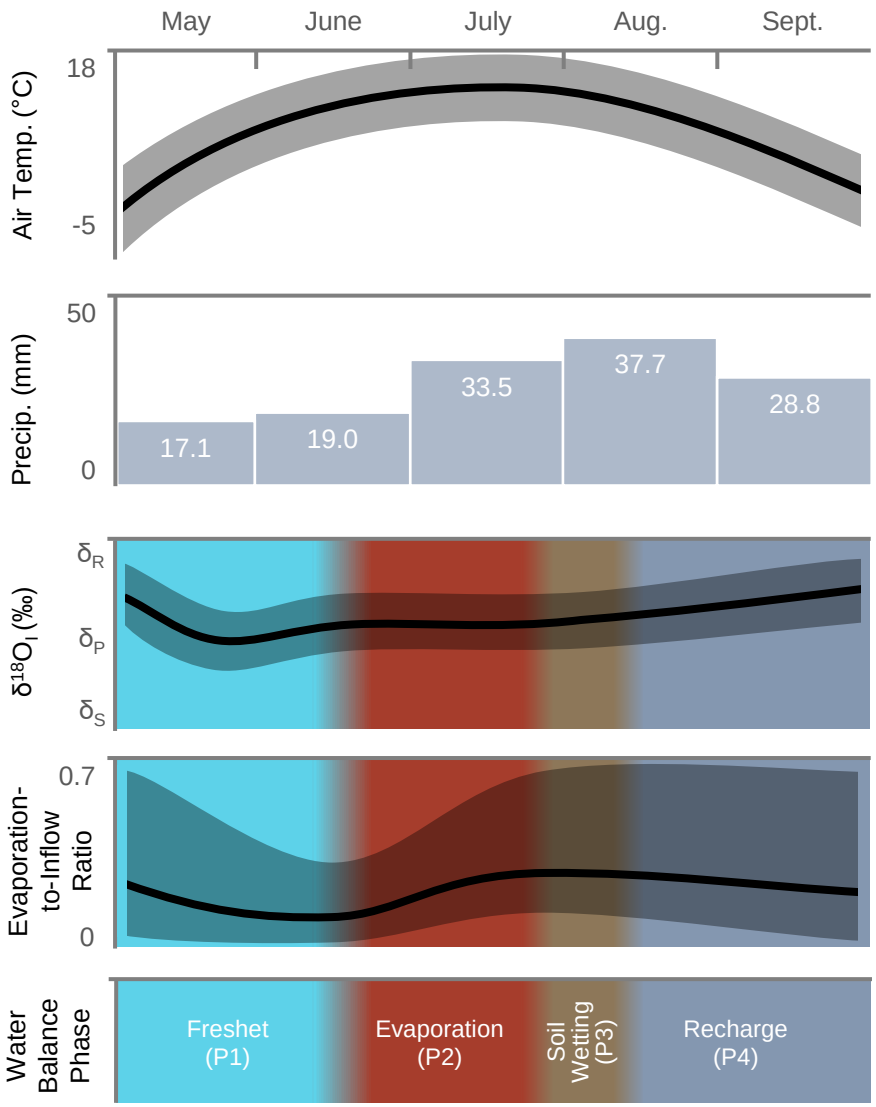

Figure 4.6 A simplified conceptual diagram showing the connections between meteorological conditions and the response of $\delta^{18}O_I$ and E/I used to designate water balance phases. Air temperature and precipitation data represent average values from 1980-2020. Shaded areas around the $\delta^{18}O_I$ and E/I lines represent the potential variability caused by lake and watershed attributes or meteorological conditions.

without becoming saturated sufficiently to generate much lateral flow. The lack of runoff in response to this rainfall event is expected given that antecedent soil moisture conditions have been observed to greatly influence the efficiency of runoff generation from rainfall events in areas underlain by continuous permafrost (Roulet and Woo, 1988; Kane et al., 1998; Favaro and Lamoureux, 2014; Stuefer et al., 2017). Since the first half of the summer is typically drier than the second half (Figure 4.6), soils generally experience drying throughout the first half of the summer before becoming rewetted.

The Recharge Phase (P4; Figure 4.6) was defined by the $\delta^{18}O_I$ of lakes becoming more similar to rainfall (Figure 4.4a) and E/I ratios decreasing to values similar to the beginning of the Freshet Phase (Figure 4.4b). The Recharge Phase of 2018 was 3.8°C cooler than average and experienced 66.1 mm of precipitation, exceeding the long-term mean of 37.2 mm (Figure 4.2). Given the cooler air temperatures, it is likely that evaporation rates also decreased and contributed to the decrease in E/I. Since the meteorological conditions were wetter and cooler than the long-term means, we expect the water balance conditions of the Recharge Phase captured in 2018 to be more representative of a later sampling date during a more normal climate year (e.g., late September). E/I ratios on May 1 were greater than September 3, suggesting that lakes received less inflow during the Recharge Phase during 2017 than during 2018 (Figure 4.4b).

Findings from previous studies of thermokarst lakes in this region imply that the four phases of lake water balance we observed are typical for this region. The four phases of seasonal water balance evolution we identified (Freshet, Evaporation, Soil Wetting, Recharge) roughly follow the pattern of seasonal changes in lake surface area observed by Cooley et al. (2019) who analyzed near-weekly satellite imagery of a large region which encompassed the lakes we studied. Cooley et al. (2019) observed initial decreases in total lake surface area during the Evaporation Phase, followed by stabilizing or increasing trends in lake surface area by the end of August. Additionally, Pohl et al. (2009) modeled the water balance for a single lake in our study region across a 30-year period, and identified that maximum lake level was most likely to occur in early June or late August/early

September, corresponding with the start of the Evaporation Phase and end of the Recharge Phase.

In comparison to the five thermokarst lake regions examined in a synthesis of isotope data by MacDonald et al. (2017), the relatively low E/I ratios and rainfall-like $\delta^{18}O_I$ values found at our study lakes compare most closely to lakes in the Alaskan Coastal Plain (ACP), where the majority of lakes also have an E/I < 0.25 and $\delta^{18}O_I$ similar to rain. This region is cooler during the summer and has a shorter ice-free season (Arp et al., 2015) than our study region, but receives less precipitation and is more lake rich (MacDonald et al., 2017), suggesting lakes likely have smaller watersheds than in our study region. The cooler and shorter summers in ACP, which decrease evaporation, may be offset by smaller watersheds and less precipitation, which decrease inflow, leading to similar E/I values as our study region. Our lakes differed from the more nearby OCF, where most lakes have an E/I between 0.25 and 0.75 but have a smaller WA/LA of ~3, whereas the average WA/LA of lakes we sampled was 9.5 (Table 4.1). OCF differs from our study region in that it is situated in a post-glacial lake bed underlain by fine-grained glaciolacustrine sediments (Hughes, 1972), resulting in a relatively flat landscape with poorer ability to convey runoff in comparison to our study region, where rolling hills are well drained by networks of peat channels with high hydraulic conductivity (Quinton and Marsh, 1998). These differences between OCF and our study region may explain the greater E/I values at the former, however our study year was cooler and wetter than average, which may also have contributed to the comparatively low E/I ratios.

4.6.2 Effects of lake and watershed attributes on E/I

While shifts in E/I over time can be attributed to changing meteorological conditions and hydrological processes, differences in E/I among lakes can be further explained by lake and watershed attributes. Most of the variability in average E/I among lakes can be explained by WA/LA (R^2 = 0.74, Figure 4.5a), as lakes with smaller WA/LA likely receive less inflow and have greater E/I ratios as a result. A similar inverse relationship between E/I ratios and WA/LA has also been observed in OCF (Turner et al., 2014), and the taiga-shield of the Northwest Territories (Gibson

and Edwards, 2002). Four of the six downstream lakes we sampled had anomalously high E/I ratios compared to their WA/LA (Figure 4.5a). Downstream lakes receive evaporated inflow from their upstream lakes, which is then evaporated further in the downstream lake, producing an enhanced E/I ratio. When downstream lakes are removed from the regression between E/I and WA/LA, the R^2 improves from 0.74 to 0.82.

We estimated E/I for lakes in the study area using the strong relationship between average E/I and WA/LA. This was done by delineating the watersheds of lakes larger than 0.25 ha in the study area (Figure 4.1) and applying the fitted regression between log(WA/LA) and average E/I for the headwater lakes we sampled:

$$AverageE/I = -0.10867 * \log(WA/LA) + 0.37007 \tag{4.3}$$

The resulting histogram of average E/I (Figure 4.7b) is primarily skewed towards larger values, because WA/LA is skewed towards smaller values (Figure 4.7a). An average E/I between 0.2 and 0.225 is most common for lakes indicating the lakes are dominated by inflow. At WA/LA >30, the estimated E/I becomes 0, and as a result 7% of lakes are predicted to have an average E/I of 0 (Figure 4.7b). None of the lakes appear to be approaching desiccation.

We note that this distribution of E/I values is dependent on the timing of our water sampling, the meteorological conditions present during the study period, and on the properties of the lakes that we selected. For example, the median lake depth of 34 lakes sampled in this region by Pienitz et al. (1997) was 3.0 m, similar to the lakes we measured (Table 4.1), however some lakes sampled by Pienitz et al. (1997) were up to 18.5 m in depth. The relationship we derived between WA/LA and E/I would likely weaken if deeper lakes had been sampled in our study, since lake surface area becomes less representative of lake volume when a wider range of lake depths are included. In that case, calculating the ratio of lake volume to watershed area could be a better predictor of E/I ratios.

We hypothesize that the hydrological response of lakes in this region to climate change will

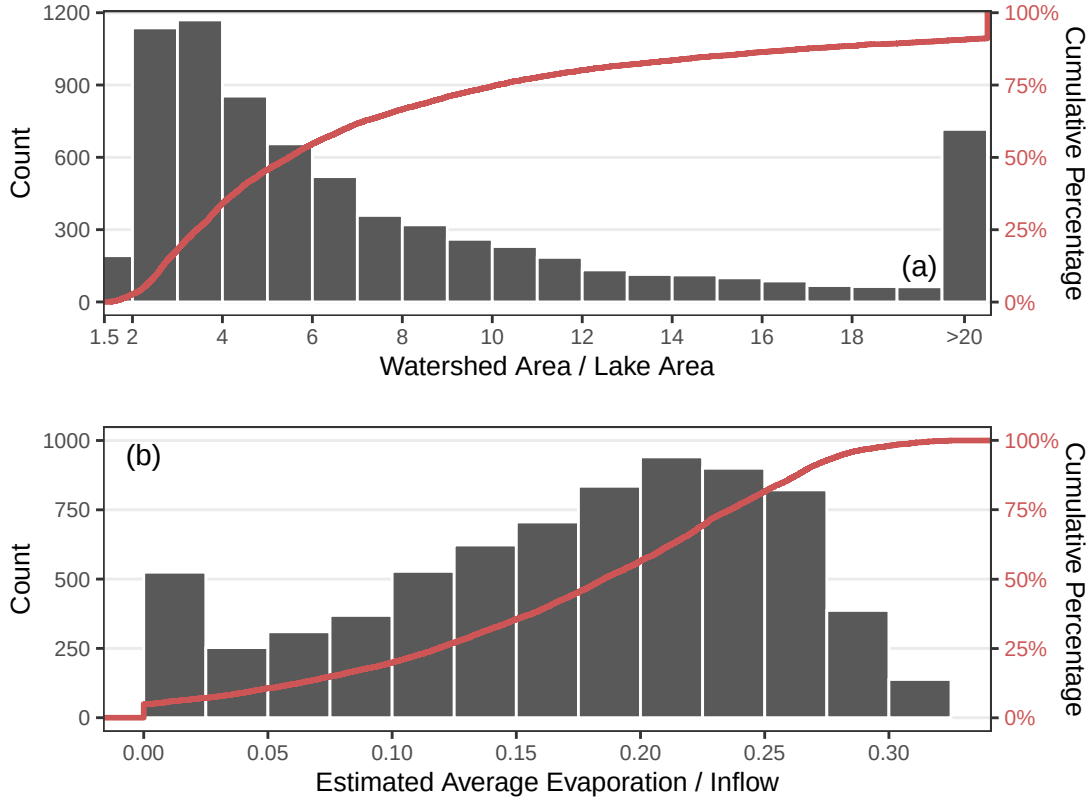

Figure 4.7 Distribution of (a) watershed area/lake area and (b) evaporation-to-inflow for 7340 lakes and their watersheds in the study area. Average evaporation-to-inflow is estimated using the relationship with watershed area/lake area of headwater lakes. Note that the leftmost bin in panel (a) is only half the width of other bins, reflecting the rejection of all WA/LA <1.5 that we applied when filtering the data.

be strongly influenced by their WA/LA. Recent predictions of future Arctic precipitation indicate greater rainfall, snowfall and more annual precipitation overall (Brown and Mote, 2009; Bintanja and Andry, 2017; Bintanja et al., 2020) and in OCF increased rainfall is already reducing lake E/I ratios (MacDonald et al., 2021). We would expect that under wetter conditions E/I ratios would decrease for all lakes, and the threshold where average E/I = 0 would also decrease. The logarithmic nature of the relationship between WA/LA and E/I indicates that average E/I is more sensitive to changes in inflow as WA/LA decreases. Therefore, we expect that lakes with smaller WA/LA would experience greater reductions in average E/I under a wetter future climate. We also hypothesize that lakes with larger WA/LA could be more vulnerable to rapid lake drainage because they receive more inflow and likely experience greater fluctuations in lake level as a result; rapid drainage is

typically triggered when extremely high water levels lead to the rapid thermo-mechanical erosion of a new lake outlet (Mackay, 1988; Brewer et al., 1993; Turner et al., 2010).

Alternatively, climate change may lead to a drier future for lakes, as ice-free periods lengthen, warmer air temperatures increase evaporation and permafrost thaw leads to landscape drying (Walvoord and Kurylyk, 2016; Koch et al., 2022; Webb and Liljedahl, 2023). A combination of such conditions has already caused lake contraction in western Greenland (Finger Higgens et al., 2019). If drier conditions prevail, given the logarithmic nature of the relationship between WA/LA and average E/I, we expect lakes with smaller WA/LA will experience greater increases in average E/I. If future climate change causes sufficiently dry conditions to cause lake desiccation, a large number of lakes in the study area could potentially be affected, given that the distribution of WA/LA in the region is skewed towards smaller values of WA/LA, with many lakes possessing a WA/LA <4 (Figure 4.7a). The 'drier future' scenario may seem less likely to result in lake desiccation given that lakes are currently dominated by inflow, however the portion of precipitation converted into runoff can be halved during dry periods when compared to wetter periods (Stuefer et al., 2017), further reducing runoff to lakes.

Future studies could build on our hypothesis that WA/LA will mediate the response of lakes to climate change by comparing past changes in lake surface area, via remote sensing and paleohydrological analyses, with WA/LA. We would expect that during drier periods, lakes with smaller WA/LA experienced greater reductions in lake surface area than lakes with larger WA/LA. Previous studies from this region have already found that lakes change in surface area in response to seasonal (Cooley et al., 2019) and multi-year (Plug et al., 2008) shifts in precipitation, indicating that changes to lake water balances can be observed by tracking changes in water surface area.

4.7 Conclusions

Water isotope-derived metrics were used to derive distinct seasonal phases of lake water balances for 25 thermokarst lakes in the tundra uplands east of the Mackenzie Delta (Northwest Territories, Canada). The Freshet Phase saw lakes experience a reduction in E/I and a shift of δ_I values towards δ_P, as a mixture of soil water and snowmelt-sourced freshet entered lakes and evaporation was minimal due to lake ice cover. Following this period was the Evaporation Phase, where minimal precipitation and warm and sunny conditions led to increasing E/I ratios and no change in δ_I. Then, a brief and intense period of rainfall led to minimal response in E/I and δ_I at lakes, as dry soils absorbed most of the precipitation during the Soil Wetting Phase. In the final stages of summer during the Recharge Phase, air temperatures declined and precipitation was unseasonably high, causing reductions in E/I and a shift of δ_I towards δ_R as lakes received increased runoff from their watersheds and evaporation rates were reduced.

Comparison of water isotope-derived lake water balance components with lake and watershed attributes shows that WA/LA explains the majority of variability in E/I among lakes. The strong relationship between average E/I and WA/LA allowed us to predict the average E/I for 7340 lakes in the study region. Predicted average E/I values were low compared to other regions of thermokarst lakes, only reaching 0.33, indicating that lakes are not currently near risk of desiccation. We hypothesize that lakes with larger WA/LA will be more prone to rapid drainage if future conditions are wetter.

Few studies have directly investigated the influence of WA/LA on E/I (Gibson and Edwards, 2002; Turner et al., 2014), but given the strong relationship we found, WA/LA could serve as a useful metric in other permafrost environments for characterizing thermokarst lake water balances and predicting the vulnerability of lakes to climate change. The non-uniform response of lake surface area to past climate change (Smith et al., 2005; Plug et al., 2008; Arp et al., 2011; Jones et al., 2011; Andresen and Lougheed, 2015) may also be explained by WA/LA; future studies could

investigate whether lakes with smaller WA/LA are more likely to decrease in surface area than lakes with larger WA/LA. Further associations between WA/LA and biogeochemical properties of lakes may also exist, as E/I has been linked to the biogeochemistry of a wide range of lakes, from tropical to tundra environments (Kosten et al., 2009).

4.8 Chapter 4 Appendix

4.8.1 Isotope framework

The calculation of the point of maximum evaporative isotopic enrichment, or the isotope composition of lake at the point of desiccation (δ^*), Gonfiantini (1986):

$$\delta^* = \frac{h * \delta_{As} + \varepsilon_k + (\varepsilon^*/\alpha^*)}{h - \varepsilon_k - (\varepsilon^*/\alpha^*)} \tag{4.4}$$

where α^* is the fractionation factor between the liquid and vapour phase of water, ε^* and ε_k are the equilibrium and kinetic separation terms, with ε^* serving as a convenient expression of α^* , where $\varepsilon^* = \alpha^* - 1$. The term h represents the relative humidity for the open water season (see below). Equilibrium fractionation (α^*) was calculated following equations from Horita and Wesolowski (1994):

$$1000ln * \alpha^* = -7.685 + 6.7123 * \frac{10^3}{T} - 1.6664 * \frac{10^6}{T^2} + 0.35041 * \frac{10^9}{T^3} \tag{4.5}$$

for δ^{18}O and

$$1000ln * \alpha^* = 1158.8 * \frac{T^3}{10^9} - 1620.1 * \frac{T^2}{10^6} + 794.84 * \frac{T}{10^3} - 161.04 + 2.9992 * \frac{10^9}{T^3} \tag{4.6}$$

for δ^2H, where T represents the temperature of the interface (K) (see below). The kinetic separation term ε_k was calculated as:

$$\varepsilon_k = x * (1 - h) \tag{4.7}$$

where $x = 0.0142$ for $\delta^{18}O$ and $x = 0.0125$ for $\delta^{2}H$ (Gonfiantini, 1986). δ_{As} represents the isotope composition of atmospheric vapour, which we assume is in equilibrium with the isotope composition of summertime precipitation (δ_{Ps}, Gibson and Edwards, 2002). We can therefore estimate δ_{As} as:

$$\delta_{As} = (\delta_{Ps} - \varepsilon^*/\alpha^*) \tag{4.8}$$

The reference point of when E/I = 1 (δ_{SSL}) was calculated using:

$$\delta_{SSL} = (\alpha^* * \delta_P * (1 - h + \varepsilon_k)) + \alpha^* * h * \delta_{As} + \alpha^* * \varepsilon_k + \varepsilon^* \tag{4.9}$$

where δ_{Ps} represents average precipitation (Gonfiantini, 1986).

Data for air temperature and relative humidity were collected at Trail Valley Creek near the centre of the study area. The time period used for the average air temperature and relative humidity spans from when lakes became ice-free (June 15, 2018) until the last day of sampling (September 3, 2018) to match the time span between the first and last sampling dates. For a few dates, air temperature was not recorded by the TVC meteorological station maintained by the Meteorological Service of Canada, and air temperature from another meteorological station at TVC was used instead.

The isotope composition of the lake-specific input water (δ_I) was calculated following Yi et al. (2008), where δ_I is estimated as the intersection of the LMWL and the lake-specific LEL, defined as the line between the measured isotope composition of the lake (δ_L) and δ_E, which is the isotope composition of vapour evaporating from the lake. δ_E was calculated following Gonfiantini (1986):

$$\delta_E = \frac{(\delta_L - \varepsilon^*)/(\alpha^* - h * \delta_{As} - \varepsilon_k)}{1 - h - \varepsilon_k} \tag{4.10}$$

δ_I, δ_E and δ_L were then used to calculate the ratio of evaporation to inflow (E/I) as described by Yi

et al. (2008) and others as:

$$\frac{E}{I} = \frac{\delta_I - \delta_L}{\delta_E - \delta_L} \tag{4.11}$$

assuming that lakes are well mixed and in hydrological and isotopic steady state.

Table 4.3 List of variables used in isotope framework and their values.

Variable (unit)	Description	Source	Value(s)
Measured			
T (K)	Average air temperature from June 15 to September 3, 2018	Trail Valley Creek (WMO ID: 71683)	281.95
h (%)	Average relative humidity from June 15 to September 3, 2018	Trail Valley Creek (WMO ID: 71683)	78.3
δ_S (^{18}O, ^{2}H) (‰)	Average isotope composition of snowpack samples.	Samples from study region	-24.61, -184.19
δ_R (^{18}O, ^{2}H) (‰)	Average isotope composition of rainfall samples.	Samples from study region	-17.03, -129.54
δ_P (^{18}O, ^{2}H) (‰)	Average of δ_S and δ_R.	Samples from study region	-21.24, -160.1
δ_{Ps} (^{18}O, ^{2}H) (‰)	Average isotope composition of precipitation during the ice-free period.	Samples from study region	-16.79, -129.15
δ_L (^{18}O, ^{2}H) (‰)	Isotope composition of lake water.	Samples from study region	*Many*
LMWL (slope, intercept (‰))	Local meteoric water line, calculated using a linear regression through δ_S and δ_R samples.	Samples from study region	7.1, -10.0
Computed			
α^* (^{18}O, ^{2}H)	Fractionation factor between the liquid and vapour phase of water.	Equation 4.5, 4.6	1.0109, 1.0986
ε^* (^{18}O, ^{2}H)	Equal to α^*-1	Equation 4.5, 4.6	0.0109, 0.0986
ε_k (^{18}O, ^{2}H)	Kinetic separation factor between liquid and vapour phases of water.	Equation 4.7	3.08, 2.71
δ_{As} (^{18}O, ^{2}H) (‰)	Isotope composition of atmospheric water vapour.	Equation 4.8	-27.58, -207.7
δ_E (^{18}O, ^{2}H) (‰)	Isotope composition of water vapour evaporating from a lake.	Equation 4.10	*Many*
δ^* (^{18}O, ^{2}H) (‰)	Theoretical isotope composition of a water body at the point of total desiccation.	Equation 4.4	-9.88, -101.1
LEL (slope, intercept (‰))	Local evaporation line, representing a theoretical lake evaporation line where $\delta_I = \delta_P$.	Equation 4.4	5.2, -48.9
δ_I (^{18}O, ^{2}H) (‰)	Estimated average isotope composition of δ_L source water.	Equation 4.10	*Many*
E/I	Evaporation-to-inflow ratio.	Equation 4.11	*Many*
δ_{SSL} (^{18}O, ^{2}H) (‰)	Isotope composition of a lake where $E/I = 1$ and $\delta_I = \delta_P$.	Equation 4.9	-12.59, -115.70

Chapter 5

Snowmelt speed, antecedent rainfall and lake ice cover duration drive year-to-year changes in thermokarst lake water balances

5.1 Abstract

During the past several decades, thermokarst lakes in the Inuvik-Tuktoyaktuk region have been observed to fluctuate in surface area in response to changing precipitation amounts and air temperature. This region is one of the fastest warming in the world, which is lengthening the time lakes are ice-free and exposed to evaporation, while precipitation amounts are also expected to increase with climate change. To understand how thermokarst lake water balances in this region vary in response to changing meteorological conditions, three years of direct water balance measurements were made at Big Bear Lake near the Trail Valley Creek research station, which is a hydroligcally-typical lake for the region (Chapter 4). Lake level (LL) was recorded with a pressure transducer, outflow (Q_{out}) was estimated with a stage-discharge relationship derived from manual discharge measurements made in the lake outlet, precipitation (P) was measured using a shielded

weighing gauge, evaporation (E) was estimated using the Priestley-Taylor model, and inflow (Q_{in}) was calculated as the unknown of the lake water balance equation: $\Delta LL = Q_{in} - Q_{out} + P - E$. Results showed that when snowmelt occurred rapidly, both the maximum lake level reached before the snow dam in the lake outlet failed, and the conversion efficiency of the snowpack into inflow (runoff ratio), were greater. During the summertime, the runoff ratio increased with precipitation and when the previous year's precipitation was greater than average, as the soil moisture conditions of the previous year are frozen into the active layer, until the active layer thaws. Evaporation losses from the lake varied between 226 to 296 mm and was predominantly affected by the length of time that the lake was ice-free. Prior to the lake becoming ice-free, the high solar radiation conditions created a high potential for evaporation (4 to 6 mm day^{-1}), suggesting that earlier ice-free dates in the future may have a disproportionate impact on evaporation losses when compared to later ice-on timing. Future responses of lake water balance to climate change will depend on the balance between increasing precipitation that could drive more runoff to lakes versus shrub expansion, permafrost thaw and hummock collapse that will reduce the ability of watersheds to convey runoff, and the lengthening ice-free period that will increase evaporative losses from lakes.

5.2 Introduction

Thermokarst lakes are common features in areas of continuous permafrost and regulate the flow of water throughout the landscape (Woo, 2012). Rapid warming in the Arctic is causing non-uniform changes to lake water balances: in some areas lake evaporation has increased enough to cause lakes to shrink or desiccate (Smol and Douglas, 2007; Finger Higgens et al., 2019), while in other areas rainfall has increased alongside air temperatures and lead to greater increases in inflow than evaporation (MacDonald et al., 2021). The rate of rapid lake drainage, which can be triggered by extremely high lake levels that lead to run-away thermomechanical erosion of a lake outlet (Brewer et al., 1993; Marsh and Neumann, 2001), is also changing throughout the Arctic as lake water

balances respond to climate change (Nitze et al., 2020; Webb et al., 2022). Many remote sensing studies have quantified changes in lake surface area and drainage around the Arctic (Smith et al., 2005; Smol and Douglas, 2007; Plug et al., 2008; Marsh et al., 2009; Arp et al., 2011; Jones et al., 2011; Anderson et al., 2013; Andresen and Lougheed, 2015; Nitze et al., 2017; Finger Higgens et al., 2019; Travers-Smith et al., 2021), but fewer studies have investigated how changes in lake water balance components, such as evaporation and inflow, may have contributed to changes in lake surface area and rapid lake drainage.

Most previous studies of lake water balance in the Arctic can be divided into two approaches. One approach involves taking direct measurements of lake water balance components using measuring devices such as water level recorders, typically in combination with a lake evaporation model (e.g. Woo et al., 1981; Roulet and Woo, 1988; Pohl et al., 2009). Another approach uses water isotope composition to estimate the ratio of evaporation-to-inflow (E/I) for many lakes using water samples taken a few times per year (e.g. Chapter 4; Turner et al., 2014; MacDonald et al., 2017). Unlike water isotope approaches, direct measurements capture changes in lake level and can be used to quantify individual components of lake water balances volumetrically at a fine temporal scale (hours, days). Also, the limited mixing between freshet and pre-freshet lake water in ice-covered lakes means water isotope methods may not capture the volumetric contributions of freshet runoff to lake inflow (Chapter 3), which is typically the largest potential water source for thermokarst lakes (Woo, 1980). Direct measurements of lake water balance components in the Arctic have been made in the past (Woo, 1980; Marsh and Bigras, 1988; Hardy, 1996; Pohl et al., 2009), but measurements longer than a year or two are rare, leaving a gap in our knowledge of how years with different meteorological conditions cause variability in individual lake water balance components.

The western Canadian Arctic contains thousands of thermokarst lakes that fluctuate in area in response to precipitation and are vulnerable to rapid drainage (Mackay, 1988; Plug et al., 2008). The rate of rapid lake drainage has increased during the past 15 years in the western Canadian

Arctic, likely in response to warmer air temperatures which have promoted permafrost thaw (Burn and Kokelj, 2009; Bush and Lemmen, 2019; Kariyawasam, 2022). Previous research by Pohl et al. (2009) modelled summertime lake levels in the region to evaluate when extremely high lake levels occurred, to better understand when lakes are vulnerable to rapid drainage. However, this study did not include the freshet period, during which the highest yearly lake levels occur as snow dams trap water in lakes until the snow dam fails (Heginbottom, 1984; Marsh and Hey, 1989; Braun et al., 2000). The high lake levels caused by snow damming can initiate rapid lake drainage (Mackay, 1988; Jones and Arp, 2015), making it important to understand the interplay between snow dams and lake level. While snow dams have been observed to increase lake levels to their yearly maximum, no research has evaluated how the maximum lake levels caused by snow damming varies from year to year.

We measured lake water balance at a thermokarst lake in the western Canadian Arctic for three years with the aim to:

1. Compare year-to-year differences in lake evaporation, inflow, and lake level to varying meteorological conditions, such as air temperature, rainfall and snowfall.

2. Evaluate the drivers of inter-annual variability in lake evaporation, inflow and lake level extremes.

3. Explore the influences on runoff ratios during the freshet and the snow-free period.

By quantifying the drivers of lake water balance components we can evaluate the sensitivity of lakes in this region to predicted increases in air temperature and precipitation (Lee et al., 2021). This study will also provide valuable data for developing and testing hydrological models needed for predicting how lakes will change into the future.

5.3 Study Area

Water balance measurements were made at Big Bear Lake, located in the Trail Valley Creek research watershed 45 km north of Inuvik and 80 km south of Tuktoyaktuk in the Northwest Territories, Canada at 68.74°N, 133.52°W (Figure 5.1). Big Bear Lake has a surface area of 6.4 ha, a watershed area of 42.9 ha, and a maximum depth of 2.75 m (Table 5.1). The vegetation cover of the watershed, based on a vegetation map generated by Grünberg and Boike (2019), comprises roughly one quarter each of tall shrubs (> 1 m height), dwarf shrubs (< 1 m height), and grass tussocks, with the remaining quarter of the watershed covered by areas of riparian shrubs (14.9%) and lichen (9.1%, Figure 5.1, Table 5.1). Based on analysis in Chapter 4, the ratio of watershed area to lake area (WA/LA = 6.7, Table 5.1) is near the median of lakes in this region (WA/LA = 5.5, Figure 4.7). The ratio of evaporation-to-inflow, based on isotope-mass balance modelling, is predominantly controlled by WA/LA (Chapter 4, Figure 4.5), meaning that Big Bear Lake likely represents a typical lake for this region.

Table 5.1 Attributes of Big Bear Lake and its watershed. Percentages refer to the % coverage of vegetation types for the watershed.

Attribute	Value
Lake Surface Area (ha)	6.4
Maximum Depth (m)	2.75
Watershed Area (ha)	42.9
Watershed Area/Lake Area	6.7
Average Watershed Slope (°)	4.9
% Tall Shrub	27.4
% Riparian Shrub	14.9
% Dwarf Shrub	22.0
% Tussock	26.5
% Lichen	9.1

Between 1991-2020, the mean annual air temperature in Inuvik was -8.0°C, while during the same period rainfall averaged 114 mm and snowfall averaged 127 mm (water equivalent). The end-of-winter snow water equivalent measured in the 58 km^2 Trail Valley Creek watershed, of

which Big Bear Lake is a part of, was 147 mm (Marsh et al., 2019). The region between Inuvik and Tuktoyaktuk comprises of mostly tundra uplands containing lichen, tussock, and shrub vegetation cover types. Thousands of thermokarst lakes inhabit this region, most ranging in area from 1 - 1000 ha and 2 - 4 m depth (Pienitz et al., 1997). The area is underlain by continuous permafrost 200 - 700 m thick and taliks (areas of permafrost-free sediment) exist beneath lakes that are deep enough to not freeze to their bed. Snowmelt runoff typically begins in mid-May and lakes usually become ice-free by mid-June before becoming ice-covered in mid-October (Burn and Kokelj, 2009). The Big Bear Lake watershed is covered by mineral earth-hummocks 0.5 to 1.0 m wide of extremely low hydraulic conductivity, with a porous peat matrix forming a network between the hummocks that facilitate subsurface runoff through the watershed (Quinton et al., 2000).

The climate is changing rapidly in this region. Mean annual air temperature has warmed by over 2.5°C degrees between 1970 and 2009, causing permafrost temperature warming by an even greater amount (Bush and Lemmen, 2019), while deciduous shrubs have been expanding their coverage by encroaching into shrub-free tundra during the past several decades (Lantz et al., 2013). Consequently, permafrost thaw has been observed in the region, leading to the degradation of mineral-earth hummocks in forested and fire-affected areas (Kokelj et al., 2007), increases in thaw slumping and rapid lake drainage (Lantz and Kokelj, 2008; Kariyawasam, 2022), and ground subsidence (O'Neill et al., 2019a).

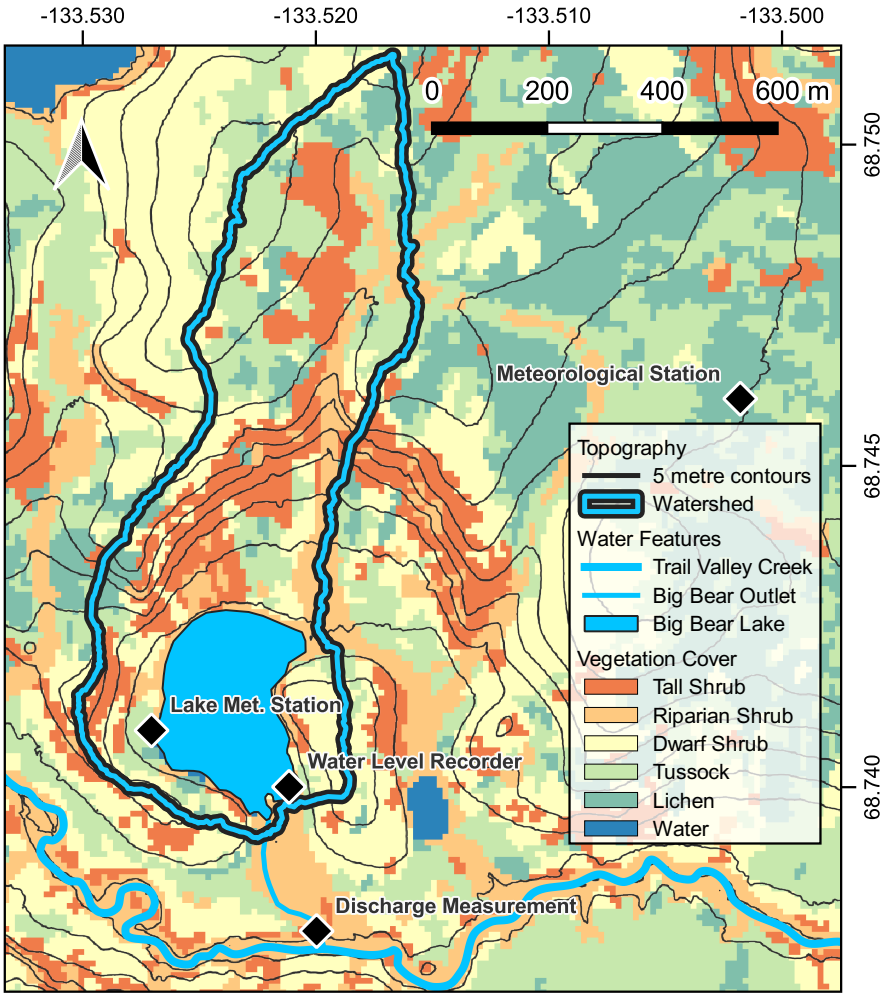

Figure 5.1 Location of Big Bear Lake and instrumentation, including meteorological stations, water level record and discharge measurement locations. Vegetation cover map sourced from Grünberg and Boike (2019).

5.4 Methods

5.4.1 Lake water balance measurements and calculation

Instrumentation installed at the Big Bear Lake watershed was used to calculate the lake water balance, following the equation:

$$\Delta LL = Q_{in} - Q_{out} + P - E \tag{5.1}$$

where ΔLL is change in lake level, Q_{in} is inflow to the lake via incoming streams or subsurface flow, Q_{out} is outflow from the outlet of the lake, P is precipitation falling directly into the lake when it is ice-free, and E is evaporation from the lake. The units of all variables in the equation are represented as changes in lake level over time (mm day^{-1}). A water balance was calculated from May 1 until October 31 of 2017, 2018 and 2020 to encompass the snowmelt period through lake and soil freeze up. The water balance in 2020 ends on October 4 as the water level recorder stopped logging data on that day. Each water balance component is calculated at a daily timescale using data that were collected hourly or half-hourly. The storage capacity of the lake (i.e., the relationship between lake level and the volume of water stored in the lake) is assumed to remain constant during the study period. The quantities of LL, Q_{out}, P and E are measured or calculated, and Q_{in} is calculated as the unknown variable in Equation 5.1, such that:

$$Q_{in} = Q_{out} - P + E + \Delta LL \tag{5.2}$$

LL was measured using a pressure transducer-type water level recorder, with water pressure corrected for changes in air pressure using data from the nearby meteorological station northeast of the lake (Figure 5.1, WMO ID = 71683). Lake level was offset at the start of every year such that LL = 0 at the start of the freshet period before any snowmelt runoff had flowed into the lake, as the lake would drain down to its sill level every autumn. Precipitation was measured using a shielded weighing gauge at the same meteorological station where air pressure was measured (Figure 5.1). On July 9, 2020 the precipitation gauge at the meteorological station stopped functioning, and precipitation data collected in Inuvik, 45 km south of Big Bear Lake, was used instead. Snow water equivalent on the ground at the end of winter was measured in the Trail Valley Creek watershed at several long-term monitoring transects representing different landscape and vegetation cover types (Marsh et al., 2019). Snow surveys were not completed at Trail Valley Creek in 2020, and data from Caribou Creek, 76 km south of Inuvik, were used to estimate snow water equivalent for 2020

(Appendix 5.8.1).

Evaporation was estimated following the Priestley-Taylor (PT) method (Priestley and Taylor, 1972) as:

$$E = \alpha'(s/(s+\gamma))Q^*/L_v\rho \tag{5.3}$$

where α' is an empirical constant that converts actual evaporation to equilibrium evaporation, s is the slope of the temperature-saturated vapour pressure curve, γ is the psychrometric constant, net radiation is Q^*, L_v is the latent heat of vapourization of water, and ρ is the density of water. An α' value of 1.26, the average found by Priestley and Taylor (1972) for saturated surfaces, was used. The value s was calculated using the equations developed by Buck (1981). The data used to calculate E with Equation 5.3 were obtained from a meteorological station at the shore of the lake that measured incoming and outgoing short and longwave radiation, air temperature, air pressure, humidity and wind speed (Figure 5.1). The radiometer was placed on an arm that overhung the lake so that the instrument measured outgoing radiation from the water surface. While PT can be inaccurate over short periods of time (hours to days), the accuracy of this method for lakes in this region was found to be within 15% over periods of one to two months (Marsh and Bigras, 1988). When the lake was ice-covered, evaporation was set to 0. Heat flux into the lake bed was not accounted for in the calculation of PT evaporation, as previous studies have found that heat flux into the lake bed typically accounts for only 2-3% of the lake energy balance in this region (Marsh and Bigras, 1988). During 2020, the radiometer was not functioning at the lake meteorological station, and radiation data from a radiometer located at the meteorological station northeast of Big Bear Lake were used to calculate evaporation. A regression between daily evaporation rates from 2017 and 2018 calculated using the Priestley-Taylor method and average incoming shortwave and longwave radiation was used to estimate evaporation for the year 2020 (R^2 = 0.97).

Outflow (Q_{out}) was initially estimated using a v-notch weir and accompanying water level recorder installed in the outlet of Big Bear Lake (Figure 5.1), however the weir was breached by strong outflows during the freshet of 2017. The weir was removed shortly after it was damaged,

after which Q_{out} was estimated using a stage-discharge relationship generated in 2017 and 2018. Discharge was measured in 2017 and 2018 using an acoustic Doppler velocimeter downstream of the lake outlet at a place where channel geometry was most suitable for Q_{out} measurements. Lake level data were then correlated with Q_{out} measurements and weir discharge measurements prior to weir failure to generate the stage-discharge relationship:

$$Q_{out} = 2527.4 * LL^2 - 125.59 * LL + 1.5602 \tag{5.4}$$

Discharge measurements of Q_{out} taken during low-flow periods were less reliable because the limited water depth (<10 cm) in the outlet channel makes it more difficult for the velocimeter to measure the speed of water flow accurately, however some amount of flow from the outlet was always observed when Q_{out} measurements were made. To account for the reduced measurement quality of Q_{out} at low-flow conditions, and reflect observations of continual outflow from the lake, Equation 5.4 was only used if Q_{out} was >1.5 litres per second, but if $Q_{out}$was <1.5 litres per second, outflow was set to equal one litre per second. On days where Q_{out} and evaporation did not fully account for losses in lake level even if Q_{in} was 0, Q_{in} was set to 0 and Q_{out} was defined as the minimum Q_{out} required to account for the loss in lake level.

In 2017 when there was a weir and water level recorder installed in the lake outlet, only a minimal amount of Q_{out} was observed (37 mm) before snowdam failure. During the lead up to snow dam failure in 2018 and 2020, we assume that Q_{out} is equal to 0, as Equation 5.4 cannot be applied because the snow dam modifies the relationship between stage and discharge. The lack of weir Q_{out} measurements in 2018 and 2020 also meant a special approach was applied to estimate Q_{out} between snowdam failure and the outlet returning to a state where the stage - discharge relationship was valid. First, the rate of Q_{in} the day before snowdam failure was assumed to be equal to the rise in lake level that day, since there is little to no outflow before snowdam failure. It was then assumed that on the day after snow dam failure that Q_{in} is equal to the day before, and that Q_{out} is equal

to the Q_{in} from the day before plus the decline in lake level on the first day of snow dam failure. Then the day when the rapid decline in lake level ended due to the erosion of the snow dam was identified, and the stage-discharge relationship to estimate Q_{out} on that day was used. For the days in between snowdam failure and complete snowdam erosion, a linear weighted average to estimate Q_{out} between the the day of snowdam failure and the day when the snowdam was fully eroded was used.

Given some of the compromises made in our water balance equation (e.g. Q_{out} set to 1.5 litres per second in low flow scenarios, Q_{in} cannot be < 0), our water balance calculations do not fully conserve mass. To evaluate the amount of error in the water balance, we also calculate the residual (e.g. whether extra water was added or subtracted from the water balance during calculation) as:

$$Residual = Q_{in} + P - \Delta LL - E - Q_{out} \tag{5.5}$$

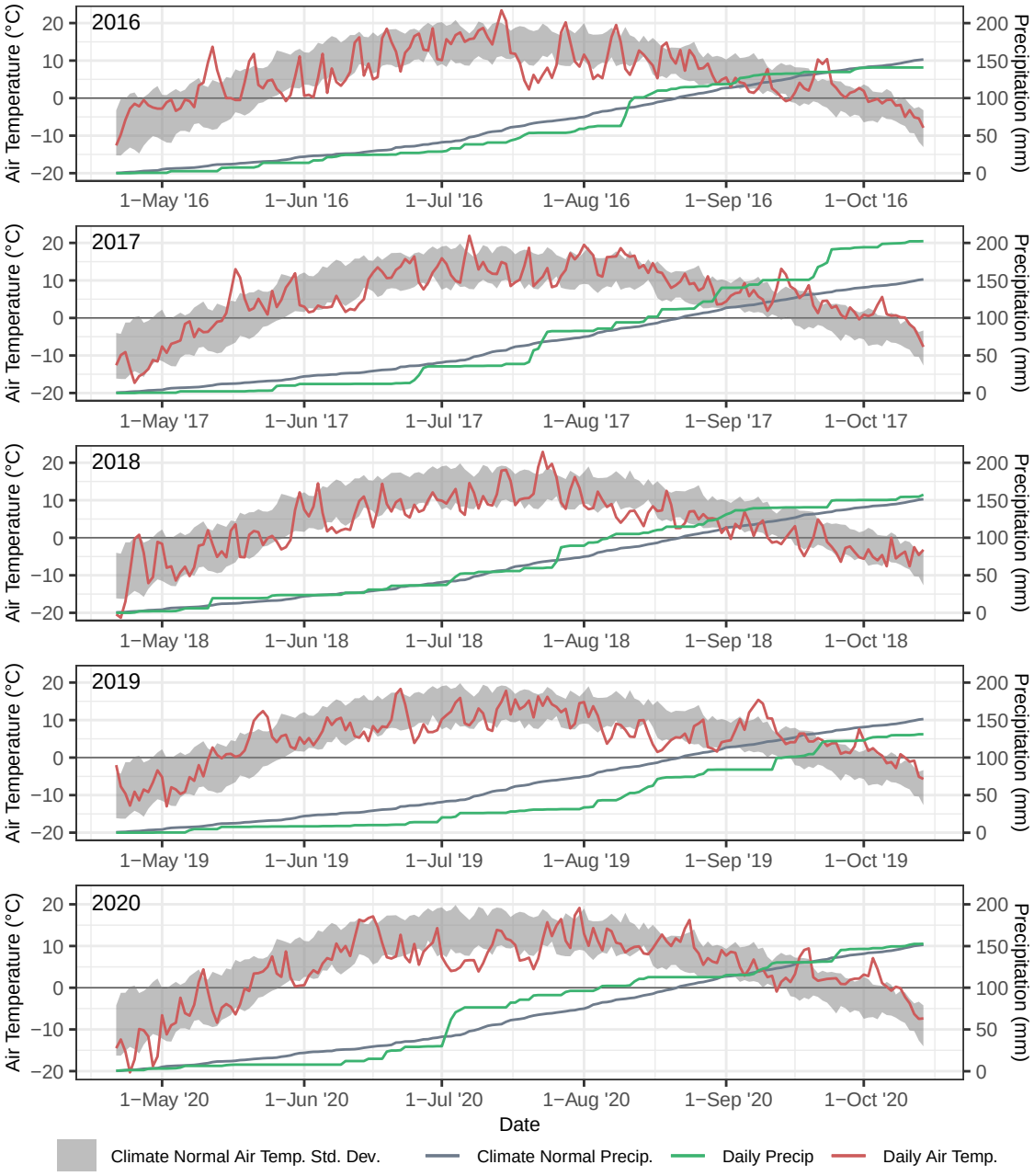

Figure 5.2 Air temperature and cumulative precipitation for the period of April 20 to October 15 for 2016-2020. Climate normals from 1991-2020 were calculated from data collected in Inuvik, 45 km south of the study site (WMO ID: 71364). The standard deviation of air temperature is lowered by one degree because Inuvik is warmer on average than Trail Valley Creek by roughly that amount, and climate normals for Trail Valley Creek are not available.

5.5 Results

5.5.1 Freshet Period

The pre-freshet snowpack stored a similar amount of water in all three years, ranging between 131 to 144 mm SWE (Table 5.2). Consistent above-zero temperatures came earlier in 2017 than in 2018 and 2020 (Figure 5.2), consequently causing Big Bear Lake to become ice-free on June 8, whereas in 2018 and 2020 the lake became ice-free on June 16 and June 17, respectively (Table 5.3). In all three freshet periods the amount of precipitation was low to average, ranging from 10 to 31 mm (Table 5.2), while the average from 1991-2020 was 29 mm (Figure 5.2).

Lake level behaviour during the freshet varied between the three years. In 2017, freshet lake level rose 0.47 m above the pre-freshet lake level before snow dam failure, whereas in 2018 and 2020 lake level maxed out at 0.27 m above pre-freshet lake levels before snowdam failure (Figure 5.3). The rise in lake level up until snow dam failure was rapid in 2017, with lake level rising several centimetres per day coinciding with abnormally warm air temperatures that were > 5°C (Figure 5.2). In 2018, lake level rose comparatively more slowly than in 2017 and 2020, taking roughly two weeks to rise 0.12 m before a sharp rise in lake level occurred on June 1, which triggered snow dam failure. Data are missing for part of 2020, but the rise in lake level when data begins is also rapid, similar to 2017. All three snow dam failures are marked by a rapid decline in lake level, however the snowdam failure in 2020 appears to have occurred more slowly, leading to a smoother transition between rapid increases and decreases in lake level. Maximum lake levels reached during the freshet were more than double the maximum lake levels reached post-freshet in all three years (Figure 5.4).

In all three years the majority of Q_{in} flowed into the lake during the freshet period, representing 53%, 62% and 58% of total yearly Q_{in} for 2017, 2018 and 2020 respectively (Table 5.2). Q_{in} was similar in 2017 (764 mm) and 2018 (718 mm), but comparably lower in 2020 (560 mm, Table 5.2). The efficiency at which the snowpack and freshet precipitation was converted into Q_{in}

Table 5.2 Yearly summary of lake water balance components for Big Bear Lake. Freshet is defined as May 1 until June 15, and June 15 until October 31 is classified as summer. Summer runoff ratios are calculated by dividing the inflow by the ratio between the lake area and watershed area, and then dividing by precipitation. Freshet runoff ratios are calculated the same as the summer, using the total of the snowpack water equivalent and freshet precipitation.[1]Snow surveys were not completed at Trail Valley Creek in 2020, and instead values from Environment and Natural Resources Northwest Territories scaled using the offset from the average at Caribou Creek, measured 76 km south of Inuvik (Appendix 5.8.1). Precipitation - Evaporation is calculated by adding freshet and summer precipitation and then subtracting by evaporation.

	Precipitation (mm)				Inflow (mm)			Runoff Ratio			Evaporation		Metrics		
Year	Snowpack	Freshet	Summer	Total	Freshet	Summer	Total	Freshet	Summer	Total	(mm)	(mm day^{-1})	Evap./Inflow	Precip.-Evap.	Inflow (% Freshet)
2017	131	11	197	208	764	669	1433	0.80	0.51	0.63	296	2.3	0.21	-88	53
2018	141	31	135	166	718	445	1163	0.62	0.49	0.57	226	2.1	0.19	-60	62
2020 [1]	144	10	142	152	560	402	962	0.58	0.42	0.49	272	2.3	0.28	-120	58

was variable: the runoff ratio during the freshet was 0.80, 0.62 and 0.57 for 2017, 2018 and 2020 respectively (Table 5.2).

5.5.2 Summertime Period

Each ice-free period encapsulates a unique set of meteorological conditions. The year 2017 received by far the most summertime precipitation, totaling 197 mm between June 15 and October 31, while 2018 received an average amount of precipitation of 135 mm and 2020 received a similar amount of precipitation (142 mm, Figure 5.2, Table 5.2). Mean air temperature during the summer period was warmest in 2017 at 7.5°C, coldest in 2018 at 4.7°C, while 2020 had an average air temperature of 5.3°C. In 2018 the lake became ice-covered on September 30, earlier than in 2017 (October 13) and 2020 (October 12) (Table 5.3).

Comparison of lake levels post-freshet reveals divergence between the three years. Lake levels remain above pre-freshet lake level for the entirety of 2017, the wettest of the three summers,

Table 5.3 Summary of yearly meteorological conditions and lake ice cover. Freshet is defined as May 1 to June 15, with summer defined as June 16 until October 31. Mean air temperature and precipitation from 1991-2020 is calculated using data from Inuvik, which is further south and typically warmer than Trail Valley Creek.

Year	Ice-off Date	Ice-on Date	Ice-free Days	Freshet Mean Air Temp. (°C)	Summer Mean Air Temp. (°C)	Summer Total Precip. (mm)
2017	08-Jun	13-Oct	127	2.1	7.5	197
2018	16-Jun	30-Sep	106	0.3	4.7	135
2020	17-Jun	12-Oct	117	1.6	5.3	142
1991-2020 Mean, Inuvik	N/A	N/A	N/A	4.0	6.3	135

while lake levels fall below pre-freshet lake levels in 2020, the driest of the three summers (Figure 5.4). Large rainfall events >15 mm drive sharp increases in lake level from 30 to 70 mm, with one or two large rainfall events visible during the first six weeks of summer in all three years (Figure 5.4).

Evaporation at the lake varied between the three summers: the wettest summer (2017) also experienced the greatest amount of total evaporation loss from the lake (296 mm) and the highest average evaporation rate (2.3 mm day^{-1}) (Table 5.2). In 2018 evaporative losses from the lake were 226 mm, 24% lower than in 2017, however the average evaporation rate in 2018 was only 9% lower (2.1 mm day^{-1}). In 2020, the average evaporation rate was the same as 2017 (2.3 mm day^{-1}), however a shorter ice-free period meant that 2020 had less evaporation (272 mm) than in 2017 (Table 5.2). The ratio of evaporation to inflow was highest in 2020 (0.28), lowest in 2018 (0.19) and slightly higher in 2017 (0.21, Table 5.2). The evaporation deficit (Freshet + summer precipitation - evaporation) was also highest in 2020 (-120 mm), lowest in 2018 (-60 mm), and slightly higher in 2017 (-88 mm, Table 5.2). Evaporation rates were highest for the first couple months after the lake became ice-free, while evaporation rates became minimal after September 1 (Figure 5.4).

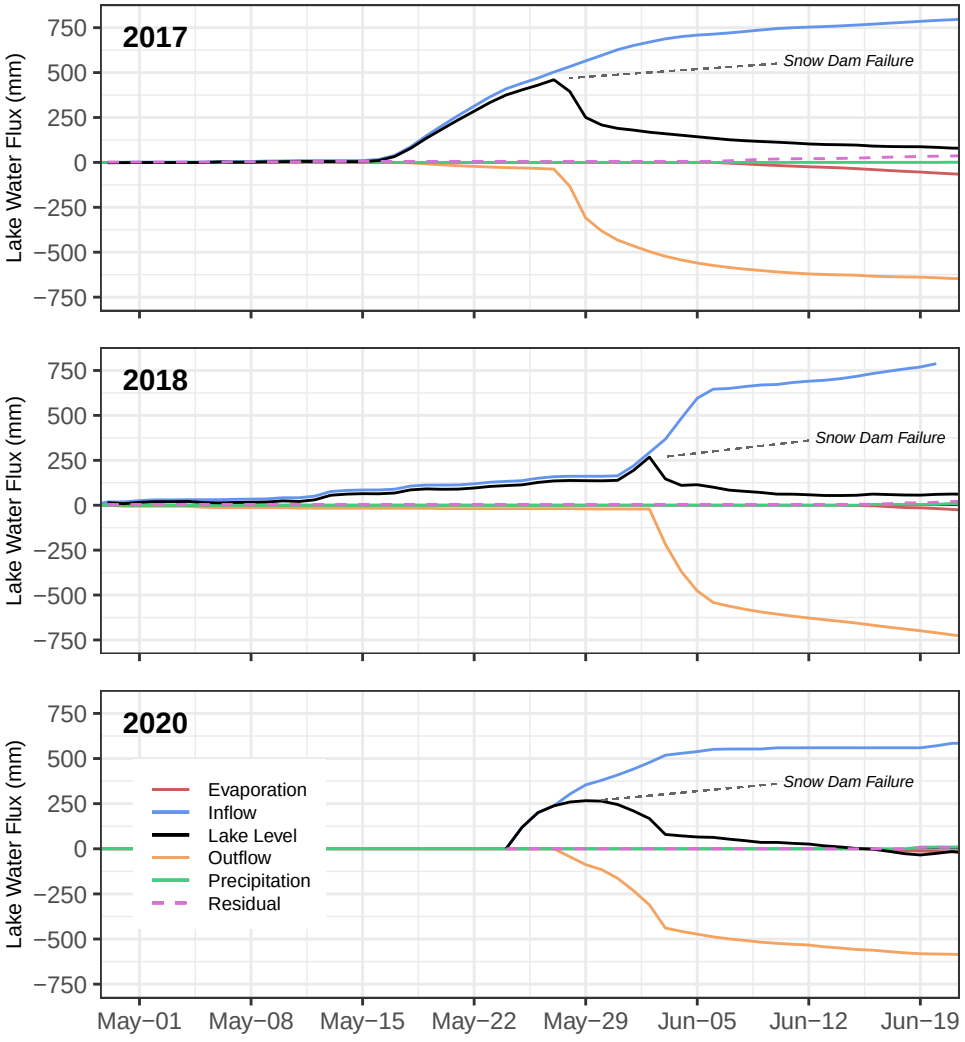

Figure 5.3 Cumulative water balance of Big Bear Lake for 2017, 2018 and 2020 during the freshet period. Snow dam failure points and subsequent declines in lake level are indicated for each year. Water flux is displayed as cumulative changes of water flux in millimetres of lake level (i.e. 1000 mm Q_{in} = 1000 mm increase in lake level).

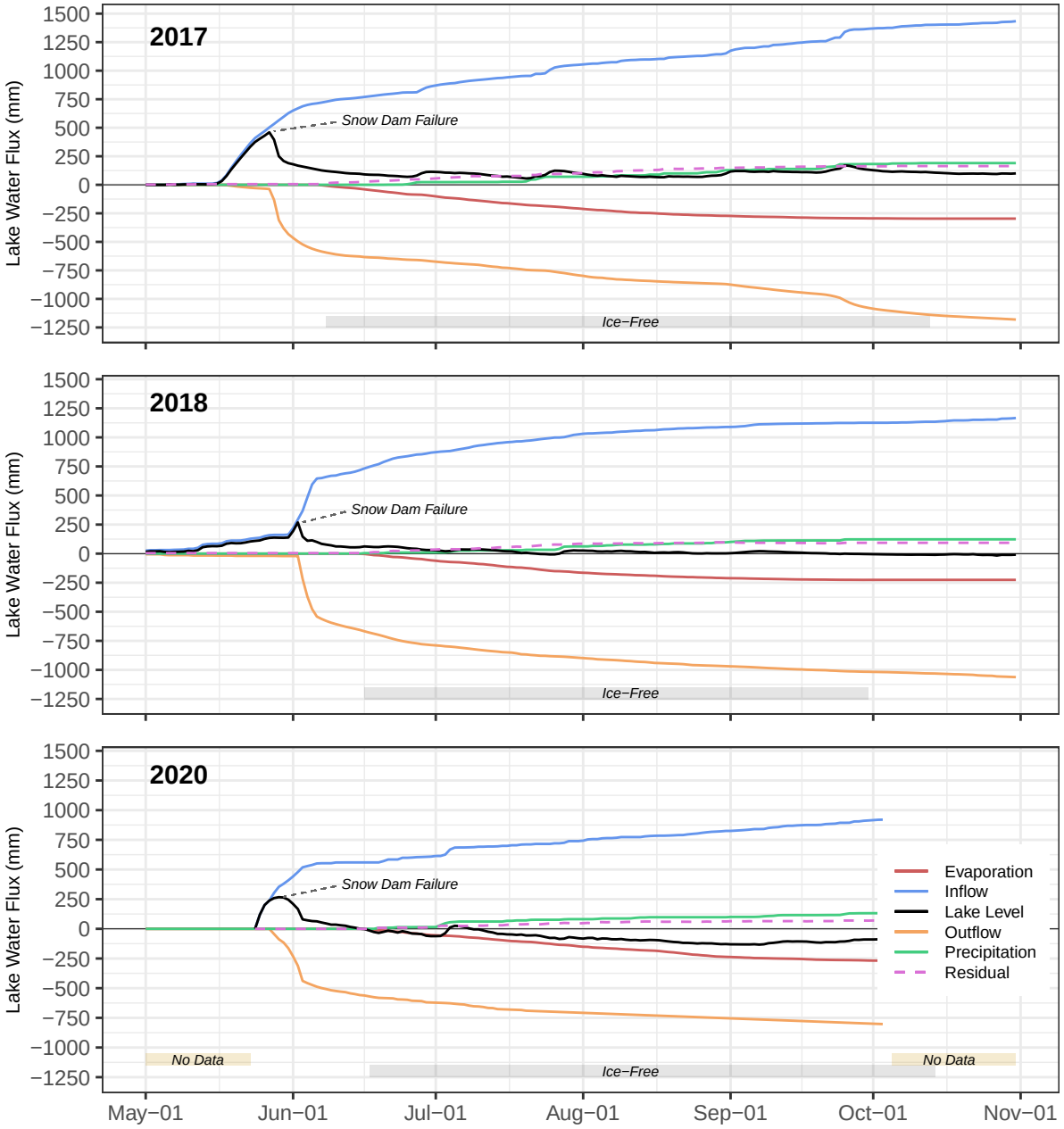

Figure 5.4 Cumulative water balance of Big Bear Lake for 2017, 2018 and 2020. Snow dam failure points and subsequent declines in lake level are indicated for each year. Water flux is displayed as cumulative changes of water flux in millimetres of lake level (i.e. 1000 mm Q_{in} = 1000 mm increase in lake level).

5.6 Discussion

5.6.1 Snow dam dynamics

Snow dam failure occurred at 270 mm above pre-freshet lake levels in 2018 and 2020, however in 2017 snow dam failure occurred at 470 mm above pre-freshet lake levels. In 2017, air temperatures rose to >10°C for two days on May 15-16 after a week of near-zero temperatures (Figure 5.2), causing a large amount of freshet runoff to flow into lakes rapidly. Snow dam failure occurred later in the snowmelt period in 2018 and 2020, making it likely that the snow dams had more time to melt before lake levels rose enough to cause failure. The snowpack in 2017 was the lowest of the three years at 131 mm, suggesting that larger snowpacks do not lead to higher lake levels at snow dam failure. These results imply that a fast snowmelt earlier in the snowmelt period may cause greater lake level maximums when snow dams are present.

The increase in lake level caused by snow dams at Big Bear Lake was at the smaller end of the range when compared to other lakes where snow dams have been studied. Heginbottom (1984) measured an 80 cm decline in lake level following snow dam failure at a lake in the Canadian High Arctic, while Woo (1980) observed declines in lake level of 40 to 120 cm following snow dam failure at a different Canadian High Arctic lake. Arp et al. (2020a) has observed smaller declines in lake level of 30 to 80 cm caused by snow dam failure in drained thaw lake basins in the northern Alaskan coast, where snow dams cause former lakes to temporarily refill until snow dam failure. Snow dams at High Arctic lakes form as a result of snow accumulation in the incised topography of the lake outlet channels (Woo, 1980; Heginbottom, 1984), while at Big Bear Lake we observed that the tall riparian vegetation (1 - 2 m) growing in lake outlet channels traps blowing snow to form the snow dam. Increased shrub growth (Lantz et al., 2013) combined with increases in snowfall in the future (Lee et al., 2021) could lead to increases in snow dam height in the future, potentially raising the lake levels required to cause snow dam failure.

Understanding the timing of snow dam failure, and the magnitude of the resulting outflow

from the lake, is important for modelling freshet runoff in lake-rich arctic watersheds, given the large amount of outflow in a short period of time after snow dam failure. Our field observations note that the initiation of streamflow in Trail Valley Creek involves substantial discharge through the snow-choked stream channel, indicative of a large release of water upstream, possibly from a lake where snow dam failure has occurred. In multi-lake watersheds, snowdam failure of an upstream lake could trigger snowdam failures at lakes downstream. Future studies could investigate such dynamics by instrumenting a chain of lakes in a watershed with water level recorders.

5.6.2 Variability of Q_{in} and runoff ratios

The runoff ratio during the freshet of 2018 was 0.69, lower than the 2017 freshet runoff ratio of 0.80 (Table 5.2). This was surprising, given that the SWE of the snowpack in 2017 and 2018 are similar (131 vs. 141 mm, respectively), and the very wet autumn of 2017 (Figure 5.2) would have left the active layer wetter than average before freezing, which typically leads to high runoff ratios during freshet in the following year (Stuefer et al., 2017). Previous isotope studies in this region have found that the water flowing through streams and remaining in lakes post-freshet is an equal mixture of snow-sourced and soil-sourced water, indicating that soil water makes a large contribution to freshet runoff (Tetzlaff et al., 2018, Chapter 3). One difference between 2017 and 2018 that may explain the lower runoff ratio in 2018 was the pace of the snowmelt. Snowmelt occurred more quickly in 2017 than in 2018, as evidenced by the much sharper rise in lake level, and shorter time period between the onset of freshet inflow and snow dam failure (Figure 5.4). The slow snowmelt of 2018 may have allowed a larger portion of the snowmelt to evaporate from the soil before being able to melt and contribute to freshet runoff; the wetter autumn of 2017 may have caused the soil surface to be more saturated and vulnerable to evaporation. Additionally, more snowmelt may have remained in the soil instead of flowing into the lake due to greater storage capacity of the soil, since the slower snowmelt would have allowed the soil in snow-free areas to thaw deeper (Chapter 2), increasing soil storage. If snow-free areas do act as a sink for snowmelt

from other areas of the watershed, it indicates that accurately representing the spatial and temporal heterogeneity of snowmelt, and subsequently active layer thawing, is important to accurately model snowmelt runoff for this region.

The year 2020 had a slightly smaller freshet runoff ratio than 2018 (0.58 vs. 0.62, Table 5.2). While 2020 also experienced a later snowmelt than 2017, the preceding year was drier than average (Figure 5.2), which likely lead to a lower runoff ratio as a result of a drier soil which required more snowmelt input before generating runoff (Stuefer et al., 2017).

The majority of Q_{in} occurred during the freshet in all three years, ranging between 53 to 62% of total Q_{in} (Table 5.2). These values match closely with the long-term averages for Trail Valley Creek, which experienced 50% of all runoff by June 15 on average between 1985 and 2011 (Shi et al., 2015). The variability in runoff ratios during the freshet controlled the volume of freshet runoff the lake received, as the variability in the the snowpack volume was comparatively small (131 - 144 mm, Table 5.2).

Runoff ratios during the summertime are markedly lower than during the freshet, ranging from 0.51 to 0.42 among the three years (Table 5.2), as the active layer thaws and slows the transit time of runoff, more soil water is lost through evapotranspiration, and rainfall is intercepted by shrubs when they have leaves and evaporates (Zwieback et al., 2019a). While the runoff ratio during the wettest summer (2017) was the highest of the three years, the lowest runoff ratio of the three years occurred in 2020, which was a slightly wetter summer than 2018 (Table 5.2). Again, we speculate that the impact of the previous year's precipitation had a strong impact on summertime runoff ratios, as observed by Stuefer et al. (2017) who found that the previous year's rainfall was as strong a predictor of runoff ratio as the current years precipitation. The year 2018 may have been drier than 2020, but 2018 followed what was an exceptionally wet year, especially prior to soil freeze-up in September (Figure 5.2). Contrarily, 2019 was a drier year than average, with little precipitation in September.

Compared to other regions, the summertime runoff ratios we observed (0.42 to 0.51) were

high. Kane et al. (1998) observed an average summertime runoff ratio of 0.36 at a 2.2 km^2 watershed in the continuous permafrost region of Alaska, while yearly runoff ratios observed by Stuefer et al. (2017) for a 0.025 km^2 watershed that is also in northern Alaska ranged from 0.34 to 0.37. The higher runoff ratios we observed may be caused by the presence of inter-hummocks in the watershed. Inter-hummock zones form a network of peat-filled channels throughout the watershed that can efficiently convey runoff due to their high hydraulic conductivity (Quinton and Marsh, 1998) and relatively shallow frost table depth (Chapter 2). In other Arctic watersheds runoff ratios for individual rainfall events typically decline to below 0.1 if the preceding days or weeks were dry (Kane et al., 1998; Favaro and Lamoureux, 2014). Inter-hummock zones are resilient to drying out because the water stored in the mineral earth hummocks is fed into inter-hummock zones during dry periods (Quinton and Marsh, 1998). This relationship between hummocks and inter-hummock zones may make the soils in our study region less susceptible to drying out, allowing runoff ratios to remain higher than other Arctic regions. The relatively high runoff ratios observed for this area may also explain why lakes in this region have relatively lower evaporation-to-inflow ratios when compared to other regions of thermokarst lakes (Chapter 4). Future runoff ratios may decrease in this region given that shrub expansion is enhancing permafrost thaw (Chapter 2), which causes hummocks to collapse and mineral soil to intrude into into inter-hummock zones (Kokelj et al., 2007), likely lowering the hydraulic conductivity of inter-hummock zones.

5.6.3 Variability in lake evaporation compared to Q_{in}

The length of the ice-free period for lakes had a strong control on the total evaporation losses - between the three years the evaporation rate was relatively stable (2.1 to 2.3 mm day^{-1}), however seasonal evaporative losses ranged from 226 to 296 mm as the length of the ice-free season varied (Table 5.3). Evaporation is expected to increase into the future as air temperatures rise and the ice-free period extends (Woolway et al., 2020). Results demonstrate that evaporation rates at ice-off are much higher than at ice-on (Figure 5.4) because incoming solar radiation is much higher at

ice-off than during ice-on. Therefore, we suggest that earlier ice-off timing may have a greater impact on increasing lake evaporation than later ice-on timing. We can estimate the impact of earlier ice-free timing on lake evaporation by using the regression between incoming radiation and evaporation developed to estimate lake evaporation in 2020. If Big Bear Lake had become ice-free 10 days earlier than it did in each year, then it would have experienced 49, 39 and 54 mm more evaporation loss in 2017, 2018 and 2020, respectively. These potential increases in evaporation represent 17 - 20% increases above the measured evaporation in those years. Global projections of future lake ice phenology predict a trend of earlier ice-off timing by two days per decade for this region (Huang et al., 2022), suggesting significant impacts on lake hydrology.

A study of evaporation-to-inflow ratios (E/I) for lakes in this region in Chapter 4 showed that variability in the ratio among lakes was driven by variability in inflow: lakes that had larger watersheds received more inflow and had lower E/I as a result. Based on our results, year-to-year variability in E/I at Big Bear Lake is affected by variability in evaporation and inflow. Even though 2018 experienced less inflow than 2017 (1163 mm vs. 1433 mm), the E/I ratio in 2018 was slightly lower than in 2017 (0.19 vs. 0.21), however this small difference may not be significant given the errors and uncertainties in calculating lake water balance. The year 2018 had a lower E/I ratio because it experienced much less evaporation than 2017 (226 mm vs. 296 mm). The range in E/I ratios between the three years at this lake (0.19 to 0.28) was much narrower than the range of E/I among the 25 lakes sampled in Chapter 4 in this region in 2018, which ranged from 0.01 to 0.43.

5.6.4 Uncertainties in water balance calculations

The residual is consistently positive in all three years, indicating that either inputs to the lake have been over-estimated, outputs have been under-estimated, or a combination of both. Of all the water balance components we have the most confidence in summer precipitation measurements, given they were taken nearby the lake using a shielded weighing gauge. Lake level is also likely well estimated given that air and water pressure were measured near each other with loggers that had

sub-millimetre accuracy. There may be some error in our estimate of daily evaporation rates, as PT has been show to be less accurate at smaller timescales (Granger and Hedstrom, 2011), however over the course of a water year PT tends to be quite accurate method in northern environments, usually within 15% of true evaporation (Marsh and Bigras, 1988). Evaporation rates measured by Marsh and Bigras (1988) at lakes in the nearby Mackenzie Delta compare closely to the evaporation rates we calculated. From mid-June until early September, Marsh and Bigras (1988) measured evaporation rates of 2.5 to 2.9 mm day^{-1} at one lake, and evaporation rates of 3.9 to 4.6 mm day^{-1} at another smaller lake which likely had higher evaporation rates due to advection. From June 17 to August 31, we estimated evaporation rates of 3.1, 2.7 and 3.1 mm day^{-1} in the years 2017, 2018 and 2020 respectively. Additionally, Pohl et al. (2009) estimated total yearly evaporation to be 317 mm from another lake in the Trail Valley Creek watershed that became ice-free on June 6, comparable to the evaporation we measured in 2017 (296 mm).

The only remaining lake water balance component that we estimated was Q_{out}, which we suspect has the greatest amount of error and is responsible for the positive residual. The residual of the water balance appears to increase during low Q_{in}/Q_{out} periods (Figure 5.4), suggesting that Q_{out} is being under-estimated by the rating curve low-flow conditions. This is unsurprising, given the challenges in accurately measuring low-flow streams with discharge measurement devices. There may also be some subsurface discharge from the lake, as we noted in the field that the lake water level was often above the frost table depth by the end of the summer.

5.7 Conclusion

Thermokarst lakes in the Arctic are responding variably to climate change, with both lake expansion, contraction, and drainage being observed. Few studies have tracked lake water balances over multiple years and measured the contribution of individual water balance components, making it difficult to attribute observed changes in thermokarst lakes to changes in different lake water

balance components. We measured lake water balance components at a thermokarst lake between Inuvik and Tuktoyaktuk, Canada for three years, finding that (a) rapid snowmelt leads to higher lake levels at snow dam failure, and higher runoff ratios during freshet, (b) runoff ratios during snowmelt appear to be driven by the speed of snowmelt, with lower runoff ratios occurring in years with slower snowmelt, (c) the runoff ratio during summertime is influenced by the wetness of the previous year, with wetter previous years causing higher runoff ratios in the following year, and (d) evaporation losses from the lake were mostly controlled by the ice-free period length, as the average evaporation rate varied minimally between the three years. Lake evaporation losses are likely more sensitive to the timing of lake-ice off rather than lake ice-on, as the greater incoming solar radiation present during the ice-off period causes higher potential evaporation rates than during during the ice-on period.

The climate in this region is predicted to become warmer, with greater snowfall and rainfall, and longer ice free seasons (Bush and Lemmen, 2019; Lee et al., 2021; Huang et al., 2022). It is difficult to know whether wetter summers in the future will lead to increased runoff ratios, as shrubification causes greater rainfall interception and evapotranspiration (Zwieback et al., 2019b; Black et al., 2021) and permafrost thaw causes hummocks to collapse into inter-hummock zones (Kokelj et al., 2007). Certainly, it seems that evaporation losses from lakes will increase as the ice-off dates advance earlier into the spring. Predicting whether these forces which are competing against each other to either wet or dry lakes will require modeling that can represent the complicated interaction between permafrost thaw, soil properties, vegetation expansion, and snow.

5.8 Chapter 5 Appendix

5.8.1 Estimating snow water equivalent for 2020

Snow surveys were unable to be completed at Trail Valley Creek in 2020, so we had to rely on the nearest snow surveys completed at Caribou Creek by Environment and National Resources

Northwest Territories to estimate what the snow water equivalent (SWE) was at Trail Valley Creek in 2020. The mean SWE over 26 years at Caribou Creek was 124 mm, while the mean SWE during the same time period at Trail Valley Creek was 148 mm (Marsh et al., 2019). The mean SWE at Trail Valley Creek was 1.19 times greater than at Caribou Creek. We multiplied the 2020 SWE value of Caribou Creek (121 mm) by this value (1.19) to estiate SWE at Trail Valley Creek for 2020 (144 mm).

Table 5.4 Comparison of Trail Valley Creek and Caribou Creek snow survey data for all years where data was collected at both sites (n = 26). On average, the SWE measured at Trail Valley Creek was 1.19 times greater than at Caribou Creek; this number was multiplied by the 2020 snow water equivalent of Caribou Creek (121 mm) to estimate Trail Valley Creek snow water equivalent in 2020.

Year	Caribou Creek (mm)	Trail Valley Creek (mm)
2020	121	N/A
2019	121	187
2018	79	141
2017	124	131
2016	95	114
2015	123	122
2014	86	155
2013	158	195
2012	103	167
2011	123	208
2010	93	177
2009	136	162
2008	106	158
2007	114	108
2006	183	193
2005	136	118
2001	180	179
2000	130	169
1999	98	137
1998	109	111
1997	140	143
1996	119	95
1995	136	133
1994	128	124
1993	153	116
1992	130	199
1991	130	107
Mean	124	148

Chapter 6

Conclusions and Recommendations for Future Research

Thermokarst lakes are common features in ice-rich permafrost areas that regulate the flow of water throughout the landscape, influence permafrost thaw and aggradation, and affect greenhouse gas fluxes (Karlsson et al., 2012; Langer et al., 2016; in 't Zandt et al., 2020). Climate change is altering lake water balances, as evidenced by changes in lake expansion, contraction and drainage during recent decades (Smith et al., 2005; Jones et al., 2011; Andresen and Lougheed, 2015; Finger Higgens et al., 2019). Research conducted within this thesis improves the ability to understand how lake water balances are being affected by climate change by (1) enhancing knowledge of snow-shrub-permafrost interactions and how they impact snowmelt and permafrost thaw, (2) documenting the controls on key freshet processes, including snow damming and snowmelt bypass, and 3) identifying the meteorological, watershed and lake characteristics that explain observed variability in lake water balances. This knowledge was generated using a variety of different methods, including direct measurements of lake water balance components and watershed characteristics, isotope analysis of lake water samples to estimate lake water balances and lake water sources, and spatial analysis of remote sensing data to quantify lake and watershed characteristics. This research

was a part of a larger research program in the Inuvik-Tuktoyaktuk region conducted by the Arctic Hydrology Research Group in coordination with partners from Wilfrid Laurier University, other universities, the Government of the Northwest Territories, and residents of the Inuvik-Tuktoyaktuk region. The main aim of this research is to better understand the impacts of climate change on the hydrology of continuous permafrost systems. This chapter details how Chapters 2, 3, 4 and 5 contribute to better understanding thermokarst lake water balances and outlines future research to address remaining knowledge gaps.

6.1 Synthesis of Thesis Contributions

6.1.1 Establishing connections between lake and watershed characteristics and lake water balance behaviour

The hypothesis that lake water balance behaviour is associated with lake and watershed characteristics is fundamental to the approach of this thesis, with Chapters 2, 3, 4 and 5 aiming to further our knowledge in specific areas of this concept. Based on water balance measurements at many lakes, using multiple methods during both the freshet and the summertime over multiple years, results demonstrate linkages between multiple components of lake water balances and lake and watershed characteristics. Chapter 2 explores how key watershed elements that influence runoff, namely snow, shrubs, and soil, interact with one another, to better understand how runoff may change as shrubs expand into shrub-free tundra, and changes occur to snowmelt and snow redistribution. Results from Chapter 2 suggest that birch shrub expansion will enhance permafrost thaw because the landscape will be snow-free earlier, thus exposing the ground to thaw earlier in the spring. As birch shrub expansion continues, the deeper frost table could cause hummocks to collapse into inter-hummock zones, reducing the ability of lake watersheds to convey runoff (Quinton, 1997; Kokelj et al., 2007). Chapter 3 concludes that deeper lakes retain less freshet runoff than shallower

lakes. The limited vertical mixing present in ice-covered open-drainage lakes causes freshet to flow into and out of lakes while only mixing with pre-snowmelt lake water in a thin layer below lake ice, a process known as "snowmelt bypass". This mixed layer of freshet runoff and pre-snowmelt lake water comprises a relatively smaller volume at deeper lakes, leading to less freshet runoff incorporated into deeper lakes. In Chapter 4, the ratio of evaporation-to-inflow (E/I) is found to be strongly related to the ratio of watershed area to lake area (WA/LA). Results show that lakes with larger WA/LA have lower E/I ratios because they receive more inflow than lakes with smaller WA/LA.

New empirical knowledge of how lake and watershed characteristics affect lake water balances allows lake and watershed characteristics to be used to predict which lakes are vulnerable to evaporative drawdown or lake drainage in response to climate change. Recent advances in remote sensing and modelling have generated many high resolution spatial datasets for the Arctic, including digital elevation models (Porter et al., 2018), waterbodies (Muster et al., 2017), vegetation height (Bartsch et al., 2020), permafrost temperature (Obu et al., 2019), and ground ice (O'Neill et al., 2019b). Such datasets can be used to correlate lake and watershed properties with lake water balance components, which can then be used to predict, or upscale, lake water balance properties for all lakes in a study region. An initial foray into statistical upscaling is applied in Chapter 4, where the empirical relationship determined for WA/LA and average E/I is used to predict the average E/I for thousands of lakes in the study region.

These upscaling approaches provide a better understanding of the total variability in lake water balances for a region, as data from sampling campaigns can be skewed depending on how randomly different lakes and their properties are sampled. For example, a statistical upscaling approach to carbon fluxes concluded that the Arctic has been a carbon sink during the last 25 years, contradicting previous literature and revealing that field-based sampling had been biased towards locations which were more likely to be carbon sources (Virkkala et al., 2021). With greater sampling of a wider range of lakes than was conducted in Chapter 4, effects of other

watershed properties, such as vegetation cover, hillslope angle, etc., may be detectable with more powerful statistical techniques, such as mixed effects models or random forest models. Statistical upscaling may simplify complicated hydrological processes into empirically-derived relationships, however other traditional modeling approaches that cover larger areas at a fine spatial scale are computationally intensive (e.g., Marsh et al., 2020b) and often require much more input data to run (e.g., soil thermal conductivity, hydraulic conductivity, energy balance), which is often spatially variable and difficult to collect in arctic environments. Therefore, there is a substantial potential to evaluate the hydrology of northern regions using statistical upscaling, given the ability to derive water balance data from large numbers of lakes using water isotope tracers, combined with recent advances in remote sensing datasets and statistical upscaling techniques.

6.1.2 A comprehensive understanding of the influence of freshet on lake water balances

This thesis has furthered understanding of various aspects of lake water balances during the freshet period, a typically underrepresented part of the year in Arctic lake water balance studies compared to the summertime. A clear description of lake water balance dynamics during the freshet can be assembled using knowledge generated in Chapters 2, 3, 4, and 5. Snowmelt is initiated in areas of birch shrubs before shrub-free areas, while areas of alder shrubs that trap snow and cause deep snow drifts are likely sources of continued snowmelt that drive runoff later in the freshet period (Chapter 2). The freshet runoff delivered to lakes is comprised of snow and soil-sourced water, with freshet becoming increasingly soil-sourced as the freshet progresses (Chapter 3). The interaction of snowmelt with soil water concurs with previous studies that observed heavy rainfalls in the previous year can increase the runoff ratio of a watershed during snowmelt by providing additional soil water that is entrained in snowmelt runoff (Stuefer et al., 2017). Concurrently, vertical mixing within the lakes is also increasing during the freshet, allowing the more soil-sourced freshet water

to be more easily mixed into lakes later during the freshet, resulting in a mixture of soil-sourced and snowmelt-sourced freshet remaining in lakes (Chapter 3). Freshet runoff represents the majority of the water delivered to lakes during the year, measuring between 52-63% of total runoff at Big Bear Lake for three years (Chapter 5). This large amount of inflow delivered in a relatively short period of time, combined with the presence of snow dams in lake outlets, cause lake levels to spike two to three times higher than during large summer rainfall events (Chapter 5). Although snowmelt bypass reduces the ability of freshet runoff to replace pre-snowmelt lake water (Chapter 3), freshet runoff still causes the greatest reduction in evaporation/inflow (E/I) ratios during the year, even when compared to unseasonably wet summers (Chapter 4).

The expansion of shrubs into shrub-free areas and the vertical growth of shrubs will impact lake water balances during the freshet. The expansion of birch shrubs will likely cause earlier snowmelt, while the expansion of alder shrubs could result in increased snow trapping and prolong the snowmelt period. The expansion of birch shrubs will advance the timing of freshet inflow to lakes, potentially leading to greater snowmelt bypass because freshet will flow into lakes at a time when mixing within the lake is more limited (Chapter 3). Such a shift could cause more soil-sourced water to be mixed into lakes during freshet, which may cause decreases in dissolved organic carbon and conductivity, and increases in pH (Marsh and Pomeroy, 1999; Finlay et al., 2006; Quinton and Pomeroy, 2006; Balasubramaniam et al., 2015). Additionally, the earlier snowmelt caused by birch shrubs could also cause snow dam failure (Chapter 5) to occur earlier during the freshet. The more rapid snowmelt caused by birch shrubs combined with the observation that rapid snowmelt causes higher lake levels when lakes are snow-dammed (Chapter 5) also implies that freshet lake levels may reach higher extremes in the future, potentially triggering more rapid lake drainage events (Mackay, 1988; Jones and Arp, 2015).

6.1.3 Direct and isotope measurements: Capturing both dimensions of lake water balances

This thesis uses a multi-method approach to characterizing lake water balances, incorporating both "direct" measurements of lake water balance components and lake water isotope derived information on lake water sources, lake water replacement, and evaporation-to-inflow ratios. The multi-method approach adds confidence to the accuracy of lake water balance measurements for either method. For example, in Chapter 4 a lake with a WA/LA of 6.7 is expected to have an E/I of 0.16, while the E/I of Big Bear Lake (which has a WA/LA of 6.7) measured using direct methods in Chapter 5 is 0.19 in 2018, giving us confidence that we have accurately measured the volumetric water balance of Big Bear Lake. However, each method also provides unique pieces of information about lake water balance, providing a wider breadth of information about lakes.

Chapters 3 and 5 illustrate the different pieces of information each method can provide, and how combining both methods can give a more complete picture of lake water balances. Direct measurements (Chapter 5) show that freshet runoff constitutes two thirds of yearly inflow, causing lake levels to reach their yearly maximum. Lake level recorders also observe that lake level maximums are enhanced by the presence of a snow dam in the lake outlet. Contrastingly, isotope measurements (Chapter 3) provide information that cannot be gathered using direct measurements. Isotope data showed that only a quarter of lake water is replaced during freshet on average, with deeper lakes retaining less freshet runoff, and the source of freshet was an equal mixture of snow and rain-sourced water. Combining the knowledge of these data reveal a more complete picture of lake water balance: i.e. snowmelt bypass causes freshet to flow in and out of lakes without mixing with pre-snowmelt lake water, causing freshet runoff to leave a disproportionately small imprint on lake water isotope composition (depending on lake depth) when compared to the relatively large volume of freshet inflow. Had only lake water isotope data been collected, information about snow dam failure would have been missed, while only direct water balance measurements could not have

captured the mixture of water sources present in freshet and the occurrence of snowmelt bypass. In short, direct measurements give information about how much water goes in and out of lakes, while isotope measurements give information about different water sources that have entered and exited lakes.

Despite the different kinds of hydrological information volume and isotope measurements generate, water balance studies including a combination of volume and isotope measurements are rare (Haig et al., 2020). Direct measurements of water balance components have lead to inaccurate hypotheses about hydrological behaviour leading researchers to call for the combination of tracers (i.e. isotopes) and direct measurements in order to better understand the behaviour of watersheds (McDonnell and Beven, 2014). The multi-method approach applied in this thesis illustrates the benefit of using both direct and isotope methods. Future studies at ice-covered lakes or other lake systems where limited mixing may occur should employ both direct and isotope measurements to fully understand lake water balances.

6.1.4 Complementary research in the Inuvik-Tuktoyaktuk Region

The studies in this thesis were completed alongside other related research that shared similar goals in better understanding the effects of climate change on the tundra-dominated permafrost environment. Further research to enhance our understanding of the interaction between snow, shrubs and soil temperature at the Siksik Creek watershed was carried out by Grünberg et al. (2020), whose findings were congruent with the results of Chapter 2. Grünberg et al. (2020) found that later snow-free dates strongly correlated with shallower active layer depth and that the timing of topsoil thawing was advanced by earlier snow-free date and shallower snow depths. The study also observed that summertime topsoil temperatures differed minimally (<1 °C) between vegetation cover types, while differences in winter topsoil temperatures varied by >5 °C, driven by variation in snow depth and density caused by shrub-affected snow redistribution. These results further exemplify the necessity for winter and springtime measurements in the Arctic.

Some of the research executed in this thesis also aided in the development of new measurement methods and protocols. The methods developed to derive snow depth from drone photos that were used in Chapter 2 and Grünberg et al. (2020) continued to be developed and were published as a methods paper (Walker et al., 2021). These drone snow depth mapping methods were then used by Meloche et al. (2022) to calibrate remote sensing data. The knowledge gained from Chapter 2 also helped inform the development of an open-source permafrost monitoring protocol (Boike et al., 2022). Specifically, Chapter 2 helped illustrate the value of making all measurements of frost table depth, vegetation, soil properties, snow, etc. in the exact same location, as the high degree of spatial heterogeneity in these variables makes it difficult to use data that are not collected in the same location. One of the principles of the protocol developed by Boike et al. (2022) is the collection of associated measurements of snow, vegetation, etc. in the exact same location where frost table depth is measured.

6.2 Predictions and future research

6.2.1 A wetter or drier future for lakes?

Most recent projections for the western Canadian Arctic predict air temperature to rise by 2-3 °C above pre-industrial levels by 2041-2060, with likely (but not certain) increases in summertime and wintertime precipitation of 10-30% by 2080-2100 (Lee et al., 2021). There is confidence that evaporation will increase for non-bedfast ice lakes in the Arctic (Arp et al., 2015; Woolway et al., 2020), as warmer air temperatures lead to longer ice-free seasons and higher evaporation rates. Whether a lake will have a wetter (increasing ratio of water input to output) or drier (decreasing ratio of water input to output) future depends on if increases in precipitation and inflow can offset expected increases in evaporation.

Future changes in lake evaporation, inflow and other water balance components will be affected by many intertwined, highly spatially variable processes and landscape elements (Figure

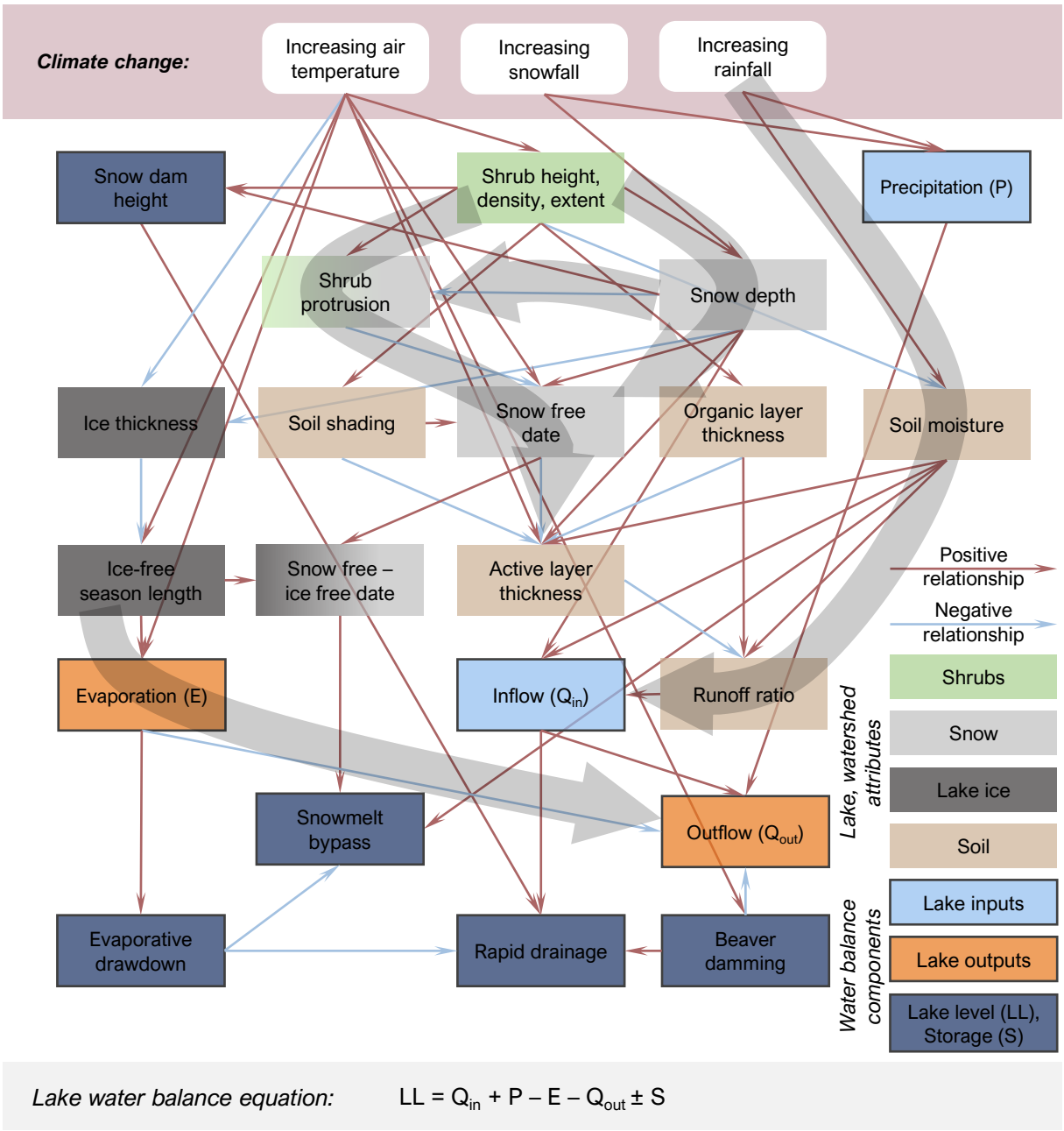

Figure 6.1 Conceptual model of the interactions between landscape elements and lake water balance components in their response to climate change at an annual to inter-annual time scale. Dominant pathways of interaction that were identified in this thesis are outlined with grey transparent arrows. Synthesized using results from Chapter 2, 3, 4 and 5, Turner et al. (2014); Heijmans et al. (2022).

6.1). Some of the resulting impacts from climate change could increase the amount of inflow for lakes, while other impacts can decrease the amount of inflow. For example, rising air temperatures cause earlier snowmelt, enhancing permafrost thaw and reducing runoff from hillslopes (Kokelj et al., 2007; Koch et al., 2022), while increases in shrub extent could lead to drier soils due to greater transpiration losses (Black et al., 2021) and rainfall interception (Zwieback et al., 2019a). Countering these drying forces include increases in precipitation, which could lead to wetter soils that convert a larger percentage of snowmelt and rainfall into runoff (i.e., greater runoff ratios, Stuefer et al., 2017), however greater rainfall enhances permafrost thaw and increases in runoff can also lead to more rapid lake drainage (Webb et al., 2022). The impact of snow-shrub-permafrost interactions on inflow are particularly difficult to predict, as shrub expansion has been observed to both inhibit (e.g. Blok et al., 2010) and advance (e.g. Chapter 2) permafrost thaw, depending on the difference between shrub height and snow depth, and resulting impacts on shrub protrusion, snow free date and soil shading (Figure 6.1).

While this thesis contributes to our understanding of how snow shrub interactions affect permafrost thaw (Chapter 2), and the conditions controlling lake inflow (Chapter 4, 5) and lake evaporation (Chapter 5), there are still many knowledge gaps in our understanding of the ultimate impact of climate change on thermokarst lake water balances. Within this thesis, predictions about how climate change will impact lake water balances are posed based on our current understanding of how landscape elements and processes influence lake water balance components (Figure 6.1). These predictions include:

1. Birch shrub expansion may amplify permafrost thaw (Chapter 2), leading to reduced runoff relative to precipitation (i.e., lower runoff ratios, Chapter 5).

2. Shrub expansion leads to earlier snowmelt timing relative to lake ice-off, causing earlier snow dam failure and more snow sourced water to bypass lakes (Chapter 2, 3, 5).

3. Lakes with smaller WA/LA ratios become disproportionately influenced by evaporation

and more vulnerable to lake-level drawdown and possibly desiccation under drier future conditions (Chapter 4).

4. Lakes with larger WA/LA ratios are more likely to experience rapid drainage because they experience greater increases in lake level in response to inflow, both during snow dam failure and summertime inflow (Chapter 4).

Below I describe some how these predictions can be tested, including ongoing work that has occurred congruently with this thesis.

Work has already begun on testing Prediction 1 using historical streamflow data. The team of researchers, including myself, are evaluating whether the Trail Valley Creek watershed is generating less runoff as the amount of shrubs in the watershed has increased over time. The data used in this study spans from 1977-2019, while 63% of the Trail Valley Creek watershed has experienced increases in shrub growth since 2000. Preliminary analyses show no clear impact of shrubification on runoff, as summertime runoff ratios have increased over time along with rainfall, whereas we hypothesized increased shrub cover may reduce runoff ratios by drying soils as a result of increasing transpiration (conference poster, Wallace et al., 2022). Even when controlling for antecedent moisture conditions, there is no clear pattern of reducing runoff ratios over time. However, this analysis is still in progress and incomplete.

Prediction 2 is more difficult to test using historical data because it requires long term measurements of lake water isotope composition, which are rare in the Arctic. When no long-term records exist, paleohydrological methods (e.g. paleolimnological records) can be used to evaluate how lake water isotope composition has evolved during past decades or centuries (e.g. Bouchard et al., 2013). One could expect that the paleohydrological data would show δ_I becoming more rainfall-like during the past several decades as shrubs have proliferated in the Arctic, if shrubs are advancing snowmelt timing and increasing snowmelt bypass. However, increases in tall, snow-trapping shrubs may supply more snowmelt to lakes later on during the freshet, potentially

offsetting increases in snowmelt bypass caused by shorter shrubs. Accurately interpreting the data obtained from a lake sediment core requires an understanding of how hydrological processes affect water isotope compositions at the lakes being studied. For example, without knowledge of the presence of snowmelt bypass at the lakes studied in this thesis (Chapter 3), one may interpret a shift to more rain-like δ_I (isotope composition of lake source water) to mean that lakes are receiving less freshet inflow relative to rainfall-sourced runoff. However, from Chapter 3, we know that freshet has an isotope composition more similar to δ_P than δ_S (Figure 3.5c), and that the volume of snowmelt inflow does not impact the replacement of lake water (Table 3.3). This exemplifies why paleohydrological data can be more confidently interpreted at locations where isotope-based hydrological investigations have already characterized the isotope hydrology of the lakes (Wolfe et al., 2005, 2008; Zabel et al., 2022). Having now described the isotope hydrology in some detail for in Chapters 3 and 4, one could now interpret isotope data from lake sediment cores the Inuvik-Tuktoyaktuk region with some confidence. However, studies deriving both δ^2H and $\delta^{18}O$ from lake sediments are rare, making it difficult to reconstruct δ_I. One would also need to make assumptions about past climate conditions during the open-water season and other isotope parameters when estimating δ_I.

Both Predictions 3 and 4 are candidates for testing with long time series of remote sensing data. Several studies have evaluated temporal changes in water surface area in the Arctic (e.g., Smith et al., 2005; Plug et al., 2008; Jones et al., 2011; Lantz and Turner, 2015; Finger Higgens et al., 2019; Nitze et al., 2020; Webb et al., 2022), however no studies have incorporated WA/LA into their analysis. Prediction 3 poses that lakes with smaller WA/LA would expand less in wetter years, and shrink more in drier years, while Prediction 4 poses that drained lakes are more likely to have a larger than average WA/LA. A Master's thesis by Kariyawasam (2022) has recently quantified changes in lake drainage during a 69-year period in the Inuvik-Tuktoyaktuk region, results of which identified that lake drainage has increased since the year 2000 following 50 years of decreasing rates of lake drainage. Testing whether the WA/LA of drained lakes identified by Kariyawasam (2022)

were larger than average would allow Prediction 4 to be tested. High resolution (3 metre), high flyover frequency (1-3 days) satellite constellations now make it possible to attribute reductions in lake surface area to either evaporative drawdown or rapid drainage.

In addition to the suggested approaches above, all predictions are candidates for testing with hydrological models. Multiple models are capable of representing high spatial resolution variability in snow, vegetation, hydrology, and permafrost conditions (e.g., Endrizzi et al., 2013; Westermann et al., 2016; Marsh et al., 2020a; Jan et al., 2020), which are necessary to accurately predict the co-evolution of the permafrost landscape in response to climate change. While models may simplify the complexity of the real world, the assumptions made using historical data are that the observed hydrological response to past changes will continue on a similar trajectory into the future. However, it becomes more difficult to rely on past observations to predict future changes as the Arctic continues to warm more rapidly and the environment reaches tipping points not previously observed (e.g., widespread talik formation, Farquharson et al., 2022), which alter the course of change. Carrying out modelling studies requires we the necessary data to drive, calibrate and validate the model, which can be a challenge to in the Arctic. Understanding the future of lake water balances will require integrating the knowledge from the multiple approaches outlined above while considering the strengths and limitations of each approach appropriately.

References

Anders, K., Marx, S., Boike, J., Herfort, B., Wilcox, E. J., Langer, M., Marsh, P., and Höfle, B.: Multitemporal terrestrial laser scanning point clouds for thaw subsidence observation at Arctic permafrost monitoring sites, Earth Surface Processes and Landforms, 45, 1589–1600, https://doi.org/10.1002/esp.4833, 2020.

Anderson, L., Birks, J., Rover, J., and Guldager, N.: Controls on recent Alaskan lake changes identified from water isotopes and remote sensing, Geophysical Research Letters, 40, 3413–3418, https://doi.org/10.1002/grl.50672, 2013.

Andresen, C. G. and Lougheed, V. L.: Disappearing Arctic tundra ponds: Fine-scale analysis of surface hydrology in drained thaw lake basins over a 65 year period (1948-2013), Journal of Geophysical Research: Biogeosciences, 120, 466–479, https://doi.org/10.1002/2014JG002778, 2015.

Anthony, K. M., Zimov, S. A., Grosse, G., Jones, M. C., Anthony, P. M., Chapin III, F. S., Finlay, J. C., Mack, M. C., Davydov, S., Frenzel, P., and Frolking, S.: A shift of thermokarst lakes from carbon sources to sinks during the Holocene epoch, Nature, 511, 452–456, https://doi.org/10.1038/nature13560, 2014.

Arp, C. D., Jones, B. M., Urban, F. E., and Grosse, G.: Hydrogeomorphic processes of thermokarst lakes with grounded-ice and floating-ice regimes on the Arctic coastal plain, Alaska, Hydrological Processes, 25, 2422–2438, https://doi.org/10.1002/hyp.8019, 2011.

Arp, C. D., Jones, B. M., Lu, Z., and Whitman, M. S.: Shifting balance of thermokarst lake ice regimes across the Arctic Coastal Plain of northern Alaska, Geophysical Research Letters, 39, n/a–n/a, https://doi.org/10.1029/2012GL052518, 2012a.

Arp, C. D., Whitman, M. S., Jones, B. M., Kemnitz, R., Grosse, G., and Urban, F. E.: Drainage Network Structure and Hydrologic Behavior of Three Lake-Rich Watersheds on the Arctic Coastal Plain, Alaska, Arctic, Antarctic, and Alpine Research, 44, 385–398, https://doi.org/10.1657/1938-4246-44.4.385, 2012b.

Arp, C. D., Jones, B. M., Liljedahl, A. K., Hinkel, K. M., and Welker, J. A.: Depth, ice thickness, and ice-out timing cause divergent hydrologic responses among Arctic lakes, Water Resources Research, 51, 9379–9401, https://doi.org/10.1016/0022-1694(68)90080-2, 2015.

Arp, C. D., Jones, B. M., Hinkel, K. M., Kane, D. L., Whitman, M. S., and Kemnitz, R.: Recurring outburst floods from drained lakes: an emerging Arctic hazard, Frontiers in Ecology and the Environment, 18, 384–390, https://doi.org/10.1002/fee.2175, 2020a.

Arp, C. D., Whitman, M. S., Kemnitz, R., and Stuefer, S. L.: Evidence of Hydrological Intensification and Regime Change From Northern Alaskan Watershed Runoff, Geophysical Research Letters, 47, https://doi.org/10.1029/2020GL089186, 2020b.

Balasubramaniam, A. M., Hall, R. I., Wolfe, B. B., Sweetman, J. N., and Wang, X.: Source water inputs and catchment characteristics regulate limnological conditions of shallow subarctic lakes (Old Crow Flats, Yukon, Canada), Canadian Journal of Fisheries and Aquatic Sciences, 72, 1058–1072, https://doi.org/10.1139/cjfas-2014-0340, 2015.

Bartsch, A., Widhalm, B., Leibman, M., Ermokhina, K., Kumpula, T., Skarin, A., Wilcox, E. J., Jones, B. M., Frost, G. V., Höfler, A., and Pointner, G.: Feasibility of tundra vegetation height retrieval from

Sentinel-1 and Sentinel-2 data, Remote Sensing of Environment, 237, 111 515, https://doi.org/10.1016/j.rse.2019.111515, 2020.

Bergmann, M. A. and Welch, H. E.: Spring Meltwater Mixing in Small Arctic Lakes, Canadian Journal of Fisheries and Aquatic Sciences, 42, 1789–1798, https://doi.org/10.1139/f85-224, 1985.

Bintanja, R. and Andry, O.: Towards a rain-dominated Arctic, Nature Climate Change, 7, 263–267, https://doi.org/10.1038/nclimate3240, 2017.

Bintanja, R. and Selten, F. M.: Future increases in Arctic precipitation linked to local evaporation and sea-ice retreat., Nature, 509, 479–82, https://doi.org/10.1038/nature13259, 2014.

Bintanja, R., van der Wiel, K., van der Linden, E. C., Reusen, J., Bogerd, L., Krikken, F., and Selten, F. M.: Strong future increases in Arctic precipitation variability linked to poleward moisture transport, Science Advances, 6, eaax6869, https://doi.org/10.1126/sciadv.aax6869, 2020.

Biskaborn, B. K., Smith, S. L., Noetzli, J., Matthes, H., Vieira, G., Streletskiy, D. A., Schoeneich, P., Romanovsky, V. E., Lewkowicz, A. G., Abramov, A., Allard, M., Boike, J., Cable, W. L., Christiansen, H. H., Delaloye, R., Diekmann, B., Drozdov, D., Etzelmüller, B., Grosse, G., Guglielmin, M., Ingeman-Nielsen, T., Isaksen, K., Ishikawa, M., Johansson, M., Johannsson, H., Joo, A., Kaverin, D., Kholodov, A., Konstantinov, P., Kröger, T., Lambiel, C., Lanckman, J. P., Luo, D., Malkova, G., Meiklejohn, I., Moskalenko, N., Oliva, M., Phillips, M., Ramos, M., Sannel, A. B. K., Sergeev, D., Seybold, C., Skryabin, P., Vasiliev, A., Wu, Q., Yoshikawa, K., Zheleznyak, M., and Lantuit, H.: Permafrost is warming at a global scale, Nature Communications, 10, 1–11, https://doi.org/10.1038/s41467-018-08240-4, 2019.

Bjorkman, A. D., Myers-Smith, I. H., Elmendorf, S. C., Normand, S., Rüger, N., Beck, P. S. A., Blach-Overgaard, A., Blok, D., Cornelissen, J. H. C., Forbes, B. C., Georges, D., Goetz, S. J., Guay, K. C., Henry, G. H. R., HilleRisLambers, J., Hollister, R. D., Karger, D. N., Kattge, J., Manning, P., Prevéy, J. S., Rixen, C., Schaepman-Strub, G., Thomas, H. J. D., Vellend, M., Wilmking, M., Wipf, S., Carbognani, M., Hermanutz, L., Lévesque, E., Molau, U., Petraglia, A., Soudzilovskaia, N. A., Spasojevic, M. J., Tomaselli, M., Vowles, T., Alatalo, J. M., Alexander, H. D., Anadon-Rosell, A., Angers-Blondin, S., te Beest, M., Berner, L., Björk, R. G., Buchwal, A., Buras, A., Christie, K., Cooper, E. J., Dullinger, S., Elberling, B., Eskelinen, A., Frei, E. R., Grau, O., Grogan, P., Hallinger, M., Harper, K. A., Heijmans, M. M. P. D., Hudson, J., Hülber, K., Iturrate-Garcia, M., Iversen, C. M., Jaroszynska, F., Johnstone, J. F., Jørgensen, R. H., Kaarlejärvi, E., Klady, R., Kuleza, S., Kulonen, A., Lamarque, L. J., Lantz, T., Little, C. J., Speed, J. D. M., Michelsen, A., Milbau, A., Nabe-Nielsen, J., Nielsen, S. S., Ninot, J. M., Oberbauer, S. F., Olofsson, J., Onipchenko, V. G., Rumpf, S. B., Semenchuk, P., Shetti, R., Collier, L. S., Street, L. E., Suding, K. N., Tape, K. D., Trant, A., Treier, U. A., Tremblay, J.-P. P., Tremblay, M., Venn, S., Weijers, S., Zamin, T., Boulanger-Lapointe, N., Gould, W. A., Hik, D. S., Hofgaard, A., Jónsdóttir, I. S., Jorgenson, J., Klein, J., Magnusson, B., Tweedie, C., Wookey, P. A., Bahn, M., Blonder, B., van Bodegom, P. M., Bond-Lamberty, B., Campetella, G., Cerabolini, B. E. L., Chapin, F. S., Cornwell, W. K., Craine, J., Dainese, M., de Vries, F. T., Díaz, S., Enquist, B. J., Green, W., Milla, R., Niinemets, Ü., Onoda, Y., Ordoñez, J. C., Ozinga, W. A., Penuelas, J., Poorter, H., Poschlod, P., Reich, P. B., Sandel, B., Schamp, B., Sheremetev, S., and Weiher, E.: Plant functional trait change across a warming tundra biome, Nature, 562, 57–62, https://doi.org/10.1038/s41586-018-0563-7, 2018.

Black, K. L., Wallace, C. A., and Baltzer, J. L.: Seasonal thaw and landscape position determine foliar functional traits and whole-plant water use in tall shrubs on the low arctic tundra, New Phytologist, 231, 94–107, https://doi.org/10.1111/nph.17375, 2021.

Blok, D., Heijmans, M. M. P. D., Schaepman-Strub, G., Kononov, A. V., Maximov, T. C., and Berendse, F.: Shrub expansion may reduce summer permafrost thaw in Siberian tundra, Global Change Biology, 16, 1296–1305, https://doi.org/10.1111/j.1365-2486.2009.02110.x, 2010.

Blöschl, G., Bierkens, M. F., Chambel, A., Cudennec, C., Destouni, G., Fiori, A., Kirchner, J. W., McDonnell,

J. J., Savenije, H. H., Sivapalan, M., Stumpp, C., Toth, E., Volpi, E., Carr, G., Lupton, C., Salinas, J., Széles, B., Viglione, A., Aksoy, H., Allen, S. T., Amin, A., Andréassian, V., Arheimer, B., Aryal, S. K., Baker, V., Bardsley, E., Barendrecht, M. H., Bartosova, A., Batelaan, O., Berghuijs, W. R., Beven, K., Blume, T., Bogaard, T., Borges de Amorim, P., Böttcher, M. E., Boulet, G., Breinl, K., Brilly, M., Brocca, L., Buytaert, W., Castellarin, A., Castelletti, A., Chen, X., Chen, Y., Chen, Y., Chifflard, P., Claps, P., Clark, M. P., Collins, A. L., Croke, B., Dathe, A., David, P. C., de Barros, F. P. J., de Rooij, G., Di Baldassarre, G., Driscoll, J. M., Duethmann, D., Dwivedi, R., Eris, E., Farmer, W. H., Feiccabrino, J., Ferguson, G., Ferrari, E., Ferraris, S., Fersch, B., Finger, D., Foglia, L., Fowler, K., Gartsman, B., Gascoin, S., Gaume, E., Gelfan, A., Geris, J., Gharari, S., Gleeson, T., Glendell, M., Gonzalez Bevacqua, A., González-Dugo, M. P., Grimaldi, S., Gupta, A. B., Guse, B., Han, D., Hannah, D., Harpold, A., Haun, S., Heal, K., Helfricht, K., Herrnegger, M., Hipsey, M., Hlaváčiková, H., Hohmann, C., Holko, L., Hopkinson, C., Hrachowitz, M., Illangasekare, T. H., Inam, A., Innocente, C., Istanbulluoglu, E., Jarihani, B., Kalantari, Z., Kalvans, A., Khanal, S., Khatami, S., Kiesel, J., Kirkby, M., Knoben, W., Kochanek, K., Kohnová, S., Kolechkina, A., Krause, S., Kreamer, D., Kreibich, H., Kunstmann, H., Lange, H., Liberato, M. L. R., Lindquist, E., Link, T., Liu, J., Loucks, D. P., Luce, C., Mahé, G., Makarieva, O., Malard, J., Mashtayeva, S., Maskey, S., Mas-Pla, J., Mavrova-Guirguinova, M., Mazzoleni, M., Mernild, S., Misstear, B. D., Montanari, A., Müller-Thomy, H., Nabizadeh, A., Nardi, F., Neale, C., Nesterova, N., Nurtaev, B., Odongo, V. O., Panda, S., Pande, S., Pang, Z., Papacharalampous, G., Perrin, C., Pfister, L., Pimentel, R., Polo, M. J., Post, D., Prieto Sierra, C., Ramos, M.-H., Renner, M., Reynolds, J. E., Ridolfi, E., Rigon, R., Riva, M., Robertson, D. E., Rosso, R., Roy, T., Sá, J. H., Salvadori, G., Sandells, M., Schaefli, B., Schumann, A., Scolobig, A., Seibert, J., Servat, E., Shafiei, M., Sharma, A., Sidibe, M., Sidle, R. C., Skaugen, T., Smith, H., Spiessl, S. M., Stein, L., Steinsland, I., Strasser, U., Su, B., Szolgay, J., Tarboton, D., Tauro, F., Thirel, G., Tian, F., Tong, R., Tussupova, K., Tyralis, H., Uijlenhoet, R., van Beek, R., van der Ent, R. J., van der Ploeg, M., Van Loon, A. F., van Meerveld, I., van Nooijen, R., van Oel, P. R., Vidal, J.-P., von Freyberg, J., Vorogushyn, S., Wachniew, P., Wade, A. J., Ward, P., Westerberg, I. K., White, C., Wood, E. F., Woods, R., Xu, Z., Yilmaz, K. K., and Zhang, Y.: Twenty-three unsolved problems in hydrology (UPH) – a community perspective, Hydrological Sciences Journal, 64, 1141–1158, https://doi.org/10.1080/02626667.2019.1620507, 2019.

Boike, J., Chadburn, S., Martin, J., Zwieback, S., Althuizen, I. H., Anselm, N., Cai, L., Coulombe, S., Lee, H., Liljedahl, A. K., Schneebeli, M., Sjöberg, Y., Smith, N., Smith, S. L., Streletskiy, D. A., Stuenzi, S. M., Westermann, S., and Wilcox, E. J.: Standardized monitoring of permafrost thaw: a user-friendly, multiparameter protocol, Arctic Science, pp. 1–30, https://doi.org/10.1139/as-2021-0007, 2022.

Bonfils, C. J. W., Phillips, T. J., Lawrence, D. M., Cameron-Smith, P., Riley, W. J., and Subin, Z. M.: On the influence of shrub height and expansion on northern high latitude climate, Environmental Research Letters, 7, https://doi.org/10.1088/1748-9326/7/1/015503, 2012.

Bonnaventure, P. P. and Lamoureux, S. F.: The active layer: A conceptual review of monitoring, modelling techniques and changes in a warming climate, Progress in Physical Geography, 37, 352–376, https://doi.org/10.1177/0309133313478314, 2013.

Bouchard, F., Turner, K. W., MacDonald, L. A., Deakin, C., White, H., Farquharson, N., Medeiros, A. S., Wolfe, B. B., Hall, R. I., Pienitz, R., and Edwards, T. W. D.: Vulnerability of shallow subarctic lakes to evaporate and desiccate when snowmelt runoff is low, Geophysical Research Letters, 40, 6112–6117, https://doi.org/10.1002/2013GL058635, 2013.

Bowling, L. C., Kane, D. L., Gieck, R. E., Hinzman, L. D., and Lettenmaier, D. P.: The role of surface storage in a low-gradient Arctic watershed, Water Resources Research, 39, 1–13, https://doi.org/10.1029/2002WR001466, 2003.

Bowser, C. and Gat, J.: On the process of lake ice formation, in: Isotopes in Water Resources Management, pp. 209–211, Vienna, 1995.

Box, J. E., Colgan, W. T., Christensen, T. R., Schmidt, N. M., Lund, M., Parmentier, F.-J. W., Brown, R., Bhatt, U. S., Euskirchen, E. S., Romanovsky, V. E., Walsh, J. E., Overland, J. E., Wang, M., Corell, R. W., Meier, W. N., Wouters, B., Mernild, S., Mård, J., Pawlak, J., and Olsen, M. S.: Key indicators of Arctic climate change: 1971–2017, Environmental Research Letters, 14, 045 010, https://doi.org/10.1088/1748-9326/aafc1b, 2019.

Braun, C., Hardy, D. R., Bradley, R. S., and Retelle, M. J.: Streamflow and suspended sediment transfer to Lake Sophia, Cornwallis Island, Nunavut, Canada, Arctic, Antarctic, and Alpine Research, 32, 456–465, https://doi.org/10.2307/1552395, 2000.

Brewer, M. C., Carter, L., Glenn, R., and Murray, R.: Sudden drainage of a thaw lake on the Alaskan Arctic coastal plain, in: Proceedings of the Sixth International Conference on Permafrost, pp. 48–53, Wushan Guangzhou: South China University of Technology Press, 1993.

Bring, A., Fedorova, I., Dibike, Y., Hinzman, L., Mård, J., Mernild, S. H., Prowse, T., Semenova, O., Stuefer, S. L., and Woo, M. K.: Arctic terrestrial hydrology: A synthesis of processes, regional effects, and research challenges, Journal of Geophysical Research: Biogeosciences, 121, 621–649, https://doi.org/10.1002/2015JG003131, 2016.

Brock, B. E., Wolfe, B. B., and Edwards, T. W. D.: Spatial and temporal perspectives on spring break-up flooding in the Slave River Delta, NWT, Hydrological Processes, 22, 4058–4072, https://doi.org/10.1002/hyp, 2008.

Brock, B. E., Yi, Y., Clogg-Wright, K. P., Edwards, T. W. D., and Wolfe, B. B.: Multi-year landscape-scale assessment of lakewater balances in the Slave River Delta, NWT, using water isotope tracers, Journal of Hydrology, 379, 81–91, https://doi.org/10.1016/j.jhydrol.2009.09.046, 2009.

Brosius, L. S., Anthony, K. M., Treat, C. C., Lenz, J., Jones, M. C., Bret-Harte, M. S., and Grosse, G.: Spatiotemporal patterns of northern lake formation since the Last Glacial Maximum, Quaternary Science Reviews, 253, 106 773, https://doi.org/10.1016/j.quascirev.2020.106773, 2021.

Brown, R. D. and Mote, P. W.: The response of Northern Hemisphere snow cover to a changing climate, Journal of Climate, 22, 2124–2145, https://doi.org/10.1175/2008JCLI2665.1, 2009.

Buck, A. L.: New Equations for Computing Vapor Pressure and Enhancement Factor, Journal of Applied Meteorology and Climatology, 20, 1527 – 1532, https://doi.org/10.1175/1520-0450(1981)020<1527:NEFCVP>2.0.CO;2, 1981.

Bui, M. T., Lu, J., and Nie, L.: A Review of Hydrological Models Applied in the Permafrost-Dominated Arctic Region, Geosciences, 10, 401, https://doi.org/10.3390/geosciences10100401, 2020.

Burn, C. and Kokelj, S.: The Environment and Permafrost of the Mackenzie Delta Area, Permafrost and Periglacial Processes, 20, 83–105, https://doi.org/10.1002/ppp, 2009.

Burn, C. R.: Tundra lakes and permafrost, Richards Island, western Arctic coast, Canada, Canadian Journal of Earth Sciences, 39, 1441, https://doi.org/10.1139/e02-903, 2002.

Burn, C. R.: Lake-bottom thermal regimes, western Arctic Coast, Canada, Permafrost and Periglacial Processes, 16, 355–367, https://doi.org/10.1002/ppp.542, 2005.

Bush, E. and Lemmen, D. S.: Canada's changing climate report, Government of Canada, URL https://publications.gc.ca/collections/collection_2019/eccc/En4-368-2019-eng.pdf, 2019.

Chapin, F. S., Sturm, M., Serreze, M. C., McFadden, J. P., Key, J. R., Lloyd, A. D., McGuire, A. D., Rupp, T. S., Lynch, A. H., Schimel, J. P., Beringer, J., Chapman, W. L., Epstein, H. E., Euskirchen, E. S., Hinzman, L. D., Jia, G., Ping, C.-L., Tape, K. D., Thompson, C. D. C., Walker, D. A., and Welker, J. M.: Role of Land-Surface Changes in Arctic Summer Warming, Science, 310, 657–660, https://doi.org/10.1126/science.1117368, 2005.

Chen, M., Rowland, J. C., Wilson, C. J., Altmann, G. L., and Brumby, S. P.: Temporal and spatial pattern of thermokarst lake area changes at Yukon Flats, Alaska, Hydrological Processes, 28, 837–852, https://doi.org/10.1002/hyp.9642, 2014.

Connon, R. F., Quinton, W. L., Craig, J. R., and Hayashi, M.: Changing hydrologic connectivity due to permafrost thaw in the lower Liard River valley, NWT, Canada, Hydrological Processes, 28, 4163–4178, https://doi.org/10.1002/hyp.10206, 2014.

Cooley, S. W., Smith, L. C., Ryan, J. C., Pitcher, L. H., and Pavelsky, T. M.: Arctic-Boreal Lake Dynamics Revealed Using CubeSat Imagery, Geophysical Research Letters, 46, 2111–2120, https://doi.org/10.1029/2018GL081584, 2019.

Coplen, T. B.: New guidelines for reporting stable hydrogen, carbon, and oxygen isotope-ratio data, Geochimica et Cosmochimica Acta, 60, 3359–3360, https://doi.org/10.1016/0016-7037(96)00263-3, 1996.

Cortés, A. and MacIntyre, S.: Mixing processes in small arctic lakes during spring, Limnology and Oceanography, 65, 260–288, https://doi.org/10.1002/lno.11296, 2020.

Cortés, A., MacIntyre, S., and Sadro, S.: Flowpath and retention of snowmelt in an ice-covered arctic lake, Limnology and Oceanography, 62, 2023–2044, https://doi.org/10.1002/lno.10549, 2017.

Craig, H.: Isotopic Variations in Meteoric Waters, Science, 133, 1702–1703, https://doi.org/10.1126/science.133.3465.1702, 1961.

Craig, H. and Gordon, L.: Deuterium and oxygen 18 variations in the ocean and the marine atmosphere, Consiglio nazionale delle richerche, Laboratorio de geologia nucleare Pisa, 1965.

De Michele, C., Avanzi, F., Passoni, D., Barzaghi, R., Pinto, L., Dosso, P., Ghezzi, A., Gianatti, R., and Vedova, G. D.: Using a fixed-wing UAS to map snow depth distribution: An evaluation at peak accumulation, Cryosphere, 10, 511–522, https://doi.org/10.5194/tc-10-511-2016, 2016.

Edwards, T. W. and McAndrews, J.: Paleohydrology of a Canadian Shield lake inferred from 18O in sediment cellulose, Canadian Journal of Earth Science, 26, 1850–1858, https://doi.org/10.1139/e89-158, 1989.

Edwards, T. W. D., Wolfe, B. B., Gibson, J. J., and Hammarlund, D.: Use of water isotope tracers in high latitude hydrology and paleohydrology, in: Long-term Environmental Change in Arctic and Antarctic Lakes, edited by Smol, J. P., Pienitz, R., and Douglas, M. S. V., vol. 8 of *Developments in Paleoenvironmental Research*, pp. 187–207, Springer Netherlands, Dordrecht, https://doi.org/10.1007/978-1-4020-2126-8_7, 2004.

Endrizzi, S. and Marsh, P.: Observations and modeling of turbulent fluxes during melt at the shrub-tundra transition zone 1: point scale variations, Hydrology Research, 41, 471–491, https://doi.org/10.2166/nh.2010.149, 2010.

Endrizzi, S., Quinton, W. L., and Marsh, P.: Modelling the spatial pattern of ground thaw in a small basin in the arctic tundra, The Cryosphere Discussions, 5, 367–400, https://doi.org/10.5194/tcd-5-367-2011, 2011.

Endrizzi, S., Gruber, S., Dall'Amico, M., and Rigon, R.: GEOtop 2.0: Simulating the combined energy and water balance at and below the land surface accounting for soil freezing, snow cover and terrain effects, Geoscientific Model Development, 7, 2831–2857, https://doi.org/10.5194/gmd-7-2831-2014, 2013.

Engram, M., Arp, C. D., Jones, B. M., Ajadi, O. A., and Meyer, F. J.: Analyzing floating and bedfast lake ice regimes across Arctic Alaska using 25 years of space-borne SAR imagery, https://doi.org/10.1016/j.rse.2018.02.022, 2018.

Environment and Climate Change Canada: Historical Climate Data, URL `https://climate.weather.gc.ca/climate_data/daily_data_e.html`, 2019a.

Environment and Climate Change Canada: Canadian Climate Normals, URL `https://climate.weather.gc.ca/climate_normals/results_1981_2010_e.html?searchType=stnProv&lstProvince=NT&txtCentralLatMin=0&txtCentralLatSec=0&txtCentralLongMin=0&txtCentralLongSec=0&stnID=1669&dispBack=0`, 2019b.

Ernakovich, J. G., Hopping, K. A., Berdanier, A. B., Simpson, R. T., Kachergis, E. J., Steltzer, H., and Wallenstein, M. D.: Predicted responses of arctic and alpine ecosystems to altered seasonality under climate change, Global Change Biology, 20, 3256–3269, https://doi.org/10.1111/gcb.12568, 2014.

ESRI: ArcGIS Desktop 10.5.1 [software], 2016.

ESRI: ArcGIS Desktop 10.7.1 [software], 2019.

Essery, R. and Pomeroy, J.: Vegetation and Topographic Control of Wind-Blown Snow Distributions in Distributed and Aggregated Simulations for an Arctic Tundra Basin, Journal of Hydrometeorology, 5, 735–744, https://doi.org/10.1175/1525-7541(2004)005<0735:VATCOW>2.0.CO;2, 2004.

Falcone, M. D.: Assessing hydrological processes controlling the water balance of lakes in the Peace-Athabasca Delta, Alberta, Canada using water isotope tracers, Msc thesis, University of Waterloo, URL https://uwspace.uwaterloo.ca/handle/10012/3081, 2007.

Farquharson, L. M., Mann, D. H., Grosse, G., Jones, B. M., and Romanovsky, V. E.: Spatial distribution of thermokarst terrain in Arctic Alaska, Geomorphology, 273, 116–133, https://doi.org/10.1016/j.geomorph.2016.08.007, 2016.

Farquharson, L. M., Romanovsky, V. E., Kholodov, A., and Nicolsky, D.: Sub-aerial talik formation observed across the discontinuous permafrost zone of Alaska, Nature Geoscience, https://doi.org/10.1038/s41561-022-00952-z, 2022.

Favaro, E. A. and Lamoureux, S. F.: Antecedent Controls on Rainfall Runoff Response and Sediment Transport in a High Arctic Catchment, Geografiska Annaler: Series A, Physical Geography, 96, n/a–n/a, https://doi.org/10.1111/geoa.12063, 2014.

Ferrick, M. G., Calkins, D. J., Perron, N. M., and Kendall, C.: Stable environmental isotopes in lake and river ice cores, in: Ice in Surface Waters, pp. 207–214, Balkema: Rotterdam, 1998.

Ferrick, M. G., Calkins, D. J., Perron, N. M., Cragin, J. H., and Kendall, C.: Diffusion model validation and interpretation of stable isotopes in river and lake ice, Hydrological Processes, 16, 851–872, https://doi.org/10.1002/hyp.374, 2002.

Finger Higgens, R. A., Chipman, J. W., Lutz, D. A., Culler, L. E., Virginia, R. A., and Ogden, L. A.: Changing Lake Dynamics Indicate a Drier Arctic in Western Greenland, Journal of Geophysical Research: Biogeosciences, 124, 870–883, https://doi.org/10.1029/2018JG004879, 2019.

Finlay, J., Neff, J., Zimov, S., Davydova, A., and Davydov, S.: Snowmelt dominance of dissolved organic carbon in high-latitude watersheds: Implications for characterization and flux of river DOC, Geophysical Research Letters, 33, n/a–n/a, https://doi.org/10.1029/2006GL025754, 2006.

Fisher, J. P., Estop-Aragonés, C., Thierry, A., Charman, D. J., Wolfe, S. A., Hartley, I. P., Murton, J. B., Williams, M., and Phoenix, G. K.: The influence of vegetation and soil characteristics on active-layer thickness of permafrost soils in boreal forest, Global Change Biology, 22, 3127–3140, https://doi.org/10.1111/gcb.13248, 2016.

Fitzgibbon, J. E. and Dunne, T.: Land surface and lake storage during snowmelt runoff in a subarctic drainage system (Knob Lake, Schefferville Quebec)., Arctic and Alpine Research, 13, 277–285, https://doi.org/10.2307/1551034, 1981.

Foster, J. L., Robinson, D. A., Hall, D. K., and Estilow, T. W.: Spring snow melt timing and changes over Arctic lands, Polar Geography, 31, 145–157, https://doi.org/10.1080/10889370802580185, 2008.

Fritz, M., Wetterich, S., McAlister, J., and Meyer, H.: A new local meteoric water line for Inuvik (NT, Canada), Earth System Science Data, 14, 57–63, https://doi.org/10.5194/essd-14-57-2022, 2022.

Gibson, J.: Short-term evaporation and water budget comparisons in shallow Arctic lakes using non-steady isotope mass balance, Journal of Hydrology, 264, 242–261, https://doi.org/10.1016/S0022-1694(02)00091-4, 2002.

Gibson, J. and Reid, R.: Water balance along a chain of tundra lakes: A 20-year isotopic perspective, Journal of Hydrology, 519, 2148–2164, https://doi.org/10.1016/j.jhydrol.2014.10.011, 2014.

Gibson, J. J. and Edwards, T. W. D.: Regional water balance trends and evaporation-transpiration partitioning from a stable isotope survey of lakes in northern Canada, Global Biogeochemical Cycles, 16, 10–11, https://doi.org/doi:10.1029/2001GB001839, 2002.

Gibson, J. J. and Prowse, T. D.: Stable isotopes in river ice: identifying primary over-winter streamflow signals and their hydrological significance, Hydrological Processes, 16, 873–890, https://doi.org/10.1002/hyp.366, 2002.

Gibson, J. J., Edwards, T. W. D., and Bursey, G. G.: Estimating Evaporation Using Stable Isotopes : Quantitative Results and Sensitivity Analysis for Two Catchments in Northern Canada, Nordic Hydrology, 24, 79–94, https://doi.org/10.2166/nh.1993.006, 1993.

Gonfiantini, R.: Environmental Isotopes in Lake Studies, in: The Terrestrial Environment, B, pp. 113–168, Elsevier, https://doi.org/10.1016/B978-0-444-42225-5.50008-5, 1986.

Granger, R. J. and Hedstrom, N.: Modelling hourly rates of evaporation from small lakes, Hydrology and Earth System Sciences, 15, 267–277, https://doi.org/10.5194/hess-15-267-2011, 2011.

Grosse, G., Romanovsky, V.E., Walter, K., Morgenstern, A., Lantuit, H., and Zimov, S. A.: Distribution of Thermokarst Lakes and Ponds at Three Yedoma Sites in Siberia, Ninth International Conferencnce on Permafrost, pp. 551–556, 2008.

Grünberg, I. and Boike, J.: Vegetation map of Trail Valley Creek, Northwest Territories, Canada, https://doi.org/10.1594/PANGAEA.904270, 2019.

Grünberg, I., Wilcox, E. J., Zwieback, S., Marsh, P., and Boike, J.: Linking tundra vegetation, snow, soil temperature, and permafrost, Biogeosciences, 17, 4261–4279, https://doi.org/10.5194/bg-17-4261-2020, 2020.

Haig, H., Hayes, N., Simpson, G., Yi, Y., Wissel, B., Hodder, K., and Leavitt, P.: Comparison of isotopic mass balance and instrumental techniques as estimates of basin hydrology in seven connected lakes over 12 years, Journal of Hydrology X, 6, 100 046, https://doi.org/10.1016/j.hydroa.2019.100046, 2020.

Hardy, D. R.: Climatic influences on streamflow and sediment flux into Lake C2, northern Ellesmere Island, Canada, Journal of Paleolimnology, 16, 133–149, https://doi.org/10.1007/BF00176932, 1996.

Harris, S. A., French, H. M., Heginbottom, J., Johnston, G. H., Ladanyi, B., Sego, D., and van Everdingen, R.: Glossary of Permafrost and Related Ground-Ice Terms, vol. 1998, https://doi.org/10.2307/1551636, 1988.

Heginbottom, J. A.: The bursting of a snow dam, Tingmisut Lake, Melville Island, Northwest Territories, Tech. rep., https://doi.org/10.4095/119574, 1984.

Heijmans, M. M. P. D., Magnússon, R. Í., Lara, M. J., Frost, G. V., Myers-Smith, I. H., van Huissteden, J., Jorgenson, M. T., Fedorov, A. N., Epstein, H. E., Lawrence, D. M., and Limpens, J.: Tundra vegetation change and impacts on permafrost, Nature Reviews Earth & Environment, 3, 68–84, https://doi.org/10.1038/s43017-021-00233-0, 2022.

Hendrey, G. R., Galloway, J. N., and Schofield, C. L.: Temporal and spatial trends in the chemistry of acidified lakes under ice cover., in: International Conference on the Ecological Impact of Acid Precipitation, Brookhaven National Lab, 1980.

Henriksen, A. and Wright, R. F.: Effects of Acid Precipitation on a Small Acid Lake in Southern Norway, Nordic Hydrology, 8, 1–10, https://doi.org/10.2166/nh.1977.0001, 1977.

Hille, E.: The effects of shoreline retrogressive thaw slumping on the hydrology and geochemistry of small tundra lake catchments, Msc thesis, University of Victoria, URL `https://dspace.library.uvic.ca/handle/1828/5887`, 2015.

Hinkel, K. M. and Nelson, F. E.: Spatial and temporal patterns of active layer thickness at Circumpolar Active Layer Monitoring (CALM) sites in northern Alaska, 1995–2000, Journal of Geophysical Research, 108, 8168, https://doi.org/10.1029/2001JD000927, 2003.

Hinzman, L. D., Kane, D. L., Gieck, R. E., and Everett, K. R.: Hydrologic and thermal properties of the active layer in the Alaskan Arctic, Cold Regions Science and Technology, 19, 95–110, https://doi.org/10.1016/0165-232X(91)90001-W, 1991.

Hopkinson, C., Pietroniro, A., and Pomeroy, J.: Hydroscan: airborne laser mapping of hydrological features and resources, URL http://scholar.ulethbridge.ca/sites/default/files/hopkinson/files/hydroscan_complete_book.pdf, 2008.

Horita, J. and Wesolowski, D. J.: Liquid-vapor fractionation of oxygen and hydrogen isotopes of water from the freezing to the critical temperature, Geochimica et Cosmochimica Acta, 58, 3425–3437, https://doi.org/10.1016/0016-7037(94)90096-5, 1994.

Huang, L., Timmermann, A., Lee, S.-s., Rodgers, K. B., Yamaguchi, R., and Chung, E.-s.: Emerging unprecedented lake ice loss in climate change projections, Nature Communications, 13, 5798, https://doi.org/10.1038/s41467-022-33495-3, 2022.

Hughes, O. L.: Surficial Geology of northern Yukon Territory and northwestern District of Mackenzie, Northwest Territories, Tech. rep., https://doi.org/10.4095/102354, 1972.

IAEA/WMO: Global Network of Isotopes in Precipitation, The GNIP Database [data set], URL https://nucleus.iaea.org/wiser, 2023.

in 't Zandt, M. H., Liebner, S., and Welte, C. U.: Roles of Thermokarst Lakes in a Warming World, Trends in Microbiology, 28, 769–779, https://doi.org/10.1016/j.tim.2020.04.002, 2020.

Jan, A., Coon, E. T., and Painter, S. L.: Evaluating integrated surface/subsurface permafrost thermal hydrology models in ATS (v0.88) against observations from a polygonal tundra site, Geoscientific Model Development, 13, 2259–2276, https://doi.org/10.5194/gmd-13-2259-2020, 2020.

Jansen, J., Thornton, B. F., Jammet, M. M., Wik, M., Cortés, A., Friborg, T., MacIntyre, S., and Crill, P. M.: Climate-sensitive controls on large spring emissions of CH4 and CO2 from northern lakes, Journal of Geophysical Research: Biogeosciences, 124, 2379–2399, https://doi.org/10.1029/2019JG005094, 2019.

Jeffries, D. S., Cox, C. M., and Dillon, P. J.: Depression of pH in Lakes and Streams in Central Ontario During Snowmelt, Journal of the Fisheries Research Board of Canada, 36, 640–646, https://doi.org/10.1139/f79-093, 1979.

Jones, B. M. and Arp, C. D.: Observing a Catastrophic Thermokarst Lake Drainage in Northern Alaska, Permafrost and Periglacial Processes, 26, 119–128, https://doi.org/10.1002/ppp.1842, 2015.

Jones, B. M., Grosse, G., Arp, C. D., Jones, M. C., Walter Anthony, K. M., and Romanovsky, V. E.: Modern thermokarst lake dynamics in the continuous permafrost zone, northern Seward Peninsula, Alaska, Journal of Geophysical Research, 116, G00M03, https://doi.org/10.1029/2011JG001666, 2011.

Jones, B. M., Grosse, G., Farquharson, L. M., Roy-Léveillée, P., Veremeeva, A., Kanevskiy, M. Z., Gaglioti, B. V., Breen, A. L., Parsekian, A. D., Ulrich, M., and Hinkel, K. M.: Lake and drained lake basin systems in lowland permafrost regions, Nature Reviews Earth & Environment, 3, 85–98, https://doi.org/10.1038/s43017-021-00238-9, 2022.

Kane, D. L., Soden, D. J., Hinzman, L. D., and Gieck, R. E.: Rainfall runoff of a nested watershed in the alaskan arctic, in: Seventh International Conference on Permafrost, 55, pp. 539–544, Nordicana, Yellowknife, 1998.

Kariyawasam, D.: Changes in lake drainage in the western Canadian Arctic, Msc thesis, Wilfrid Laurier University, URL https://scholars.wlu.ca/etd/2458, 2022.

Karlsson, J. M., Lyon, S. W., and Destouni, G.: Thermokarst lake, hydrological flow and water balance indicators of permafrost change in Western Siberia, Journal of Hydrology, 464-465, 459–466, https://doi.org/10.1016/j.jhydrol.2012.07.037, 2012.

Kemppinen, J., Niittynen, P., Virkkala, A.-m., Happonen, K., Riihima, H., Aalto, J., and Luoto, M.: Dwarf Shrubs Impact Tundra Soils : Drier, Colder, and Less Organic Carbon, https://doi.org/10.1007/s10021-020-00589-2, 2021.

Kirillin, G., Hochschild, J., Mironov, D., Terzhevik, A., Golosov, S., and Nützmann, G.: FLake-Global: Online lake model with worldwide coverage, Environmental Modelling and Software, 26, 683–684, https://doi.org/10.1016/j.envsoft.2010.12.004, 2011.

Koch, J. C., Sjoberg, Y., O'Donnell, J., Carey, M., Sullivan, P. F., and Terskaia, A.: Sensitivity of headwater streamflow to thawing permafrost and vegetation change in a warming Arctic, Environmental Research Letters, 2, 0–31, https://doi.org/10.1088/1748-9326/ac5f2d, 2022.

Kokelj, S., Burn, C., and Tarnocai, C.: The Structure and Dynamics of Earth Hummocks in the Subarctic Forest near Inuvik, Northwest Territories, Canada, Arctic, Antarctic and Alpine Research, 39, 99–109, https://doi.org/10.1657/1523-0430(2007)39[99:TSADOE]2.0.CO;2, 2007.

Kosten, S., Huszar, V. L., Mazzeo, N., Scheffer, M., Sternberg, L. d. S., and Jeppesen, E.: Lake and watershed characteristics rather than climate influence nutrient limitation in shallow lakes, Ecological applications, 19, 1791–1804, https://doi.org/10.1890/08-0906.1, 2009.

Krogh, S. A. and Pomeroy, J. W.: Impact of future climate and vegetation on the hydrology of an Arctic headwater basin at the tundra-taiga transition, Journal of Hydrometeorology, 20, 197–215, https://doi.org/10.1175/JHM-D-18-0187.1, 2019.

Lafleur, P. M. and Humphreys, E. R.: Tundra shrub effects on growing season energy and carbon dioxide exchange, Environmental Research Letters, 13, https://doi.org/10.1088/1748-9326/aab863, 2018.

Langer, M., Westermann, S., Boike, J., Kirillin, G., Grosse, G., Peng, S., and Krinner, G.: Rapid degradation of permafrost underneath waterbodies in tundra landscapes—Toward a representation of thermokarst in land surface models, Journal of Geophysical Research: Earth Surface, 121, 2446–2470, https://doi.org/10.1002/2016JF003956, 2016.

Lantz, T. C. and Kokelj, S. V.: Increasing rates of retrogressive thaw slump activity in the Mackenzie Delta region, N.W.T., Canada, Geophysical Research Letters, 35, 1–5, https://doi.org/10.1029/2007GL032433, 2008.

Lantz, T. C. and Turner, K. W.: Changes in lake area in response to thermokarst processes and climate in Old Crow Flats, Yukon, Journal of Geophysical Research G: Biogeosciences, 120, 513–524, https://doi.org/10.1002/2014JG002744, 2015.

Lantz, T. C., Gergel, S. E., and Kokelj, S. V.: Spatial heterogeneity in the shrub tundra ecotone in the Mackenzie Delta region, Northwest territories: Implications for Arctic environmental change, Ecosystems, 13, 194–204, https://doi.org/10.1007/s10021-009-9310-0, 2010.

Lantz, T. C., Marsh, P., and Kokelj, S. V.: Recent Shrub Proliferation in the Mackenzie Delta Uplands and Microclimatic Implications, Ecosystems, 16, 47–59, https://doi.org/10.1007/s10021-012-9595-2, 2013.

Lawrence, D. M. and Swenson, S. C.: Permafrost response to increasing Arctic shrub abundance depends on the relative influence of shrubs on local soil cooling versus large-scale climate warming, Environmental Research Letters, 6, https://doi.org/10.1088/1748-9326/6/4/045504, 2011.

Lee, J.-Y., Marotzke, J., Bala, G., Cao, L., Corti, S., Dunne, J., Engelbrecht, F., Fischer, E., Fyfe, J., Jones, C., Maycock, A., Mutemi, J., Ndiaye, O., Panickal, S., and Zhou, T.: Future Global Climate: Scenario-Based Projections and Near Term Information, in: Climate Change 2021: The Physical Science Basis. Contribution of Working Group I to the Sixth Assessment Report of the Intergovernmental Panel on Climate Change, chap. 4, pp. 553–672, Cambridge University Press, Cambridge, United Kingdom and New York, NY, USA, https://doi.org/10.1017/9781009157896.006, 2021.

Lefcheck, J. S.: piecewiseSEM: Piecewise structural equation modelling in R for ecology, evolution, and systematics, Methods in Ecology and Evolution, 7, 573–579, https://doi.org/10.1111/2041-210X.12512, 2016.

Liljedahl, A. K., Boike, J., Daanen, R. P., Fedorov, A. N., Frost, G. V., Grosse, G., Hinzman, L. D., Iijma, Y., Jorgenson, J. C., Matveyeva, N., Necsoiu, M., Raynolds, M. K., Romanovsky, V. E., Schulla, J.,

Tape, K. D., Walker, D. A., Wilson, C., Yabuki, H., and Zona, D.: Pan-Arctic ice-wedge degradation in warming permafrost and influence on tundra hydrology, Nature Geoscience, 9, 312 – 318, https://doi.org/10.1038/ngeo2674, 2016.

Lindgren, P. R., Farquharson, L. M., Romanovsky, V. E., and Grosse, G.: Landsat-based lake distribution and changes in western Alaska permafrost regions between the 1970s and 2010s, Environmental Research Letters, 16, https://doi.org/10.1088/1748-9326/abd270, 2021.

Lopez Caceres, M. L., Takakai, F., Iwahana, G., Fedorov, A. N., Iijima, Y., Hatano, R., and Fukuda, M.: Snowmelt and the hydrological interaction of forest-grassland ecosystems in Central Yakutia, eastern Siberia, Hydrological Processes, 29, 3074–3083, https://doi.org/10.1002/hyp.10424, 2015.

Loranty, M. M. and Goetz, S. J.: Shrub expansion and climate feedbacks in Arctic tundra, Environmental Research Letters, 7, https://doi.org/10.1088/1748-9326/7/1/011005, 2012.

Loranty, M. M., Abbott, B. W., Blok, D., Douglas, T. A., Epstein, H. E., Forbes, B. C., Jones, B. M., Kholodov, A. L., Kropp, H., Malhotra, A., Mamet, S. D., Myers-Smith, I. H., Natali, S. M., O'Donnell, J. A., Phoenix, G. K., Rocha, A. V., Sonnentag, O., Tape, K. D., and Walker, D. A.: Reviews and syntheses: Changing ecosystem influences on soil thermal regimes in northern high-latitude permafrost regions, https://doi.org/10.5194/bg-15-5287-2018, 2018.

MacDonald, L. A., Wolfe, B. B., Turner, K. W., Anderson, L., Arp, C. D., Birks, S. J., Bouchard, F., Edwards, T. W., Farquharson, N., Hall, R. I., McDonald, I., Narancic, B., Ouimet, C., Pienitz, R., Tondu, J., and White, H.: A synthesis of thermokarst lake water balance in high-latitude regions of North America from isotope tracers, Arctic Science, 3, 118–149, https://doi.org/10.1139/as-2016-0019, 2017.

MacDonald, L. A., Turner, K. W., McDonald, I., Kay, M. L., Hall, R. I., and Wolfe, B. B.: Isotopic evidence of increasing water abundance and lake hydrological change in Old Crow Flats, Yukon, Canada, Environmental Research Letters, 16, 124 024, https://doi.org/10.1088/1748-9326/ac3533, 2021.

Mackay, J. R.: The origin of hummocks, western Arctic coast, Canada, Canadian Journal Earth Science, 17, 996–1006, https://doi.org/10.1139/e80-100, 1980.

Mackay, J. R.: Catastrophic lake drainage, Tuktoyaktuk Peninsula area, District of Mackenzie, in: Current research part D: interior plains and Arctic Canada, pp. 83–90, Geological Survey of Canada, https://doi.org/10.4095/122651, 1988.

MacKay, M. D., Verseghy, D. L., Fortin, V., and Rennie, M. D.: Wintertime Simulations of a Boreal Lake with the Canadian Small Lake Model, Journal of Hydrometeorology, 18, 2143–2160, https://doi.org/10.1175/JHM-D-16-0268.1, 2017.

Macrae, M. L., Brown, L. C., Duguay, C. R., Parrott, J. a., and Petrone, R. M.: Observed and Projected Climate Change in the Churchill Region of the Hudson Bay Lowlands and Implications for Pond Sustainability., Arctic, Antarctic and Alpine Research, 46, 272–285, https://doi.org/10.1657/1938-4246-46.1.272, 2014.

Mann, P.: Spatial and temporal variability of the snow environment in the Western Canadian Arctic, MSc Thesis, Wilfrid Laurier University, URL https://scholars.wlu.ca/etd/2011, 2018.

Marsh, C. B., Pomeroy, J. W., Spiteri, R. J., and Wheater, H. S.: A Finite Volume Blowing Snow Model for Use With Variable Resolution Meshes, Water Resources Research, 56, 1–28, https://doi.org/10.1029/2019WR025307, 2020a.

Marsh, C. B., Pomeroy, J. W., and Wheater, H. S.: The Canadian Hydrological Model (CHM) v1.0: a multi-scale, multi-extent, variable-complexity hydrological model – design and overview, Geoscientific Model Development, 13, 225–247, https://doi.org/10.5194/gmd-13-225-2020, 2020b.

Marsh, P. and Bigras, S. C.: Evaporation from Mackenzie Delta Lakes, N.W.T., Canada, Arctic and Alpine Research, 20, 220, https://doi.org/10.2307/1551500, 1988.

Marsh, P. and Hey, M.: The flooding hydrology of Mackenzie Delta Lakes near Inuvik, N.W.T., Canada, Arctic, 42, 41–49, https://doi.org/10.14430/arctic1638, 1989.

Marsh, P. and Lesack, L. F. W.: The hydrologic regime of perched lakes in the Mackenzie Delta: Potential responses to climate change, Limnology and Oceanography, 41, 849–856, https://doi.org/10.4319/lo.1996.41.5.0849, 1996.

Marsh, P. and Neumann, N. N.: Processes controlling the rapid drainage of two ice-rich permafrost-dammed lakes in NW Canada, Hydrological Processes, 15, 3433–3446, https://doi.org/10.1002/hyp.1035, 2001.

Marsh, P. and Pomeroy, J.: Meltwater Fluxes At an Arctic Forest-Tundra Site, Hydrological Processes, 10, 1383–1400, https://doi.org/10.1002/(sici)1099-1085(199610)10:10<1383::aid-hyp468>3.3.co;2-n, 1996.

Marsh, P. and Pomeroy, J. W.: Spatial and temporal variations in snowmelt runoff chemistry, Northwest Territories, Canada, Water Resources Research, 35, 1559–1567, https://doi.org/10.1029/1998WR900109, 1999.

Marsh, P., Russell, M., Pohl, S., Haywood, H., and Onclin, C.: Changes in thaw lake drainage in the Western Canadian Arctic from 1950 to 2000, Hydrological Processes, 23, 145–158, https://doi.org/10.1002/hyp.7179, 2009.

Marsh, P., Bartlett, P., MacKay, M., Pohl, S., and Lantz, T.: Snowmelt energetics at a shrub tundra site in the western Canadian Arctic, Hydrological Processes, 24, 3603–3620, https://doi.org/10.1002/hyp.7786, 2010.

Marsh, P., Mann, P., and Walker, B.: Changing snowfall and snow cover in the western Canadian Arctic, in: 22nd Northern Research Basins Symposium and Workshop, pp. 1–10, Yellowknife, 2019.

Marushchak, M. E., Kiepe, I., Biasi, C., Elsakov, V., Friborg, T., Johansson, T., Soegaard, H., Virtanen, T., and Martikainen, P. J.: Carbon dioxide balance of subarctic tundra from plot to regional scales, Biogeosciences, 10, 437–452, https://doi.org/10.5194/bg-10-437-2013, 2013.

McDonnell, J. J. and Beven, K.: Debates-The future of hydrological sciences: A (common) path forward? A call to action aimed at understanding velocities, celerities and residence time distributions of the headwater hydrograph, Water Resources Research, 50, 5342–5350, https://doi.org/10.1002/2013WR015141, 2014.

Meloche, J., Langlois, A., Rutter, N., Royer, A., King, J., Walker, B., Marsh, P., and Wilcox, E. J.: Characterizing tundra snow sub-pixel variability to improve brightness temperature estimation in satellite SWE retrievals, The Cryosphere, 16, 87–101, https://doi.org/10.5194/tc-16-87-2022, 2022.

Muster, S., Roth, K., Langer, M., Lange, S., Cresto Aleina, F., Bartsch, A., Morgenstern, A., Grosse, G., Jones, B., Sannel, A. B. K., Sjöberg, Y., Günther, F., Andresen, C., Veremeeva, A., Lindgren, R. P., Bouchard, F., Lara, J. M., Fortier, D., Charbonneau, S., Virtanen, A. T., Hugelius, G., Palmtag, J., Siewert, B. M., Riley, J. W., Koven, D. C., and Boike, J.: PeRL: A circum-Arctic Permafrost Region Pond and Lake database, vol. 9, https://doi.org/10.5194/essd-9-317-2017, 2017.

Myers-Smith, I. H. and Hik, D. S.: Shrub canopies influence soil temperatures but not nutrient dynamics: An experimental test of tundra snow-shrub interactions, Ecology and Evolution, 3, 3683–3700, https://doi.org/10.1002/ece3.710, 2013.

Myers-Smith, I. H., Forbes, B. C., Wilmking, M., Hallinger, M., Lantz, T., Blok, D., Tape, K. D., Macias-Fauria, M., Sass-Klaassen, U., Lévesque, E., Boudreau, S., Ropars, P., Hermanutz, L., Trant, A., Collier, L. S., Weijers, S., Rozema, J., Rayback, S. A., Schmidt, N. M., Schaepman-Strub, G., Wipf, S., Rixen, C., Ménard, C. B., Venn, S., Goetz, S., Andreu-Hayles, L., Elmendorf, S., Ravolainen, V., Welker, J., Grogan, P., Epstein, H. E., and Hik, D. S.: Shrub expansion in tundra ecosystems: dynamics, impacts and research priorities, Environmental Research Letters, 6, https://doi.org/10.1088/1748-9326/6/4/045509, 2011.

Narancic, B., Wolfe, B. B., Pienitz, R., Meyer, H., and Lamhonwah, D.: Landscape-gradient assessment of thermokarst lake hydrology using water isotope tracers, Journal of Hydrology, 545, 327–338, https://doi.org/10.1016/j.jhydrol.2016.11.028, 2017.

Nauta, A. L., Heijmans, M. M. P. D., Blok, D., Limpens, J., Elberling, B., Gallagher, A., Li, B., Petrov, R. E., Maximov, T. C., van Huissteden, J., and Berendse, F.: Permafrost collapse after shrub removal shifts tundra

ecosystem to a methane source, Nature Climate Change, 5, 67–70, https://doi.org/10.1038/nclimate2446, 2015.

Nitze, I., Grosse, G., Jones, B. M., Arp, C. D., Ulrich, M., Fedorov, A., and Veremeeva, A.: Landsat-based trend analysis of lake dynamics across Northern Permafrost Regions, Remote Sensing, 9, 1–28, https://doi.org/10.3390/rs9070640, 2017.

Nitze, I., W. Cooley, S., R. Duguay, C., M. Jones, B., and Grosse, G.: The catastrophic thermokarst lake drainage events of 2018 in northwestern Alaska: Fast-forward into the future, Cryosphere, 14, 4279–4297, https://doi.org/10.5194/tc-14-4279-2020, 2020.

Obu, J., Westermann, S., Bartsch, A., Berdnikov, N., Christiansen, H. H., Dashtseren, A., Delaloye, R., Elberling, B., Etzelmüller, B., Kholodov, A., Khomutov, A., Kääb, A., Leibman, M. O., Lewkowicz, A. G., Panda, S. K., Romanovsky, V., Way, R. G., Westergaard-Nielsen, A., Wu, T., Yamkhin, J., and Zou, D.: Northern Hemisphere permafrost map based on TTOP modelling for 2000–2016 at 1 km2 scale, Earth-Science Reviews, 193, 299–316, https://doi.org/10.1016/j.earscirev.2019.04.023, 2019.

O'Callaghan, J. F. and Mark, D. M.: The extraction of drainage networks from digital elevation data, Computer Vision, Graphics, and Image Processing, 28, 323–344, https://doi.org/10.1016/S0734-189X(84)80011-0, 1984.

Olefeldt, D. and Roulet, N. T.: Effects of permafrost and hydrology on the composition and transport of dissolved organic carbon in a subarctic peatland complex, Journal of Geophysical Research: Biogeosciences, 117, https://doi.org/10.1029/2011JG001819, 2012.

O'Neill, H. B., Smith, S. L., and Duchesne, C.: Long-Term Permafrost Degradation and Thermokarst Subsidence in the Mackenzie Delta Area Indicated by Thaw Tube Measurements, in: 18th International Conference on Cold Regions Engineering and 8th Canadian Permafrost Conference, pp. 643–651, https://doi.org/10.1061/9780784482599.074, 2019a.

O'Neill, H. B., Wolfe, S. A., and Duchesne, C.: New ground ice maps for Canada using a paleogeographic modelling approach, The Cryosphere, 13, 753–773, https://doi.org/10.5194/tc-13-753-2019, 2019b.

Pan, X., Yu, Q., You, Y., Chun, K. P., Shi, X., and Li, Y.: Contribution of supra-permafrost discharge to thermokarst lake water balances on the northeastern Qinghai-Tibet Plateau, Journal of Hydrology, 555, 621–630, https://doi.org/10.1016/j.jhydrol.2017.10.046, 2017.

Pienitz, R., Smol, J. P., and Lean, D. R.: Physical and chemical limnology of 59 lakes located between the southern Yukon and the Tuktoyaktuk Peninsula, Northwest Territories (Canada), Canadian Journal of Fisheries and Aquatic Sciences, 54, 330–346, https://doi.org/10.1139/f96-274, 1997.

Pinheiro, J. C., Bates, D., DebRoy, S., Sarkar, D., and Team, R. C.: nlme: Linear and Nonlinear Mixed Effects Models, URL `https://cran.r-project.org/package=nlme`, 2018.

Pitcher, L. H., Smith, L. C., Cooley, S. W., Zaino, A., Carlson, R., Pettit, J., Gleason, C. J., Minear, J. T., Fayne, J. V., Willis, M. J., Hansen, J. S., Easterday, K. J., Harlan, M. E., Langhorst, T., Topp, S. N., Dolan, W., Kyzivat, E. D., Pietroniro, A., Marsh, P., Yang, D., Carter, T., Onclin, C., Hosseini, N., Wilcox, E., Moreira, D., Berge-Nguyen, M., Cretaux, J.-F., and Pavelsky, T. M.: Advancing Field-Based GNSS Surveying for Validation of Remotely Sensed Water Surface Elevation Products, Frontiers in Earth Science, 8, 1–20, https://doi.org/10.3389/feart.2020.00278, 2020.

Pix4D SA: Pix4Dmapper [software], 2019.

Plug, L. J. and West, J. J.: Thaw lake expansion in a two-dimensional coupled model of heat transfer, thaw subsidence, and mass movement, Journal of Geophysical Research: Earth Surface, 114, 1–18, https://doi.org/10.1029/2006JF000740, 2009.

Plug, L. J., Walls, C., and Scott, B. M.: Tundra lake changes from 1978 to 2001 on the Tuktoyaktuk Peninsula, western Canadian Arctic, Geophysical Research Letters, 35, 1–5, https://doi.org/10.1029/2007GL032303, 2008.

Pohl, S., Marsh, P., Onclin, C., and Russell, M.: The summer hydrology of a small upland tundra thaw lake: implications to lake drainage, Hydrological Processes, 23, 2536–2546, https://doi.org/10.1002/hyp.7238, 2009.

Pointner, G., Bartsch, A., Forbes, B. C., and Kumpula, T.: The role of lake size and local phenomena for monitoring ground-fast lake ice, International Journal of Remote Sensing, 40, 832–858, https://doi.org/10.1080/01431161.2018.1519281, 2019.

Pomeroy, J. W., Marsh, P., and Gray, D. M.: Application of a Distributed Blowing Snow Model To the Arctic, Hydrological Processes, 11, 1451–1464, https://doi.org/10.1002/(SICI)1099-1085(199709)11:11<1451::AID-HYP449>3.0.CO;2-Q, 1997.

Pomeroy, J. W., Bewley, D. S., Essery, R. L. H., Hedstrom, N. R., Link, T., Granger, R. J., Sicart, J. E., Ellis, C. R., and Janowicz, J. R.: Shrub tundra snowmelt, Hydrological Processes, 20, 923–941, https://doi.org/10.1002/hyp.6124, 2006.

Porter, C., Morin, P., Howat, I., Noh, M.-J., Bates, B., Peterman, K., Keesey, S., Schlenk, M., Gardiner, J., Tomko, K., Willis, M., Kelleher, C., Cloutier, M., Husby, E., Foga, S., Nakamura, H., Platson, M., Wethington, Michael, J., Williamson, C., Bauer, G., Enos, J., Arnold, G., Kramer, W., Becker, P., Doshi, A., D'Souza, C., Cummens, P., Laurier, F., and Bojesen, M.: ArcticDEM [data set], https://doi.org/10.7910/DVN/OHHUKH, 2018.

Priestley, C. and Taylor, R.: On the assessment of surface heat flux and evaporation using large-scale parameters, Montly Weather Review, 100, https://doi.org/10.1175/1520-0493(1972)100<0081:OTAOSH>2.3.CO;2, 1972.

Prowse, T., Alfredsen, K., Beltaos, S., Bonsal, B., Duguay, C., Korhola, A., McNamara, J., Pienitz, R., Vincent, W. F., Vuglinsky, V., and Weyhenmeyer, G. A.: Past and future changes in arctic lake and river ice, Ambio, 40, 53–62, https://doi.org/10.1007/s13280-011-0216-7, 2011.

Quinton, W. L.: Runoff from hummock-covered arctic tundra hillslopes in the continuous permafrost zone, Ph.D. thesis, https://doi.org/10.16953/deusbed.74839, 1997.

Quinton, W. L. and Marsh, P.: The influence of mineral earth hummocks on subsurface drainage in the continuous permafrost zone, Permafrost and Periglacial Processes, 9, 213–228, https://doi.org/10.1002/(SICI)1099-1530(199807/09)9:3<213::AID-PPP285>3.0.CO;2-E, 1998.

Quinton, W. L. and Marsh, P.: A Conceptual Framework for Runoff Generation in a Permafrost Environment, Hydrological Processes, 13, 2563–2581, https://doi.org/10.1002/(SICI)1099-1085(199911)13:16<2563::AID-HYP942>3.0.CO;2-D, 1999.

Quinton, W. L. and Pomeroy, J. W.: Transformations of runoff chemistry in the Arctic tundra, Northwest Territories, Canada, Hydrological Processes, 20, 2901–2919, https://doi.org/10.1002/hyp.6083, 2006.

Quinton, W. L., Gray, D. M., and Marsh, P.: Subsurface drainage from hummock-covered hillslopes in the arctic tundra, Journal of Hydrology, 237, 113–125, https://doi.org/10.1016/S0022-1694(00)00304-8, 2000.

R Core Team: R: A Language and Environment for Statistical Computing [software], URL `https://www.r-project.org/`, 2021.

Rampton, V. and Wecke, M.: Surficial Geology, Tuktoyaktuk Coastlands, District of Mackenzie, Northwest Territories, Geological Survey of Canada, https://doi.org/10.4095/125160, 1987.

Rampton, V. N.: Quaternary geology of the Tuktoyaktuk coastlands, Northwest Territories, Geological Survey of Canada, https://doi.org/10.4095/126937, 1988.

Rantanen, M., Karpechko, A. Y., Lipponen, A., Nordling, K., Hyvärinen, O., Ruosteenoja, K., Vihma, T., and Laaksonen, A.: The Arctic has warmed nearly four times faster than the globe since 1979, Communications Earth & Environment, 3, 1–10, https://doi.org/10.1038/s43247-022-00498-3, 2022.

Remmer, C. R., Owca, T., Neary, L., Wiklund, J. A., Kay, M., Wolfe, B. B., and Hall, R. I.: Delineating extent and magnitude of river flooding to lakes across a northern delta using water isotope tracers, Hydrological Processes, 34, 303–320, https://doi.org/10.1002/hyp.13585, 2020.

Riordan, B., Verbyla, D., and McGuire, A. D.: Shrinking ponds in subarctic Alaska based on 1950-2002 remotely sensed images, Journal of Geophysical Research: Biogeosciences, 111, https://doi.org/10.1029/2005JG000150, 2006.

Roulet, N. T. and Woo, M. K.: Runoff generation in a low Arctic drainage basin, Journal of Hydrology, 101, 213–226, https://doi.org/10.1016/0022-1694(88)90036-4, 1988.

Scheffé, H.: A method for judging all contrasts in the analysis of variance, Biometrika, 40, 87–104, https://doi.org/10.1093/biomet/40.1-2.87, 1953.

Schiff, S. and English, M.: Deuterium/hydrogen as a tracer of snowmelt mixing in a small subarctic and a small northern temperate lake., in: Interaction between groundwater and surface water. International symposium., pp. 136–170, Ystad, Sweden, 1988.

Schunke, E. and Zoltai, S. C.: Earth Hummocks, Advances in Periglacial Geomorphology, 10, 231–245, 1988.

SenseFly: eBee Classic [fixed-wing drone], 2015.

Shi, X., Marsh, P., and Yang, D.: Warming spring air temperatures, but delayed spring streamflow in an Arctic headwater basin, Environmental Research Letters, 10, https://doi.org/10.1088/1748-9326/10/6/064003, 2015.

Smith, L. C., Sheng, Y., MacDonald, G. M., and Hinzman, L. D.: Disappearing Arctic Lakes, Science, 308, 1429–1429, https://doi.org/10.1126/science.1108142, 2005.

Smol, J. P. and Douglas, M. S. V.: Crossing the final ecological threshold in high Arctic ponds, Proceedings of the National Academy of Sciences, 104, 12 395–12 397, https://doi.org/10.1073/pnas.0702777104, 2007.

Souchez, R., Tison, J.-L., and Jouzel, J.: Freezing Rate Determination by the Isotopic Composition of the Ice, Geophysical Research Letters, 14, 599–602, https://doi.org/10.1029/GL014i006p00599, 1987.

Stuefer, S. L., Arp, C. D., Kane, D. L., and Liljedahl, A. K.: Recent Extreme Runoff Observations From Coastal Arctic Watersheds in Alaska, Water Resources Research, 53, 9145–9163, https://doi.org/10.1002/2017WR020567, 2017.

Sturm, M. and Holmgren, J.: An Automatic Snow Depth Probe for Field Validation Campaigns, Water Resources Research, 54, 9695–9701, https://doi.org/10.1029/2018WR023559, 2018.

Sturm, M. and Wagner, A. M.: Using repeated patterns in snow distribution modeling : An Arctic example, Water Resources Research, 46, 1–15, https://doi.org/10.1029/2010WR009434, 2010.

Sturm, M., Racine, C., and Tape, K.: Increasing shrub abundance in the Arctic., Nature, 411, 546–547, https://doi.org/10.1038/35079180, 2001.

Surdu, C. M., Duguay, C. R., Brown, L. C., and Fernández Prieto, D.: Response of ice cover on shallow lakes of the North Slope of Alaska to contemporary climate conditions (1950-2011): Radar remote-sensing and numerical modeling data analysis, Cryosphere, 8, 167–180, https://doi.org/10.5194/tc-8-167-2014, 2014.

Swann, A. L., Fung, I. Y., Levis, S., Bonan, G. B., and Doney, S. C.: Changes in arctic vegetation amplify high-latitude warming through the greenhouse effect, Proceedings of the National Academy of Sciences of the United States of America, 107, 1295–1300, https://doi.org/10.1073/pnas.0913846107, 2010.

Tananaev, N. and Lotsari, E.: Defrosting northern catchments: Fluvial effects of permafrost degradation, Earth-Science Reviews, p. 103996, https://doi.org/10.1016/j.earscirev.2022.103996, 2022.

Tape, K., Sturm, M., and Racine, C.: The evidence for shrub expansion in Northern Alaska and the Pan-Arctic, Global Change Biology, 12, 686–702, https://doi.org/10.1111/j.1365-2486.2006.01128.x, 2006.

Tarnocai, C. T. and Zoltai, S.: Earth Hummocks of the Canadian Arctic and Subarctic, Arctic and Alpine Research, 10, 581–594, https://doi.org/10.2307/1550681, 1978.

Tetzlaff, D., Piovano, T., Ala-Aho, P., Smith, A., Carey, S. K., Marsh, P., Wookey, P. A., Street, L. E., and Soulsby, C.: Using stable isotopes to estimate travel times in a data-sparse Arctic catchment: Challenges and possible solutions, Hydrological Processes, 32, 1936–1952, https://doi.org/10.1002/hyp.13146, 2018.

Townsend-Small, A., McClelland, J. W., Max Holmes, R., and Peterson, B. J.: Seasonal and hydrologic drivers of dissolved organic matter and nutrients in the upper Kuparuk River, Alaskan Arctic, Biogeochemistry, 103, 109–124, https://doi.org/10.1007/s10533-010-9451-4, 2011.

Travers-Smith, H. Z., Lantz, T. C., and Fraser, R. H.: Surface Water Dynamics and Rapid Lake Drainage in the Western Canadian Subarctic (1985–2020), Journal of Geophysical Research: Biogeosciences, 126, e2021JG006 445, https://doi.org/10.1029/2021JG006445, 2021.

Turner, K. W., Wolfe, B. B., and Edwards, T. W.: Characterizing the role of hydrological processes on lake water balances in the Old Crow Flats, Yukon Territory, Canada, using water isotope tracers, Journal of Hydrology, 386, 103–117, https://doi.org/10.1016/j.jhydrol.2010.03.012, 2010.

Turner, K. W., Wolfe, B. B., Edwards, T. W. D., Lantz, T. C., Hall, R. I., and Larocque, G.: Controls on water balance of shallow thermokarst lakes and their relations with catchment characteristics: a multi-year, landscape-scale assessment based on water isotope tracers and remote sensing in Old Crow Flats, Yukon (Canada), Global Change Biology, 20, 1585–1603, https://doi.org/10.1111/gcb.12465, 2014.

Vachon, D., Langenegger, T., Donis, D., and McGinnis, D. F.: Influence of water column stratification and mixing patterns on the fate of methane produced in deep sediments of a small eutrophic lake, Limnology and Oceanography, 64, 2114–2128, https://doi.org/10.1002/lno.11172, 2019.

Virkkala, A.-M., Aalto, J., Rogers, B. M., Tagesson, T., Treat, C. C., Natali, S. M., Watts, J. D., Potter, S., Lehtonen, A., Mauritz, M., Schuur, E. A. G., Kochendorfer, J., Zona, D., Oechel, W., Kobayashi, H., Humphreys, E., Goeckede, M., Iwata, H., Lafleur, P. M., Euskirchen, E. S., Bokhorst, S., Marushchak, M., Martikainen, P. J., Elberling, B., Voigt, C., Biasi, C., Sonnentag, O., Parmentier, F.-J. W., Ueyama, M., Celis, G., St.Louis, V. L., Emmerton, C. A., Peichl, M., Chi, J., Järveoja, J., Nilsson, M. B., Oberbauer, S. F., Torn, M. S., Park, S.-J., Dolman, H., Mammarella, I., Chae, N., Poyatos, R., López-Blanco, E., Christensen, T. R., Kwon, M. J., Sachs, T., Holl, D., and Luoto, M.: Statistical upscaling of ecosystem CO2 fluxes across the terrestrial tundra and boreal domain: Regional patterns and uncertainties, Global Change Biology, 27, 4040–4059, https://doi.org/10.1111/gcb.15659, 2021.

Vucic, J. M., Gray, D. K., Cohen, R. S., Syed, M., Murdoch, A. D., and Sharma, S.: Changes in water quality related to permafrost thaw may significantly impact zooplankton in small Arctic lakes, Ecological Applications, 30, https://doi.org/10.1002/eap.2186, 2020.

Walker, B., Wilcox, E. J., and Marsh, P.: Accuracy assessment of late winter snow depth mapping for tundra environments using Structure-from-Motion photogrammetry, Arctic Science, 7, 588–604, https://doi.org/10.1139/as-2020-0006, 2021.

Walker, D. A., Raynolds, M. K., Daniëls, F. J., Einarsson, E., Elvebakk, A., Gould, W. A., Katenin, A. E., Kholod, S. S., Markon, C. J., Melnikov, E. S., Moskalenko, N. G., Talbot, S. S., Yurtsev, B. A., and The other members of the CAVM Team: The Circumpolar Arctic vegetation map, Journal of Vegetation Science, 16, 267–282, https://doi.org/10.1111/j.1654-1103.2005.tb02365.x, 2005.

Wallace, C. A. and Baltzer, J. L.: Tall Shrubs Mediate Abiotic Conditions and Plant Communities at the Taiga – Tundra Ecotone, Ecosystems, https://doi.org/10.1007/s10021-019-00435-0, 2019.

Wallace, C. A., Berg, A. A., Chang, Q., Coles, A. E., Marsh, P., Sonnentag, O., Wilcox, E. J., and Baltzer, J. L.: Impacts of tall shrub expansion on the hydrological dynamics of a low-arctic catchment, in: Global Water Futures Annual Open Science Meeting, URL https://www.gwf2022.com/_files/ugd/55a6d6_a27a6420335e4af1942cbcae3555c358.pdf, 2022.

Walsh, J. E., Overland, J. E., Groisman, P. Y., and Rudolf, B.: Ongoing Climate Change in the Arctic, AMBIO, 40, 6–16, https://doi.org/10.1007/s13280-011-0211-z, 2011.

Walvoord, M. A. and Kurylyk, B. L.: Hydrologic Impacts of Thawing Permafrost—A Review, Vadose Zone Journal, 15, 2–20, https://doi.org/10.2136/vzj2016.01.0010, 2016.

Wan, C., Gibson, J. J., and Peters, D. L.: Isotopic constraints on water balance of tundra lakes and watersheds affected by permafrost degradation, Mackenzie Delta region, Northwest Territories, Canada, Science of the Total Environment, 731, 139 176, https://doi.org/10.1016/j.scitotenv.2020.139176, 2020.

Wang, X. and Meijer, H. A.: Ice–liquid isotope fractionation factors for 18O and 2H deduced from the isotopic correction constants for the triple point of water, Isotopes in Environmental and Health Studies, 54, 304–311, https://doi.org/10.1080/10256016.2018.1435533, 2018.

Wang, Z., Kim, Y., Seo, H., Um, M. J., and Mao, J.: Permafrost response to vegetation greenness variation in the Arctic tundra through positive feedback in surface air temperature and snow cover, Environmental Research Letters, 14, https://doi.org/10.1088/1748-9326/ab0839, 2019.

Webb, E. E. and Liljedahl, A. K.: Diminishing lake area across the northern permafrost zone, Nature Geoscience, pp. 1–8, 2023.

Webb, E. E., Liljedahl, A., Cordeiro, J., Loranty, M., Witharana, C., and Lichstein, J.: Permafrost thaw drives surface water decline across lake-rich regions of the Arctic, Nature Climate Change, https://doi.org/10.1038/s41558-022-01455-w, 2022.

Wen, Z., Yang, Z., Yu, Q., Wang, D., Ma, W., Niu, F., Sun, Z., and Zhang, M.: Modeling thermokarst lake expansion on the Qinghai-Tibetan Plateau and its thermal effects by the moving mesh method, Cold Regions Science and Technology, 121, 84–92, https://doi.org/10.1016/j.coldregions.2015.10.012, 2016.

Westermann, S., Langer, M., Boike, J., Heikenfeld, M., Peter, M., Etzelmüller, B., and Krinner, G.: Simulating the thermal regime and thaw processes of ice-rich permafrost ground with the land-surface model CryoGrid 3, Geoscientific Model Development, 9, 523–546, https://doi.org/10.5194/gmd-9-523-2016, 2016.

Wilcox, E. J., Keim, D., de Jong, T., Walker, B., Sonnentag, O., Sniderhan, A. E., Mann, P., and Marsh, P.: Tundra shrub expansion may amplify permafrost thaw by advancing snowmelt timing, Arctic Science, 5, 202–217, https://doi.org/10.1139/as-2018-0028, 2019.

Wilcox, E. J., Keim, D., de Jong, T., Walker, B., Mann, P., and Marsh, P.: Frost table depth with associated snow and landscape variables at Trail Valley Creek, NT, 2015., https://doi.org/10.5683/SP2/9ZGR5U, 2020.

Wilcox, E. J., Wolfe, B., and Marsh, P.: Isotope data and associated attributes for 25 thermokarst lakes along the Inuvik – Tuktoyaktuk Highway, 2018, https://doi.org/10.5683/SP3/AZE4ER, 2022a.

Wilcox, E. J., Wolfe, B. B., and Marsh, P.: Assessing the influence of lake and watershed attributes on snowmelt bypass at thermokarst lakes, Hydrology and Earth System Sciences, 26, 6185–6205, https://doi.org/10.5194/hess-26-6185-2022, 2022b.

Wilcox, E. J., Wolfe, B. B., and Marsh, P.: Hydrological, Meteorological and Watershed Controls on the Water Balance of Thermokarst Lakes between Inuvik and Tuktoyaktuk, Northwest Territories, Canada, https://doi.org/10.5194/hess-2022-279, under rev.

Wiltse, B., Yerger, E. C., and Laxson, C. L.: A reduction in spring mixing due to road salt runoff entering Mirror Lake (Lake Placid, NY), Lake and reservoir management, 36, 109–121, https://doi.org/10.1080/10402381.2019.1675826, 2020.

Wolfe, B. B., Karst-Riddoch, T. L., Vardy, S. R., Falcone, M. D., Hall, R. I., and Edwards, T. W.: Impacts of climate and river flooding on the hydro-ecology of a floodplain basin, Peace-Athabasca Delta, Canada since A.D. 1700, Quaternary Research, 64, 147–162, https://doi.org/10.1016/j.yqres.2005.05.001, 2005.

Wolfe, B. B., Hall, R. I., Edwards, T. W. D., Vardy, S. R., Falcone, M. D., Sjunneskog, C., Sylvestre, F., McGowan, S., Leavitt, P. R., and van Driel, P.: Hydroecological responses of the Athabasca Delta, Canada, to changes in river flow and climate during the 20th century, Ecohydrology, 1, 131–148, https://doi.org/10.1002/eco.13, 2008.

Wolfe, B. B., Light, E. M., MacRae, M. L., Hall, R. I., Eichel, K., Jasechko, S., White, J., Fishback, L., and Edwards, T. W.: Divergent hydrological responses to 20th century climate change in shallow tundra ponds, western Hudson Bay Lowlands, Geophysical Research Letters, 38, 1–6, https://doi.org/10.1029/2011GL049766, 2011.

Woo, M.: Hydrology of a Small Lake in the Canadian High Arctic, Arctic and Alpine Research, 12, 227, https://doi.org/10.2307/1550519, 1980.

Woo, M.-K.: Permafrost Hydrology, Springer Berlin Heidelberg, Berlin, Heidelberg, https://doi.org/10.1007/978-3-642-23462-0, 2012.

Woo, M. K., Heron, R., and Steer, P.: Catchment hydrology of a High Arctic lake, Cold Regions Science and Technology, 5, 29–41, https://doi.org/10.1016/0165-232X(81)90038-0, 1981.

Woo, M.-K., Kane, D. L., Carey, S. K., and Yang, D.: Progress in permafrost hydrology in the new millennium, Permafrost and Periglacial Processes, 19, 237–254, https://doi.org/10.1002/ppp.613, 2008.

Woolway, R. I. and Merchant, C. J.: Worldwide alteration of lake mixing regimes in response to climate change, Nature Geoscience, 12, 271–276, https://doi.org/10.1038/s41561-019-0322-x, 2019.

Woolway, R. I., Kraemer, B. M., Lenters, J. D., Merchant, C. J., O'Reilly, C. M., and Sharma, S.: Global lake responses to climate change, Nature Reviews Earth & Environment, 1, 388–403, https://doi.org/10.1038/s43017-020-0067-5, 2020.

Xia, Z. and Woo, M.-k.: Theoretical analysis of snow-dam decay, Journal of Glaciology, 38, 191–199, https://doi.org/10.3189/S0022143000009722, 1992.

Yang, B., Wells, M. G., McMeans, B. C., Dugan, H. A., Rusak, J. A., Weyhenmeyer, G. A., Brentrup, J. A., Hrycik, A. R., Laas, A., Pilla, R. M., Austin, J. A., Blanchfield, P. J., Carey, C. C., Guzzo, M. M., Lottig, N. R., MacKay, M. D., Middel, T. A., Pierson, D. C., Wang, J., and Young, J. D.: A New Thermal Categorization of Ice-Covered Lakes, Geophysical Research Letters, 48, 1–11, https://doi.org/10.1029/2020GL091374, 2021.

Yi, Y., Brock, B. E., Falcone, M. D., Wolfe, B. B., and Edwards, T. W. D.: A coupled isotope tracer method to characterize input water to lakes, Journal of Hydrology, 350, 1–13, https://doi.org/10.1016/j.jhydrol.2007.11.008, 2008.

Yin, P. and Fan, X.: Estimating R^2 Shrinkage in Multiple Regression: A Comparison of Different Analytical Methods, The Journal of Experimental Education, 69, 203–224, https://doi.org/10.1080/00220970109600656, 2001.

Yoshikawa, K. and Hinzman, L. D.: Shrinking thermokarst ponds and groundwater dynamics in discontinuous permafrost near Council, Alaska, Permafrost and Periglacial Processes, 14, 151–160, https://doi.org/10.1002/ppp.451, 2003.

Zabel, N. A., Soliguin, A. M., Wiklund, J. A., Birks, S. J., Gibson, J. J., Fan, X., Wolfe, B. B., and Hall, R. I.: Paleolimnological assessment of past hydro-ecological variation at a shallow hardwater lake in the Athabasca Oil Sands Region before potential onset of industrial development, Journal of Hydrology: Regional Studies, 39, 100 977, https://doi.org/10.1016/j.ejrh.2021.100977, 2022.

Zwieback, S., Chang, Q., Marsh, P., and Berg, A.: Shrub tundra ecohydrology: rainfall interception is a major component of the water balance, Environmental Research Letters, https://doi.org/10.1088/1748-9326/ab1049, 2019a.

Zwieback, S., Westermann, S., Langer, M., Boike, J., Marsh, P., and Berg, A.: Improving Permafrost Modeling by Assimilating Remotely Sensed Soil Moisture, Water Resources Research, 55, 1814–1832, https://doi.org/10.1029/2018WR023247, 2019b.